Marie Curie Industry-Academia Partnerships and Pathways
Call: FP7-People-2011-IAPP

Long Life Bridges – Research Report

Secondment 1.1b
Adaptive and semi-active vibration control of railway bridge dynamics

Deliverable No: 1.1

Roughan & O'Donovan
Innovative Solutions

March 2013

Project Title:	Long Life Bridges
Deliverable No:	1.1
Deliverable Title:	Secondment 1.1b Adaptive and semi-active vibration control of railway bridge dynamics
Dissemination Level:	RE
Document No:	LLB-RODIS-REP-1.1b-Railway_Dynamics
Created by:	Andreas Andersson
Checked by:	Alan O'Connor
Approved by:	Eugene O'Brien

Description	Issue	Created	Checked	Approved	Date
Research Report	1.0	14/3/13			2/4/13
1st revision	1.1	29/3/13			2/4/13

The research leading to these results has received funding from the European Union's Seventh Framework Programme (FP7/2007-2013) under the Marie Curie, Industry and Academia Partnerships and Pathways (IAPP) call, Grant agreement no. 286276

Acknowledgements

Long Life Bridges is a Marie Curie 7th Framework Project funded under the Industry and Academia Partnerships and Pathways call, Grant Agreement No. 286276. The Project commenced in September 2011 and is continuing for 4 years until August 2015. The author wishes to acknowledge the financial contribution by the European Commission in supporting the project and funding this research.

The work presented in this report has been conducted at Roughan & O'Donovan Innovative Solutions, Dublin, Ireland, during the period of January to December 2012, under supervision of Associate Professor Alan O'Connor. The author has been seconded from the Royal Institute of Technology (KTH), Division of Structural Engineering and Bridges.

Within the project, experimental work to develop a prototype damper has been carried out at Trinity College Dublin (TCD), Department of Civil, Structural and Environmental Engineering. A special thank goes to Dr. Kevin Ryan and the laboratory staff at the Department for the help in manufacturing and testing the prototype damper.

Full-scale testing has been performed on a railway bridge in Sweden. The tests were funded directly by the Swedish Transport Administration (Trafikverket). The instrumentation and field measurements were performed by KTH in collaboration with the author.

Stockholm, April 2013

Andreas Andersson

List of publications

Within the project, the following publications have been produced.

I. Attenuating resonant behaviour of a tied arch railway bridge using increased hanger damping. *Taylor & Francis, IABMAS 2012, Stresa, Italy, July 8-12 2012*. (*Conference paper, published*)

II. Semi active damping systems for railway bridges. *BCRI 2012, Dublin, Ireland, September 6-7 2012.* (*Conference paper, published*)

III. Vibration mitigation of railway bridges using adaptive damping control. *IABSE 2013, Rotterdam, The Netherlands, May 6-8 201*3. (*Conference paper, accepted*)

IV. Passive and adaptive damping systems for vibration mitigation and increased fatigue service life of a tied arch railway bridge. *(Journal paper. submitted to ASCE Journal of Bridge Engineering, February 2013*)

V. Development and testing of a bi-directional multi-passive tuned mass damper. (*Journal paper. submitted to ASCE Journal of Structural Engineering, February 2013*)

VI. External damping of stay cables using adaptive and semi-active vibration control. *ICSBOC 2013, Edinburgh, Scotland, June 3-5 2013*. (*Conference paper, accepted*)

Contents

Chapter 1. Introduction

1.1. The Long Life Bridges project

Long Life Bridges is a European Union 7th framework funded project led by Roughan & O'Donovan Innovative Solutions, Dublin, Ireland. The project vision is to extend the service lives of bridges through development of advanced assessment methods.

The project is organized as an Industry-Academia Partnership involving the following partners:

- Roughan & O'Donovan (ROD), Ireland,
- Royal Institute of Technology (KTH), Sweden,
- Phi-Meca (Phimeca), France,
- Aalborg University (AAU), Denmark.

The work consists of seven secondments organized in three different tasks as follows:

Task 1.1: Railway Bridge Dynamics

1.1a) Probabilistic Evaluation of Allowance for Dynamics.

1.1b) Adaptive and semi-active control of railway bridges.

Task 1.2: Life Cycle Evaluation

1.2a) Probabilistic life cycle evaluation of cable stayed bridges.

1.2b) Probabilistic life cycle evaluation of cable stayed bridges.

1.2c) Structural Health Monitoring.

Task 1.3: Fatigue Evaluation

1.3a) Probabilistic Approach to Fatigue.

1.3b) Probabilistic Fatigue Model using Fracture Mechanics.

The goal of the Long Life Bridges project is to extend the lives of bridges and to get more from the transport structures for less. The project aims to deliver:

- more road and rail bridges being proven to be in a safe state and
- higher speeds on our (non-high-speed) railway lines,
- with less demand for non-renewable and carbon intensive resources and
- for less cost.

The work is organised in work packages (WP) following the structure of Figure 1.

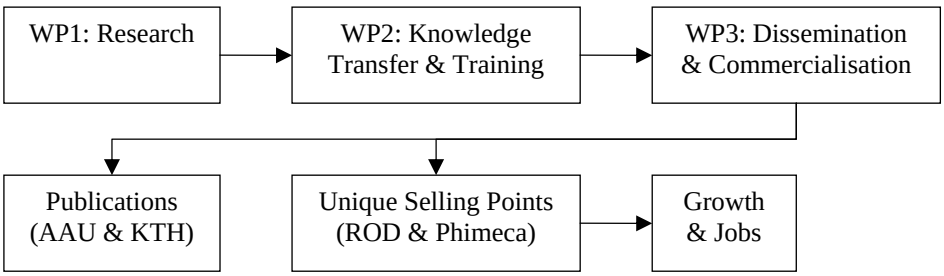

Figure 1: Structure of the work packages within the Long Life Bridges project.

1.2. Secondment 1.1b

Secondment 1.1b deals with development of adaptive and semi-active damping systems for railway bridges. The aim of the project is to develop methods for structural vibration control with applications for railway bridge dynamics. Much of the work has been related to a case study bridge, further described in Section 2.1.

There is constant demand on rail authorities to increase both the allowable axle loads and the allowable speed on existing railway lines. As an example, the Swedish Transport Administration has recently investigated the possibility of upgrading part of the main lines to allow for future high-speed trains. Some lines are also being investigated with the aim of allowing ore transports with higher axle loads and longer trains. A large portion of the bridge stock was designed for significantly lower axle loads and only very few have been designed to account for dynamic effects. Increased dynamic effects may result in exceedance of dynamic design criteria, reduced service life due to fatigue, or even failure. Through better quantification of risk, it is often possible to prove that speeds can be increased with no adverse effect. However, for bridges where the level of risk is too high, a cost-effective means of reducing dynamic effects on bridges are active and semi-active control system. Semi-active control is well established in other fields and could prove to be a beneficial technique to allow train speeds to be increased.

The concept of structural vibration control is to attenuate the dynamic response of a structure by means of an external damping device. Due to changes in either loading or structural behaviour, the properties of the damper device may need to be changed to efficiently mitigate vibrations. Two main principles of damper devices are commonly used; tuned mass dampers and shock absorbers. Tuned mass dampers consist of a suspended mass mounted on the main structure. Due to a phase-shift, the vibration of the suspended mass partly counteracts the corresponding motion of the main structure. Changing the stiffness of the suspended mass results in a variable adaptive tuned mass damper. Shock absorbers rely on producing the counteracting force by means of increased viscous damping. Devices with variable viscous damping are often categorised as semi-active. Fully active systems rely on producing the counteracting force by means of a load actuator. Adaptive and semi-active systems generally require much less energy to operate compared to fully active systems.

1.3. Knowledge transfer

The transfer of knowledge during the secondment from KTH to ROD is summarised below.

- The author has gained increased analytical skills in structural dynamics and vibration control, partly by progressing from work by previous ROD member Dr. John Arrigan.
- The author has gained increased knowledge in statistics by discussion with Prof. Alan O'Connor, especially on the use of fragility curves that has been adopted in paper V.
- The routines developed by the author (summarised in Appendix A) have been delivered to ROD and ROD-staff has been inducted on how to use it.
- The author has given two presentations to ROD-staff; one on the topic of fatigue assessment of steel railway bridges and one on the content of secondment 1.1b.
- The author has gained increased laboratory skills during the development of a prototype damper, performed in the laboratory at TCD under supervision of Dr. Kevin Ryan.

1.4. Format of the report

This report consists of an extended summary of the published and submitted papers. The full papers are appended in the end of the report.

Within the project, numerous routines and numerical models have been created. All relevant material has been delivered in digital format to Roughan & O'Donovan Innovative Solutions at the end of the

secondment. Due to the extent of the developed codes and input files, the content is not included in the report. The structure and the outline of the data files are however presented in Appendix A.

In November 2012, additional field measurements were performed on the case study bridge. The performance of a developed prototype damper was tested. The instrumentation programme from the tests is found in Appendix B.

Chapter 2. Extended summary

The following chapter contains an extended summary of the publications produced during the research period of secondment 1.1b. The publications are appended in the end of this report.

2.1. Case study bridge

The developed theories and experiments are demonstrated on a case study bridge. The bridge is located approximately 110 km West of Sundsvall, a municipality in central Sweden. It is part of the Northern main line and is important for ore transports as well as commuter trains. The bridge was built in 1959 and is designed as a single span single track tied arch railway bridge. A photo of the bridge is presented in Figure 2. The mid-support is a remnant from the previous bridge and is not utilized.

Figure 2: View of the Ljungan railway bridge.

The deck is designed as an unballasted steel grillage consisting of main beams, cross beams and stringers. Wooden sleepers are supported directly by the stringers. A cross-section of the deck is illustrated in Figure 3. The distance between the cross beams is 3.75 m, which is the same for the hangers. The hangers consist of solid steel rods with a diameter of 80 mm above the threaded section. The arch has a circular shape with a radius of 31.9 m and a height of 8.9 m, measured from the top of the main beam to the arch centre line.

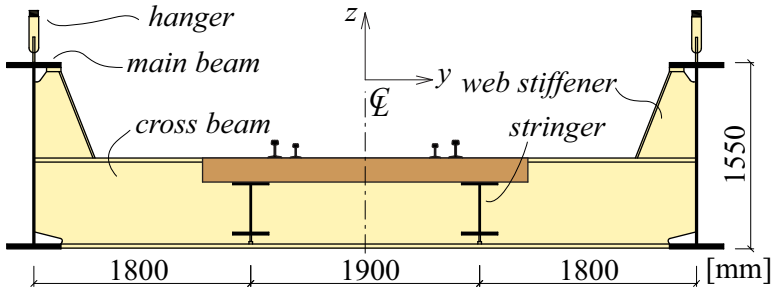

Figure 3: Cross-section of the grillage deck.

The dimensions of the beams are presented in Table 1. In addition, secondary bracing systems with profile L90×90×9 connects to the upper flange of the stringers and with profile L140×140×13 to the lower flange of the main beams and cross beams. Due to excessive vibration of the hangers, a system of diagonal RHS-beams was installed in the 1980's as an attempt to stabilize the hangers. This system was replaced by individual pendulum dampers in 2005.

Table 1: Beam cross-sectional properties. The arch has a rectangular hollow section; all I-beams are doubly symmetric.

(mm)	h	b_f	t_f	t_w
main beam	1550	450	40	16
cross beam	750	300	34	18
stringer	440	300	22	12
arch	350	600	16	20

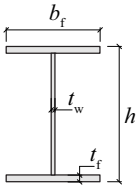

Field measurements were carried out in June 2003, comprising 16 strain gauges and 12 accelerometers, mounted on hangers 2 to 5. During field measurements, the stabilizing system of RHS-beams was removed. The position of the gauges and details of the hangers are presented in Figure 4a . The total length of L_h and distance L_a to the accelerometers are given by Table 2. At each position, three accelerometers are mounted together, measuring in xyz-directions. Also, four strain gauges are instrumented at the distance z_1 = 100 mm above the threaded section, spaced 90° apart along the perimeter of the hanger. Gauge e1, e5, e9, e13 are closest to the track.

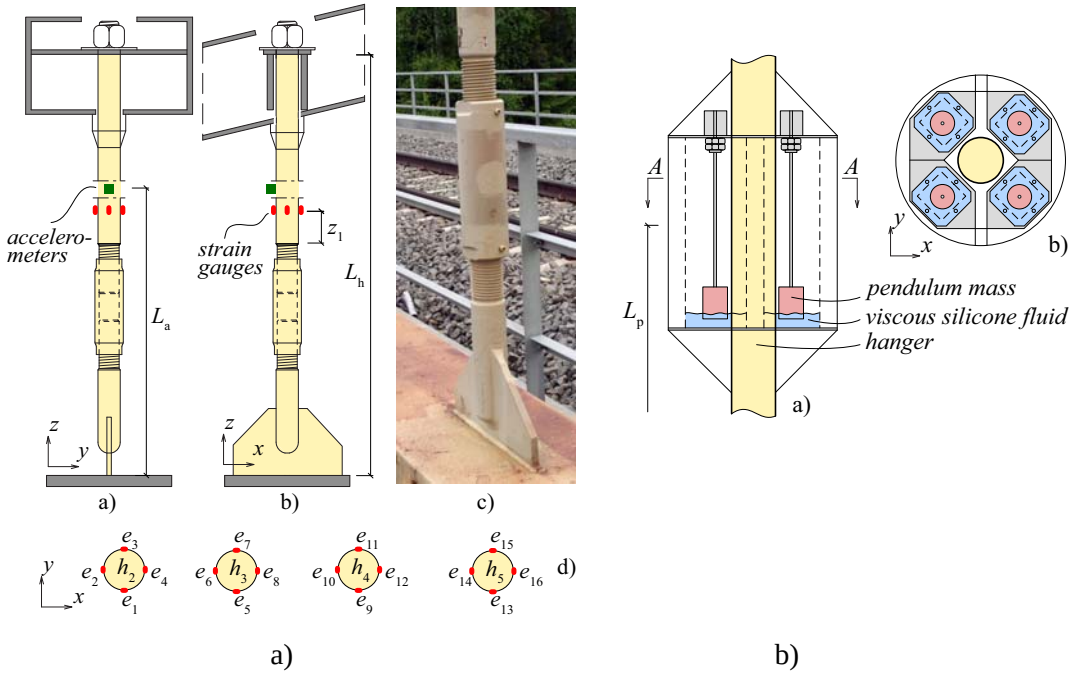

Figure 4: Details of a) the instrumentation from 2003, b) installed pendulum damper from 2005.

Table 2: Length of the hangers L_h (according to original drawings) and position of accelerometers L_a, rounded to 5 cm. L_p is the position of installed passive pendulum dampers.

hanger	h_1	h_2	h_3	h_4	h_5	h_6
L_h (m):	1.30	3.54	5.20	6.30	6.95	7.15
L_a (m):	–	1.55	1.90	2.15	2.30	–
L_p (m):	–	–	3.12	3.67	4.00	4.10

2.2. Paper I – Case study bridge (IABMAS 2012)

Paper I was presented at the IABMAS-conference in Stresa, Italy, in July 2012. The paper was submitted prior to the start of the secondment and only contains background knowledge. The main content of the paper is summarised below.

- The case study bridge is introduced and is briefly described.
- The instrumentation and field measurements from 2003 is presented and partly re-analysed. Natural frequencies and structural damping of the hangers are estimated based on free vibration measurements of the unloaded bridge.
- From several strain gauges located along the perimeter of the hanger, the stress components during train passage related to axial force and bending moments in two directions are separated. Noticeable bi-axial bending is found. For the case of a passing freight train, significant resonance during the free vibration is measured.
- The cumulative fatigue damage due to the train passage is performed using Palmgren-Miners linear damage rule. The stress collective is calculated using a Rain-flow counting algorithm.
- The lateral displacement of the studied hanger is estimated based on measured acceleration and a Newmark time integration algorithm.
- A 2D finite element model of the bridge is created. From an Eigen-value analysis, good agreement in natural frequencies is found compared to the measured response. It is shown that the pre-stress of the hangers influence the natural frequencies significantly and need to be included in the analysis. It is further concluded that the additional axial force due to passing trains need to be accounted for. As a result, the analyses are nonlinear and the dynamic response needs to be analysed by direct time integration instead of modal analysis.
- Dynamic simulations of the response due to passing trains are performed. The train is considered as moving point loads. Rayleigh-damping is used, based on damping ratios estimated from the free vibration tests. Considering that the 2D-model does not include the transverse behaviour, good agreement in response is found compared to the field measurements.
- It is concluded that the resonant behaviour of the bridge significantly decreases the fatigue service life. Based on field measurement of one of the longer hangers, 50 % of the fatigue damage was related to free vibrations after train passage. Simulations with increased damping show great potential in increasing the service life.

2.3. Paper II – Adaptive control (BCRI 2012)

Paper II was presented at the BCRI-conference in Dublin, in September 2012. The paper describes the use of tuned mass dampers (TMD) and applications on the case study bridge. The main content of the paper is summarised below.

- The case study bridge and key results estimated from the field measurements is briefly introduced.
- The 2D FE-model of the bridge is briefly presented.
- The concept of the TMD is introduced. A 2DOF-model representing a bridge hanger and the TMD is analysed. A parametric study on the influence of the mass and viscous damping of the TMD is performed. The influence of a detuned TMD is investigated, both based on the steady-state response and a direct time response. The load block in the direct time response corresponds to the forces acting on the hanger during train passage.
- The use of a variable frequency semi-active system is presented. A developed algorithm for a Short Time Fourier Transform (STFT) is used to determine the real-time dominant frequency. The performance of the semi-active TMD is studied for the 2DOF-model.
- The 2D FE-model is modified to include a TMD on one of the hangers. The damper is modelled as a lumped mass and connects to the hanger by a spring and dashpot element.
- Simulations of passing trains show that a passive TMD tuned to the unloaded bridge efficiently attenuates the free vibrations. During train passage however, the passive TMD experience detuning and provides little improvement. The detuning is due to an increased natural frequency of the loaded hanger, caused by the additional axial force from the passing train. An STFT-analysis of the measured response confirms this change in frequency.
- Similar simulations using the developed algorithm for the variable stiffness semi-active TMD shows a significant improvement for the forced vibration.

2.4. Paper III – Adaptive control (IABSE 2013)

Paper III has been accepted for publication and presentation at the IABSE-conference in Rotterdam, May 2013. The paper progress from paper II and the outline is summarised below.

- The concepts of the TMD and the governing equations are presented. The use of pendulum dampers is introduced and equation for a pinned and a fixed pendulum is presented. Passive pendulum dampers were installed in the hangers in 2005.
- The semi-active algorithm is updated resulting in increased performance and accuracy. In addition to the STFT, a Short Time Wavelet Transform (STWT) is used.
- The performance of both the TMD and the pendulum damper is studied for 2DOF and MDOF models under different loadings and conditions. The best performance is found for an adaptive variable stiffness TMD using the STWT-routine.
- The 2D FE-model is updated to include the pendulum damper. The results from simulations of passing trains are presented and a comparison between the different dampers and methods of analysis is made.
- From the simulations, the passive pendulum damper shows better performance than the passive TMD. However, both experience significant detuning during the forced vibration. The adaptive TMD shows an overall better performance, both using the STFT or STWT methods.
- The adaptive TMD also shows much smaller amplitude for the free vibrations, although tuned to the same frequency as its passive counterpart. The reason is that the free vibrations start at a lower amplitude since the forced vibrations have been attenuated in the adaptive case.

2.5. Paper IV –Vibration control and fatigue (ASCE)

Paper IV was submitted to ASCE Journal of Bridge Engineering in February 2013. It includes a more detailed description of the bridge, the instrumentation from 2003 and installed pendulum dampers from 2005. It further describes the theory for TMD and pendulum dampers in more detail than the conference papers. The equations for incremental time-frequency estimation are presented. In addition, the following new content is included.

- A 3D FE-model of the bridge is presented. Due to the detail of the hanger to main beam connection, the hangers are considered clamped for longitudinal bending and pinned for transverse bending. As a result, the natural frequencies are lower in the transverse direction than the longitudinal direction. This is confirmed by the result from the field measurements and a good agreement is found in comparison with the model.
- Dynamic simulations of passing trains are performed to investigate the resonance behaviour at different speeds. Due to low structural damping, the stresses at resonance are significantly higher than off resonance. The results are also sensitive to the train speed, inducing different modes of vibration, either in the transverse or longitudinal direction. At higher speeds, the global bending mode of the bridge is set in motion, causing resonance of many hangers simultaneously. Similar analyses are performed on the 2D-model, not including the transverse bending.
- Time-variant combination of normal force and bi-axial bending results in a variable stress field along the perimeter of the hanger at each increment of time.
- For each train passage at each speed, the stress variation along each hanger is calculated for each increment of time. The Rain-flow counting method is used to calculate the corresponding stress collectives, one for each studied position along the perimeter of each hanger.
- The mixed train traffic on the real bridge is simulated by two generic train types, a typical freight train and a typical passenger train. The estimated fatigue service life is found highly dependent on the train speed.
- Fragility curves are adopted as a method to relate the fatigue service life to a probability of failure. The results from the simulations are considered to be deterministic and the only stochastic process is related to the train speed. Based on long-term measurements of passing trains at another railway bridge, a triangular probability distribution function (pdf) is assumed. The limits of the pdf are determined by the allowable train speed. The FE-model predicts non-negligible stresses even at significantly lower speeds. From the train speed measurements, some trains were found to travel at very low speed, possibly due to traffic diversions. To account for this, a tri-linear pdf is used.
- Fragility curves are calculated for both the 2D and 3D-model. For the 2D-model, the influence of different damping systems is also included. The results show that for a probability $P<0.8$, the fatigue damage is generally low. For $P>0.8$ however, extreme increases in fatigue damage is obtained, allowing only a few thousand train passages.
- The passive dampers are shown to have a moderate influence on the cumulative damage whereas the variable stiffness adaptive damper shows a great improvement. For $P>0.8$ however, less improvement is found for all damper types. This is likely due to the influence of global modes of the bridge, setting all hangers in motion.

2.6. Paper V – Laboratory work on prototype damper (ASCE)

Paper V was submitted to ASCE Journal of Structural Engineering in February 2013. The paper contains the experimental results of a prototype damper, developed by the author at the laboratory in Trinity College Dublin (TCD).

In the previous theoretical simulations, the adaptive and semi-active dampers are governed by a variable stiffness control. This is found to be an efficient and robust method to account for detuning and load-dependent frequency changes. However, most physical dampers in the literature that are based on similar concepts consist of complicated mechanical systems. As an alternative, a bi-directional Multi-Passive Tuned Mass Damper (bi-MTMD) was developed. The damper accounts for both the unloaded and loaded conditions of the hanger for both longitudinal and transverse motion.

Although the developed damper is tailor-made for a specific hanger on the case study bridge, the concept may have a wider application, e.g. cable structures. The main content of the paper is summarised below.

- A 3D FE-model of the damper is presented. The damper consists of two steel rings suspended in wires and connected to the hanger by spring and dashpot elements. An Eigen-value analysis shows the four main modes of vibration. Although the two rings are coupled in series, the modes are shown to be rather independent.
- The physical damper device and its components are described. The hanger consists of a steel tube mounted on a sliding table. The base of the table is connected to a load shaker. The steel rings are suspended in nylon wires and connected to the hanger by tailor-made coil springs and foam material.
- The experimental setup and instrumentation is described. Separate tests are performed to determine the accuracy of the sensors and the signal quality.
- The steady-state response of the damper is estimated by slowly increasing the frequency of the load shaker. Based on the results, a frequency response function (FRF) is calculated.
- The damper is calibrated to target frequencies obtained from the field measurements in 2003. The natural frequencies depend both on the stiffness of the coil spring and the foam material, whereas the damping mainly depends on the foam material.
- The influence of the foam is shown from experiments only including the coil springs. For the case of only coil springs, torsional modes of the steel rings were found. This is prevented by the foam material due to its shear stiffness.
- To simulate the conditions of passing trains, the damper is subjected to a set of harmonic load blocks at different frequencies. The results are compared with the FE-model of the damper and generally show good agreement.

2.7. Paper VI – Cable dynamics (ICSBOC'13)

Paper VI is accepted for publication and presentation at the ICBOC-conference in Edinburgh, Scotland, in June 2013. In this paper, the work developed in relation to the case study bridge is applied to stay cables for stay cable bridges. A single cable is analysed, having properties of a reference case found in the literature. The content of the paper is summarised below.

- The cable is modelled as a horizontal beam with negligible flexural stiffness. A pre-stress is included to obtain the prescribed natural frequency. The influence of cable sag is neglected.
- Two different dampers are studied, a near anchorage viscous damper and a TMD. The viscous damper is mounted at $0.02L$ and the TMD at $0.4L$, where L is the length of the cable.
- The cable and the dampers are described by a 2D FE-model and results are based on steady-state analyses.
- Near anchorage dampers are based on introducing additional structural damping to the cable. For the above mentioned conditions, a closed form solution exists. A passive viscous damper is often calibrated based on optimal performance for the fundamental mode of vibration. The same equation is valid for higher order modes and results in another optimal viscous damping.
- For a TMD, the influence of the mass and viscous damping on the resulting cable damping is determined by a numerical parametric study. A significantly smaller viscous component can be used in the TMD compared to the near anchorage damper for the same resulting cable damping.
- The adaptive control developed for the case study bridge is modified to fit with the cable model. Two different adaptive strategies are used for the TMD; a continuous variable tuning frequency and an incremental frequency based on the four lowest modes of vibration. Both are based on a variable stiffness control. For the adaptive near anchorage damper, the viscous damping is controlled based on the dominate mode of vibration.
- The results show that the near anchorage damper has a rather limited performance, depending on the relatively short distance between the anchorage point and the connection with the damper. This decreased for longer cables.
- The adaptive viscous damper shows moderate improvement for higher modes compared to the corresponding passive damper.
- A TMD can result in significant vibration mitigation, even for a moderate damper mass.
- For the TMD, an optimal damping value exists, that increases with increased damper mass.
- The passive TMD is sensitive to detuning, resulting in a poor performance for higher modes.
- An adaptive/semi-active TMD can increase the vibration mitigation significantly for higher modes. The best performance was obtained by a continuously variable stiffness TMD.

Appendix A. Structure of developed routines

A.1. Overview

Within the project, numerous routines and numerical models have been created. All relevant material has been delivered in digital format to Roughan & O'Donovan Innovative Solutions at the end of the secondment. Due to the extent of the developed codes and input files, only the structure of the content is presented below.

Source: \\roddubfp1\P_drive\Proj\2011\11150\11150-12-RODDOCs\Andreas - Secondment\

\Admin

Misc admin documents, contacts, meeting minutes, PDP, document templates, time sheet

\FEM\Beam_dynamic\Main.m

Routines for a simply supported beam subjected to dynamics of high-speed trains. Requires Matlab and the FE-software SOLVIA03 to run. Includes:

- Frequency analysis
- Steady-state analysis
- modal dynamics
- direct dynamics
- point loads vs. moving mass and vehicle interaction
- Influence of track stiffness and load distribution

\FEM\Cable_dynamic\Main.m

Routines for dynamics of a single stay cable. Requires Matlab and the FE-software SOLVIA03 to run. Includes:

- Frequency analysis
- Steady state analysis
- Direct dynamics

\FEM\Case_study_bridge

Main directory for FE-models related to the case study bridge (2D and 3D models). Requires Matlab and the FE-software SOLVIA03 to run. Includes:

- Frequency analysis
- Dynamics of passing trains
- Passive damper
- Adaptive damper
- Pendulum damper
- Multi-passive TMD
- STFT vs. STWT analysis
- Results from cumulative fatigue damage
- Code for fragility curve analysis

\FEM\Dampers

Main directory for development of damper models (prior to experimental work). Requires Matlab and the FE-software SOLVIA03 to run. Some models created in Abaqus. Includes:

- Clamped beam model, passive and adaptive
- Hula-hoop models, passive, multi-passive, adaptive, friction, taut wires
- MDOF-models, coupled and decoupled
- MR-damper, dynamic-mechanical models for MR-dampers, comparison with literature data
- Algorithms for semi-active control
- Pendulum dampers, clamped pendulum, adaptive pendulum, MDOF models
- Romb-piston model
- General routines for semi-active (adaptive) MDOF-systems

\FEM\DEMO

Contains demo-files and templates for vibration control. Requires Matlab and the FE-software SOLVIA03 to run. Includes:

- 2D bridge models (with and without damper)
- 3D bridge models (with and without damper)
- Bi-directional multi-passive TMD
- MR-damper models
- FRF (Frequency response function analysis)
- Matrix-Porthole feature in SOLVIA03, read from Matlab
- Matlab script LL_Misc.m, TestCumulativeDamage.m, TestDamping.m for dynamics

\Field measurements

Contains documentation related to the field measurements on the case study bridge.

- Measurements performed 2003 (by KTH)
- Reports from damper design and field tests 2005 (by Sedlacek & Partners)
- Measurements performed 2012 (by KTH)
- Original drawings and instrumentation programmes

\Lab work

Main directory for files related to the laboratory work performed at TCD. Contains:

- Data files from experiments
- Documentation and sensor specifications
- FE-model of the developed damper

\Literature

Main directory for literature related to dynamics and vibration control. Contains:

- SOLVIA03 FE-manual
- Misc books on structural dynamics and vibration control
- Cable dynamics
- MR dampers and semi-active control
- Theories for TMD
- Wavelets
- Fatigue
- Fragility curves and probabilistic analysis
- Misc documents and lecture notes on dynamics

\Matlab

Directory for developed Matlab-functions. Contains:

- Damping estimators, Damp_logdec.m, Damp_logdec2.m, Damp_HPB.m
- Rayleigh damping, Rayleigh.m
- Time integration, newmark_3.m
- Real-time frequency estimators, STFT and STWT
- Triangular distribution functions, TriaPDF.m, Tria2PDF.m
- Fast Fourier Transform freq.m
- Cumulative fatigue damage, CalcDamage.m
- WAFO toolbox for signal analysis, probabilistic and cumulative damage
- CalFEM toolbox, open source FE-code for Matlab

\Presentation

Presentations related to the Long Life Bridges project.

\Publications

Main directory for publications related to the Long Life Bridges project

\Reports

Contains temporary documents and draft work material, used as basis for meeting discussion.

Appendix B. Instrumentation of the case study bridge

B.1. Content

In the following appendix, the instrumentation of the case study bridge performed in November 2012 is presented.

KTH Architecture and
the Built Environment

Ljungan vid Alby nsp, km 469 + 116

Instrumentation and field measurement, 12-15 November 2012

Andreas Andersson, 30/11/2012

Division of Structural Engineering and Bridges
KTH – Brinellvägen 23, SE-100 44 Stockholm
http://www.kth.se/abe/inst/byv/avd/bro

Content

1 Introduction

1.1 Scope

The following report contains the documentation and instrumentation for the field measurements performed on the bridge "Ljungan vid Alby, nsp", during the period 12-15 November 2012. The field measurements were funded by the Swedish Transport Administration (Trafikverket) and performed by KTH, Division of Structural Engineering and Bridges. The purpose of the measurements was to:

- estimate the dynamic properties of all hangers by free vibration tests,
- measure the stress in selected hangers during train passages,
- measure local stress concentrations on selected stringer and cross beam connections,
- demonstrate a developed bi-directional multi-passive tuned mass damper.

1.2 The bridge

The bridge is located in Ånge, 110 km West of Sundsvall, Sweden. It was built in 1959 and is designed as a steel tied arch railway bridge, carrying a single track. The bridge deck consists of a steel grillage, the track is supported by wooded sleepers directly onto the stringer beams. The span length is 45 m, the distance between the cross beams are 3.75 m, the same as the distance between the hangers. The arch has a circular shape with a radius of 31.9 m. The distance from the main beam upper flange to the arch centre line is 8.9 m. General bridge data is presented in Table 1, geometry of the beams are given by Table 2. A cross-section of the bridge deck is shown in Figure 1. More details about the geometry of the bridge and the hangers are given in the instrumentation section of this report.

Table 1: Bridge data.

name:	Ljungan vid Alby nsp	*built:*	1959
location:	bdl 215, km 469+116	*design load:*	085F + load gr. 1
knr.	3500-1587-1	*material:*	Steel S1411
type:	Tied arch bridge	*Span:*	45 m
WGS 84:	N62 ° 27.9', E15 ° 27.0'	*tracks:*	1

Table 2: Beam geometry data. All I-beams are double symmetric, the arch has a rectangular hollow section.

(mm)	h	b_f	t_f	t_w
main beam	1550	450	40	16
cross beam	750	300	34	18
stringer	440	300	22	12
arch	350	600	16	20

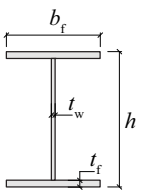

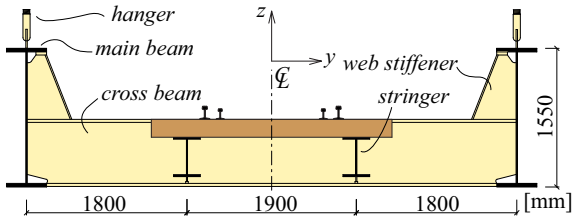

Figure 1: Cross-section of the bridge deck.

2 Instrumentation

2.1 Data acquisition

The main instrumentation consists of 12 accelerometers (SiFlex) and 18 strain gauges (LS31). Data was collected using a HBM MGCPlus data acquisition system. The sample frequency was set to 600 Hz with a Bessel lowpass filter at 250 Hz. Data was stored in binary files using the CaTMan software.

In addition, a tri-axial accelerometer (Sensr CX1) was used. Data from the CX1 sensor was sampled with 2000 Hz and a low pass filter at 200 Hz. The data from the CX1 sensor was collected directly with a separate PC and LAN connection. The sensor details are given below.

- Accelerometer (uni-axial): SiFlex SF1500S (±3g), ±12V input.
- Accelerometer (tri-axial): Sensr CX1 (±1.5g), ±5V input.
- Strain gauge: HBM LS31, 6 mm (weldable).
- HBM MGCPlus 24 bit data acquisition system with ML801 module.

2.2 Position of sensors

The instrumentation was performed on November 12$^{\text{th}}$, 2012. Strain gauges and accelerometers were installed on hanger 3 to 6 on the North-East side of the bridge. An overview of the instrumentation is given in Figure 3.The hangers are denoted with index N (North), S (South), NE (North-East), NW (North-West), SE (South-East) and SW (South-West).

The geometry of the hangers is illustrated in Figure 2. The strain gauges are instrumented a distance $L_{\text{e}} = 0.95$ m above the upper flange of the main beam, corresponding to about 100 mm above the upper threaded section of the hanger. The accelerometers are installed at the distance L_{a} and the total hanger length is L_{h}. The numbering of the sensors are given by Figure 4. Pendulum dampers were installed in 2005 and are located the distance L_{p} on hanger 3-6. During the field measurements, the pendulum damper on hanger $h5_{\text{NE}}$ was removed. The distances are given in Table 3.

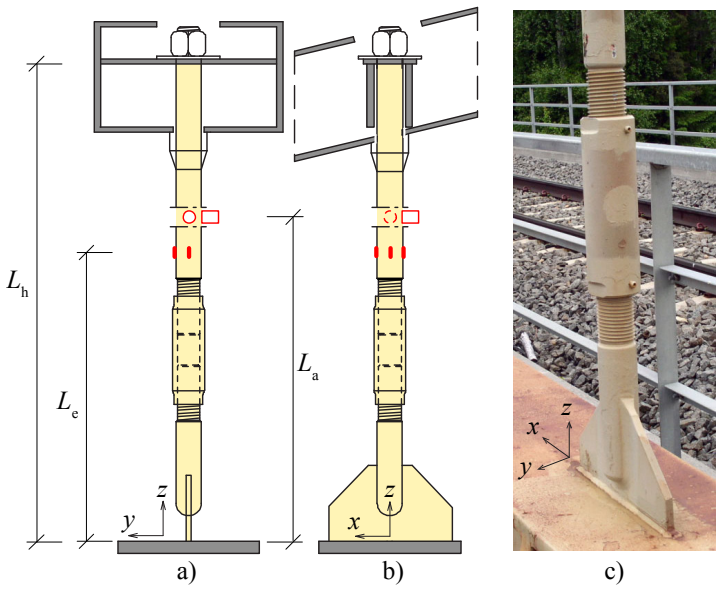

Figure 2: Geometry of the hangers and the sensors, a) across the bridge, b) along the bridge, c) photo of the hanger turn-buckle and connection with the main beam.

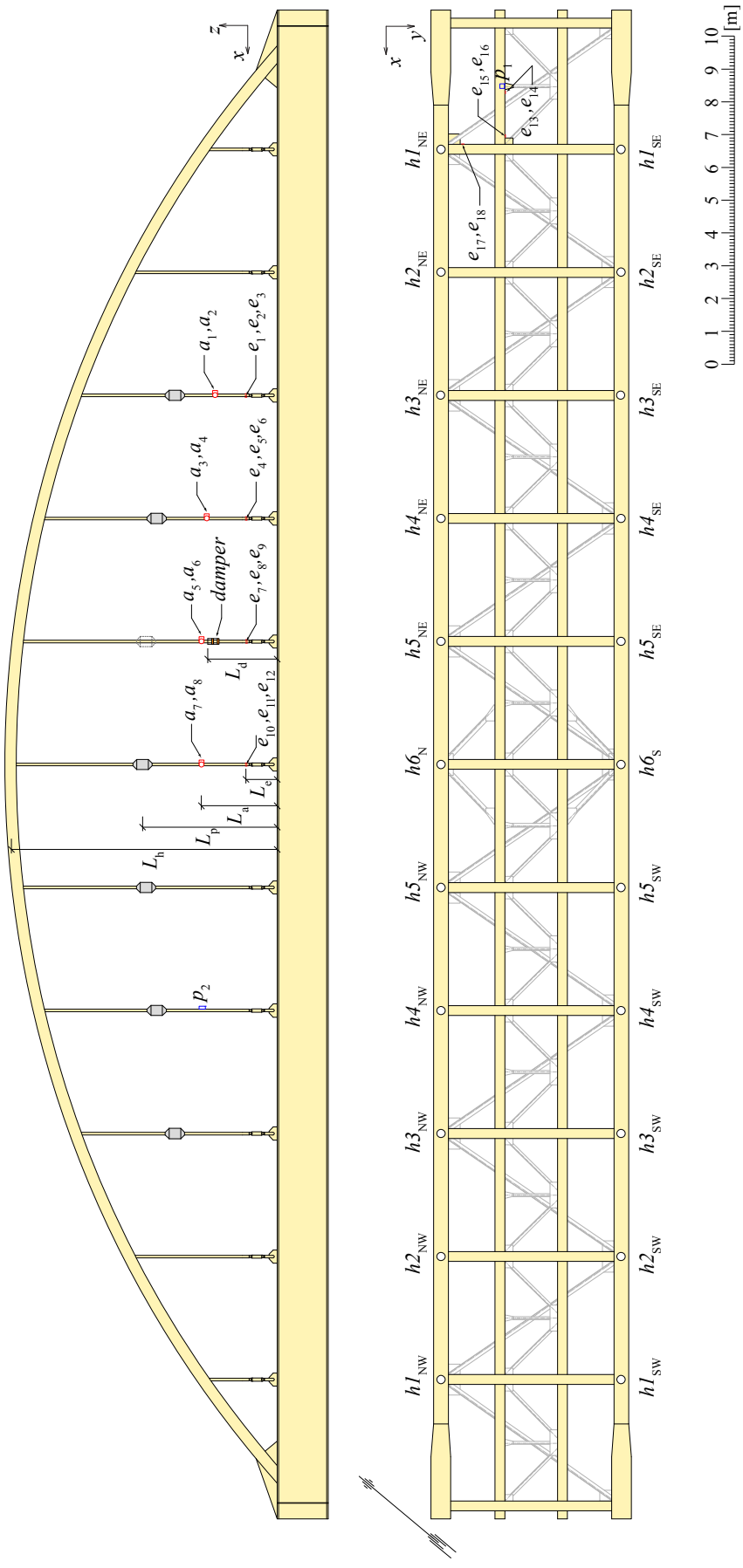

Figure 3: Elevation and plan view of the bridge, notations of hangers and position of sensors.

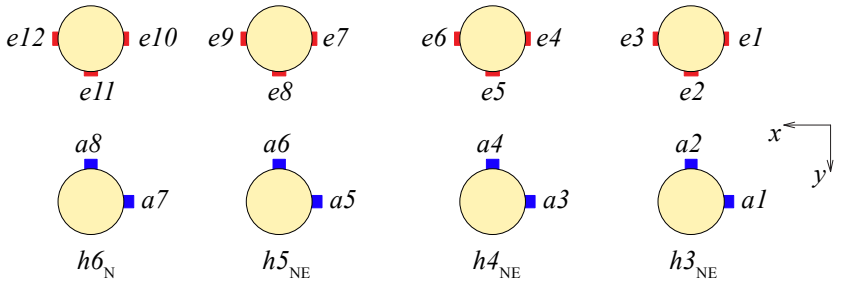

Figure 4: Numbering of strain gauges (e1-e12) and accelerometers (a1-a8) on hanger 3 to 6 on the North-East side of the bridge.

Table 3: Hanger length and position of dampers and accelerometers.

hanger:	*h1*	*h2*	*h3*	*h4*	*h5*	*h6*
L_h (m):	2.30	4.55	6.20	7.30	7.95	8.15
L_p (m):	-	-	3.12	3.67	4.00	4.10
L_a (m):	1.20	1.55	1.90	2.10	2.30	2.30

Three sections on the steel grillage was instrumented with strain gauges for estimation of local stress concentrations, Figure 5. Gauge e13,e14 and e15,e16 is positioned on the upper flange of the stringer, near connecting gusset plates. Gauge e17,e18 is positioned on the lower flange of the cross beam at similar locations. The detailed positions of the strain gauges are presented in Figure 6. The target distance was $0.4t + 0.6t$ measured from the weld toe, where t is the thickness of the flange plate. For e14 and e15 however, a longer distance was needed due to the size of the strain gauges.

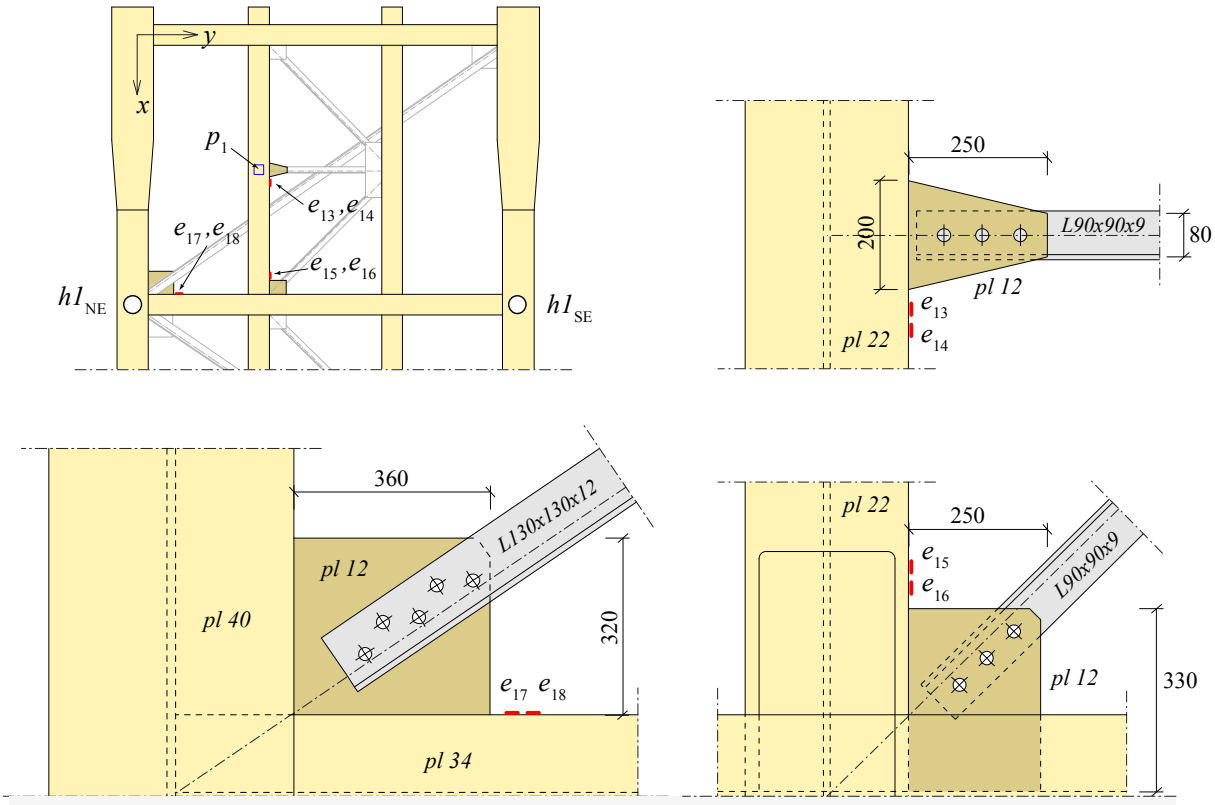

Figure 5: Instrumentation strain gauges the stringer and cross beam, details of intersecting gusset plates.

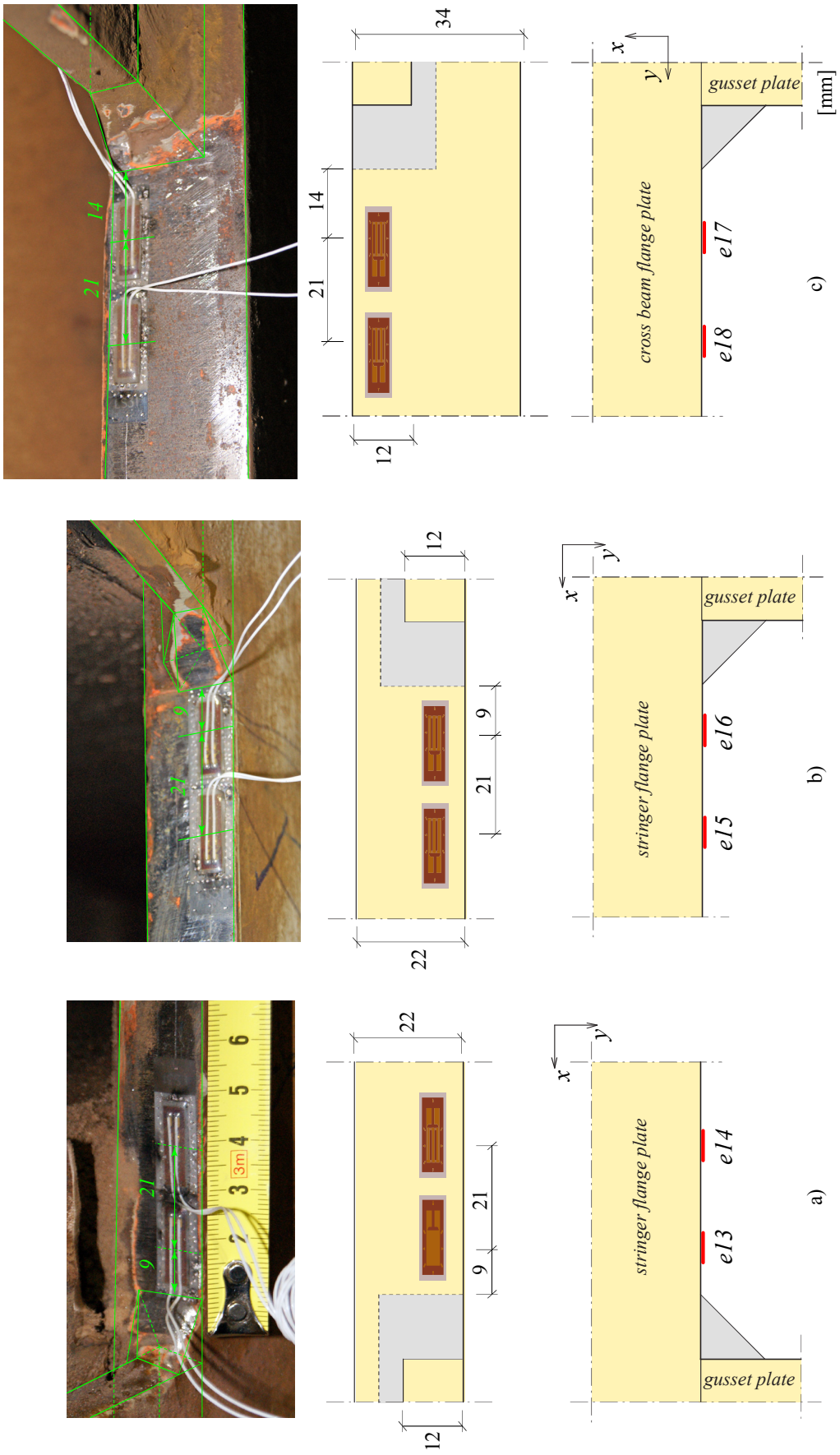

Figure 6: Strain gauges for hotspot measurements on a) the stringer upper flange at support, b) stringer upper flange at midpoint, c) cross beam lower flange at midpoint.

Photos of the dampers on the hangers are shown in Figure 7. A schematic of the dampers are illustrated in Figure 8, also showing the instrumentation on the bi-directional TMD on hanger $h5_{\mathrm{NE}}$.

a) b)

Figure 7: Installed dampers, a) pendulum damper, installed on hanger 3-6.b) bi-directional multi-passive TMD on hanger $h5_{\mathrm{NE}}$,

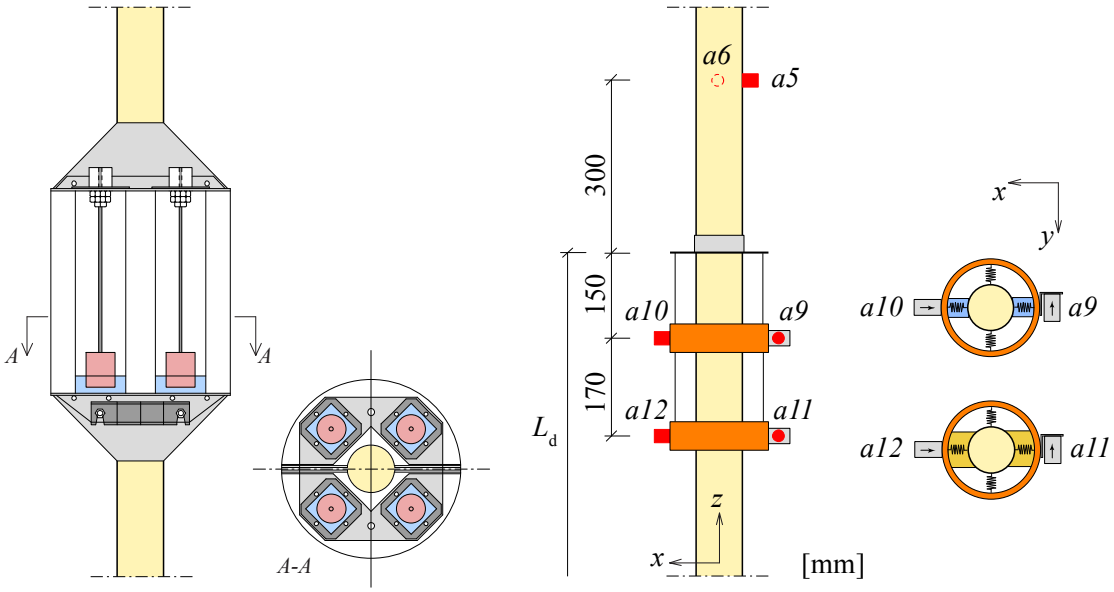

a) b)

Figure 8: Details of the dampers, a) pendulum damper on hanger 3-6, b) bi-directional multi-passive TMD installed on hanger $h5_{\mathrm{NE}}$.

2.3 Calibration factors

The raw data was stored in CatMan *.bin files. The results need to be divided with the calibration factors in Table 4 to obtain relevant units. The acceleration was recorded in [mV] on November 12th and in [V] the remaining days. The strain was measured in [μm/m] on November 13th but need to be divided by the below factors on the remaining days. Results from the CX1 accelerometer (denoted a13,a14,a15) are measured in [g]. Relevant parts of the raw data have been sorted and stored in *.mat files, where all accelerations are in [m/s^2] and all strains in [μm/m]. This conversion was performed on the 29th November 2012.

Table 4: Calibration factors for accelerometers and strain gauges.

Acc No.	*ID:*	V/(m/s^2)	*strain No.*	V/(μm/m)	*strain No.*	V/(μm/m)
a1:	604	0.27734	e1	1.005025	e10	1.015228
a2:	616	0.25859	e2	1.005025	e11	0.990099
a3:	608	0.26342	e3	1.005025	e12	0.990099
a4:	162-17	0.25970	e4	1.005025	e13	1.015228
a5:	611	0.25756	e5	1.005025	e14	0.990099
a6:	140-01	0.25040	e6	1.005025	e15	0.990099
a7:	605	0.26741	e7	1.005025	e16	1.015228
a8:	175-44	0.25540	e8	1.005025	e17	0.990099
a9:	603	0.26446	e9	1.005025	e18	0.990099
a10	622	0.27209				
a11	610	0.26564				
a12	617	0.27292				

3 Field measurements

3.1 Short log of procedure

Table 5: Short log.

Date:	*Event:*
12/11/2012	Free vibration tests of all hangers. Only accelerometer a1 (x-dir) and a2 (y-dir) in use, positioned at the distance L_a according to Table 3. Excitation by a swift knock on the hangers, 3 times in the x-dir and 3 times in the y-dir. Data from each hanger stored in a separate file, following the notations of Figure 3. All sorted data later stored in data_all.mat. Strain gauges installed during the same time period.
13/11/2012	Accelerometer a1-a6 first mounted on hanger $h5_{NE}$, located at L_a = 1.1, 1.7, 2.3 m. a1, a3, a5 in x-dir, a2,a4,a6 in y-dir. Free vibration tests, 3 times in the x-dir and 3 times in the y-dir (test_1.bin). Then same order but forced vibration obtained by hand (test_2.bin). Mounted accelerometer a1-a8 on hanger h3-h6 according to Figure 3 at distances according to Table 3. Free vibration test of hanger 3-6, 1 time in x-dir and y-dir (test_3.bin). Accelerometer CX1 mounted on the stringer lower flange, position p_1.Free vibration tests of the stringer, 3 times in y-dir, z-dir, x-dir (test_cx1.csv). Measurements of passing trains (11 AM to 2:40 PM). A total of 8 train passages, stored in files data_1.bin to data_7.bin. Separate files for the CX1 sensor, data_5.csv to data_7.csv. Each train later stored in train_1.mat to train_8.mat, including all sensors.
14/11/2012	Installed the bi-directional TMD on hanger $h5_{NE}$. Acc a5,a6 moved to 2.4 m to accommodate the damper. Acc a9 – a12 installed on the damper according to Figure 8b. Acc CX1 installed on hanger $h5_{NW}$, position p_2 at L_a = 2.3 m. Vibration tests of hanger $h5_{NE}$, after installation of the damper. 3 swift knock on the hanger in each of the x-dir and y-dir (test_1.bin). Excite the damper 3 times in each DOF (test_2.bin). Excite the hanger with forced vibration, 1 time in x-dir and y-dir (test_3.bin). Later additional tests, test_4.bin to test_6.bin. Measurements of passing trains (11 AM to 9:45 PM). A total of 12 train passages, stored in files data_1.bin to data_9.bin. Separate files for the CX1 sensor, data_4.csv to data_9.csv. Each train later stored in train_1.mat to train_12.mat, including all sensors.
15/11/2012	Replaced power supply batteries for the accelerometers. CX1-sensor not working. Measurements of passing trains (9 AM to 9 PM). A total of 15 train passages, stored in files data_1.bin to data_8.bin. Each train later stored in train_1.mat to train_12.mat.
16/11/2012	Removed all instrumentation (no measurements performed).

3.2 Recorded train passages

Table 6: Recorded train passages, 13/11/2012.

Time:	**.bin*	**.mat*	*Type:*	*Direction:*
12:00	data_1	train_1	Freight train 2*Rc + 22 wagons (incomplete data)	to Ljusdal
12:22	data_2	train_2	Freight train, Rc + 29 wagons (mostly empty)	to Ånge
13:18	data_3	train_3	Single Rc4 locomotive	to Ljusdal
14:10	data_4	train_4	Freight train, Rc4+2 wagons (incomplete data)	to Ånge
15:00	data_5	train_5	Freight train, Rc4 + 8 wagons (loaded wagons)	to Ånge
15:15	data_6	train_6	2 locomotives (HektorRail)	to Ånge
15:26	data_7	train_7	Rail alignment wagon	to Ljusdal
15:35	data_7	train_8	Freight train, steel slabs, 2*loco + 34 wagons	to Ljusdal

Table 7: Recorded train passages, 14/11/2012.

Time:	**.bin*	**.mat*	*Type:*	*Direction:*
11:47	data_1	train_1	Freight train, 2*Rc4 + 30 wagons (mixed weight)	to Ånge
12:05	data_2	train_2	Commuter train, Rc6 + 4 wagons	to Ånge
14:32	data_3	train_3	Freight train, loco + 30 wagons (mostly loaded)	to Ånge
14:43	data_3	train_4	2 loco (HektorRail) + empty wagon	to Ånge
	data_4	train_5	Freight train, 2 loco + wagons (mixed weight)	to Ånge
	data_5	train_6	Freight train (loaded)	to Ljusdal
18:21	data_6	train_7	Freight train (mixed weight)	
	data_7	train_8	Commuter train, Rc + 4 wagons	
	data_8	train_9	Freight train, Rc + 10 wagons (mixed weight)	
	data_8	train_10	Freight train, Rc + wagons (mostly empty)	
	data_9	train_11	Commuter train, 4 wagons (no locomotive?)	
	data_9	train_12	Freight train, 2*Rc + wagons (mixed weight)	

Table 8: Recorded train passages, 15/11/2012.

Time:	**.bin*	**.mat*	*Type:*	*Direction:*
9:00	data_1	train_1	Single locomotive, Rush-Rail	to Ljusdal
9:05	data_1	train_2	Freight train, Rc4 + 5 wagons (partly loaded)	to Ljusdal
13:02	data_2	train_3	Freight train, 2*Rc4 + wagons (mixed weight)	to Ljusdal
13:12	data_3	train_4	Freight train, Rc4 + empty wagons	to Ljusdal
15:32	data_4	train_5	Freight train, 2*Rc4 + 32 wagons (mostly loaded)	to Ljusdal
15:51	data_5	train_6	Freight train, steel slabs, 2 locomotives + 30 wagons	to Ljusdal
16:12	data_6	train_7	Freight train, 2*Rc4 + 21 wagons (mixed weight)	to Ånge
	data_7	train_8	Freight train 2*Rc + 21 wagons (mostly loaded)	to Ljusdal
	data_7	train_9	Commuter train, Rc + 5 wagons	to Ljusdal
18:35	data_8	train_10	Freight train, (mostly empty)	
18:46	data_8	train_11	Freight train (mixed weight)	
18:52	data_8	train_12	Freight train, 2 locomotives + 16 wagons (empty)	to Ljusdal
19:22	data_8	train_13	Freight train, loco + wagons (mostly empty)	
19:43	data_8	train_14	Freight train? Rc + 6 empty wagons	
20:55	data_8	train_15	Freight train, 2*Rc + wagons (mostly empty)	to Ånge

Paper I.

Attenuating resonant behaviour of a tied arch railway bridge using increased hanger damping

Andreas Andersson, Raid Karoumi, Alan O'Connor

Taylor & Francis, IABMAS 2012, Stresa, Italy, July 8-12 2012.
(*Conference paper, published*)

Bridge Maintenance, Safety, Management, Resilience and Sustainability – Biondini & Frangopol (Eds)

Attenuating resonant behavior of a tied arch railway bridge using increased hanger damping

A. Andersson & R. Karoumi
Division of Structural Engineering and Bridges, KTH Royal Institute of Technology

ABSTRACT: In this paper, dynamic analyses and field measurements of a tied arch railway bridge is presented. Excessive vibrations of the hangers were obtained, caused by resonance during train passages. The resulting increase of the stress level and number of stress cycles were shown to decrease the fatigue service life significantly. The most critical section is a threaded turnbuckle connection of the hangers. Due to low damping of the hangers, more than 50 % of the cumulative fatigue damage was related to free vibrations after train passage. Passive dampers were installed to attenuate the vibrations by means of increased damping. A combination of field measurements and numerical models are used to investigate the behavior of the bridge and the impact of increased hanger damping.

1 INTRODUCTION

There is a constant demand on the railway authorities to increase both the allowable axle loads and the allowable speed on existing railway lines. An increased utilization of the bridges can sometimes be justified based on refined capacity assessments and field measurements.

In design of railway bridges, dynamic effects are most often accounted for by dynamic amplification factors (DAF) of the static response. This does not account for resonant behavior. Only for bridges on high-speed lines (defined as an allowable speed more than 200 km/h), separate dynamic calculations are required.

A refined dynamic assessment of a tied arch railway bridge is presented. The project was initiated since excessive vibrations of the hangers were detected. Based on field measurements and numerical simulations, the remaining fatigue service life of the hangers was estimated, further presented in Andersson & Malm (2004) and Malm & Andersson (2006). An existing stabilizing system was later replaced with passive dampers, mounted on the longer hangers, Hortmanns & Schäfer (2005) and Hortmanns (2005).

In this paper, some of the previous field measurements have been reanalyzed and used for updating a simplified 2D finite element model of the bridge. Also, the effect of increased damping measured by Hortmanns & Schäfer (2005) after installation of the passive dampers are analyzed.

2 THE BRIDGE

The bridge was built in 1959 and is designed as a single span tied arch railway bridge. A photo of the bridge is presented in Figure 1. The mid-support is a remain from the previous bridge and is not utilized.

Figure 1. View of the Ljungan railway bridge.

The deck is designed as an unballasted steel grillage consisting of main beams, cross beams and stringers. The wooden sleepers are supported directly by the stringers. A cross-section of the deck is illustrated in Figure 2. The distance between the cross-beams is 3.75 m, same as for the hangers. The hangers consists of solid steel rods with a diameter of 80 mm at the threaded section. The arch has a circular shape with a radius of 31.9 m and a height of 8.9 m, measured from the top of the main beam to the arch centre line. More details regarding the geometry can be found in Andersson & Malm (2004).

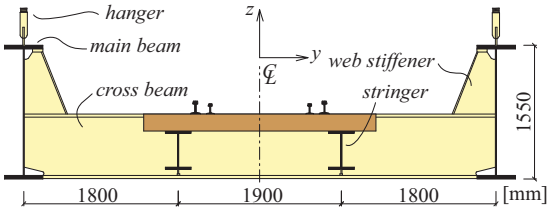

Figure 2. Cross-section of the grillage deck.

Already in the early 1980's, excessive vibration of the hangers was noticed. A system of diagonal RHS-beams (*Rectangular Hollow Section*) was installed to stabilize the hangers. These beams can be seen in Figure 1. In 2005, the RHS-beams were replaced with passive dampers on hangers no. 3 – 9 on each side of the bridge. The hangers are numbered 1 to 11 where 1 is the shortest and 6 the longest.

3 FIELD MEASUREMENTS

3.1 *Instrumentation*

Field measurements were carried out in June 2003, comprising 16 strain gauges and 12 accelerometers, mounted on hanger 2 to 5. During the measurements, the stabilizing system of RHS-beams was removed. The position of the gauges and details of the hangers are presented in Figure 3. The total length L_h and the position of the accelerometers L_a are given in Table 1. At each position, three accelerometers are mounted together, measuring in *xyz*-directions.

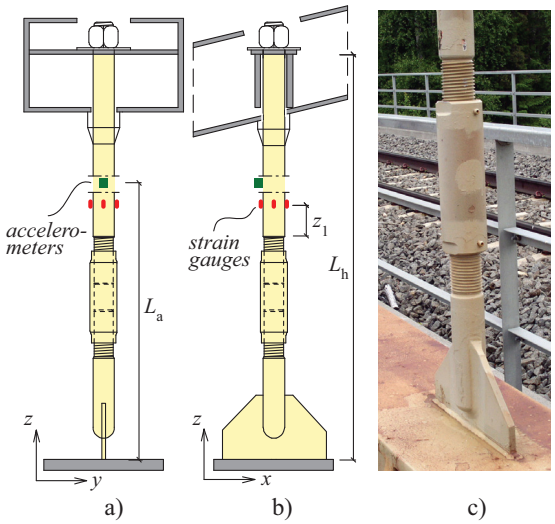

Figure 3. Detail of the hangers, a) section across the bridge, b) section along the bridge, c) detail of the turn buckle connection.

Table 1. Length of the hangers L_h (according to original drawings) and position of accelerometers L_a, rounded to 5 cm.

Hanger:	1	2	3	4	5	6
L_h (m):	1.30	3.54	5.20	6.30	6.95	7.15
L_a (m):	-	1.55	1.90	2.15	2.30	-

Four strain gauges were instrumented at each of the studied hangers, positioned z_1 = 100 mm above the threaded section and spaced 90° apart along the perimeter of the hanger. The notation of the strain gauges follows Figure 4. Gauge e1, e5, e9, e13 are closest to the track.

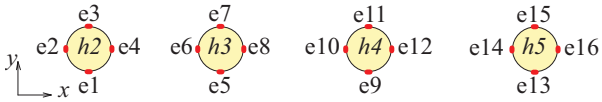

Figure 4. Numbering of the strain gauges on hanger 2 to 5.

Two different data acquisition systems were used, *HBM MGCPlus* for the strain gauges and a *Sony PC216AX* with an *UNO-MWL006* amplifier for the accelerometers. The sampling frequency was set to 2 kHz for the strain gauges and 6 kHz for the accelerometers. To avoid overloading, an analogue 20 Hz low-pass filter (*PCP-848*) was used for the accelerometers. To synchronize the signals from the two systems, strain gauge no. 1, 2, 15, 16 were connected to both systems.

A total of six train passages were recorded, four freight trains and two passenger trains. In addition, free vibration tests were performed to determine the natural frequencies of the hangers without disturbance from passing trains.

3.2 *Natural frequencies and damping*

The natural frequencies and damping ratios of the hangers were estimated based on free vibration tests. Each hanger was excited by a swift knock in each direction. Based on a Maximum Likelihood estimate of the free decay of motion, the results in Table 2 Table 3 are obtained. Similar measurements reported by Hortmanns & Schäfer (2005) generally show very good agreement. The average difference in estimated frequency was about 0.1 %. The difference of individual damping ratio scatters significantly, but the average for all hangers is 0.2 %, both from Hortmanns & Schäfer (2005) and in Table 3.

Table 2. Estimated natural frequencies, based on free vibration measurements.

Hanger	$f_{1,x}$ (Hz)	$f_{2,x}$ (Hz)	$f_{1,y}$ (Hz)	$f_{2,y}$ (Hz)
2	16.0	44.9	10.9	34.0
3	7.9	23.1	6.1	18.9
4	7.2	19.2	6.0	16.5
5	4.3	13.5	3.6	11.4

Table 3. Estimated damping ratios, based on free vibration measurements.

Hanger	$\zeta_{1,x}$ (%)	$\zeta_{2,x}$ (%)	$\zeta_{1,y}$ (%)	$\zeta_{2,y}$ (%)
2	0.33	0.18	0.14	0.46
3	0.16	0.22	0.42	0.16
4	0.09	0.08	0.14	0.19
5	0.15	0.05	0.30	0.24

3.3 *Plane stress components*

The total stress in the hangers is due to the combination of axial forces and bending moments in two directions. Since four strain gauges are available at each section, the system is over-determined. This facilitates including the torsion component, resulting in Equation (1). The torsion is however found to give small contribution in stresses and mainly serves as indication that no torsion is present. The stresses due to axial force and bending moments are similar for either including torsion or using any given combination of three strain gauges.

$$\sigma = \frac{N}{A} \pm \frac{M_x}{W_x} \pm \frac{M_y}{W_y} \pm \frac{T}{J} r \tag{1}$$

During train passage, resonant behavior of several hangers was obtained. Due to very low damping, this results in significant increase of both stress range and number of stress cycles. The stress components of hanger 5 during passage of a freight train are presented in Figure 5. The train consists of one locomotive and 19 wagons, transporting steel ingot.

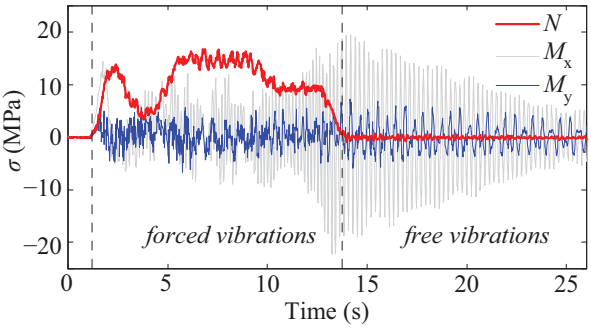

Figure 5. Stress components in hanger 5 during passage of a freight train.

During the train passage, the main stress contribution is due to the axial force. For the following free vibrations however, bending stresses longitudinal to the track is of the same amplitude. The hanger is mainly oscillating with its first natural frequency at 4.3 Hz, causing a significant amount of stress cycles.

3.4 *Cumulative fatigue damage*

The most fatigue critical part of the hangers is the threaded section at the turn buckle, illustrated in Figure 3. According to Eurocode 3 (CEN, 2005), threaded bolts are assigned a detail category $C = 50$. This corresponds to a fatigue service life of 2 million stress cycles at a constant stress range of 50 MPa. Due to size effects, a correction factor k_s shall be accounted for, if the diameter is larger than 30 mm. for the present case $k_s = 0.8$, resulting in $C = 40$. Similar results are obtained using the Swedish design code BSK 07, Boverket (2007).

Palmgren-Miners cumulative damage rule (Palmgren, 1924 and Miner, 1945) is used according to Equation (2), where n_{Ei} is the number of stress cycles with a stress range $\Delta\sigma_{Ri}$ and N_{Ri} is the maximum number of stress cycles until failure for a constant stress range. The fatigue strength is governed by Equation (3). The stress range shall be multiplied with a safety factor $\gamma_{Mf} = 1.35$. The effective area in the threaded section is 74 mm compared to the gross diameter of 80 mm at the position of the strain gauges. Since most of the fatigue-induced stresses are due to bending, the measured strains are multiplied with the factor $(80/74)^3 = 1.26$.

$$D_d = \sum_{i=1}^{n} \frac{n_{Ei}}{N_{Ri}} \tag{2}$$

$$\begin{aligned} \Delta\sigma_R^m N_R &= \Delta\sigma_C^m 2\times10^6, \quad m = 3, \ N \le 5\times10^6 \\ \Delta\sigma_R^m N_R &= \Delta\sigma_C^m 5\times10^6, \quad m = 5, \ 5\times10^6 \le N \le 10^8 \end{aligned} \tag{3}$$

The stress collective is calculated using a Rainflow counting algorithm according to Rychlik (1987) and the measured response of the freight train in Figure 5. The theoretical fatigue service life is obtained when $D_d = 1$ and the corresponding number of train passages is presented in Table 4. Two cases are studied, $\gamma_{Mf} = 1.35$ and $\gamma_{Mf} = 1.0$. The fatigue service life is proportional to γ_{Mf}^m, for the present case corresponding to an average reduction factor of 3. A parametric study of the influence of the safety factor on the fatigue service life is shown in Leander et al. (2010). Assuming 2 similar trains per day, results in a total service life of merely 20 years for hanger 5, provided that no other trains contribute to fatigue. If instead using $\gamma_{Mf} = 1.0$, the corresponding service life would be 50 years. The fatigue damage due to free vibrations was negligible for hanger 2 and 3. For hanger 4 and 5 however, it constituted 10 % and 60 % respectively. No knowledge of hanger 6 is available since it was not instrumented.

Table 4. Number of train passages until $D_d = 1$.

Hanger:	$\gamma_{Mf} = 1.35$	$\gamma_{Mf} = 1.0$
2	281 400	831 300
3	113 000	402 200
4	33 400	105 900
5	13 400	36 300

3.5 *Accelerations and displacements*

To attenuate the vibrations of mainly the longer hangers, a system of passive dampers was installed in 2005, Hortmanns (2005). One of the design conditions for the dampers was the amplitude of displacement of the hangers.

The displacement of the hangers was estimated based on the measured accelerations, positioned according to Table 1, at about $0.4L_h$. A Newmark time

integration routine according to Equation (4) was adopted, using $\beta = 0.25$ and $\gamma = 0.5$ according to the trapezoidal rule. The measured acceleration had previously been subjected to an analogue low-pass filter at 20 Hz. To attenuate deviating trends due to time integration, a digital high-pass filter at 0.5 Hz was used. Since the lowest measured natural frequency of the hangers was 3.6 Hz this does not influence the resonant behaviour. Global displacements of the bridge during train passage may however not be obtained.

$$\begin{aligned} \dot{u}_i &= \dot{u}_{i-1} + (1-\gamma)\Delta t \ddot{u}_{i-1} + \gamma \Delta t \ddot{u}_i, \\ u_i &= u_{i-1} + \Delta t \dot{u}_{i-1} + (0.5-\beta)\Delta t^2 \ddot{u}_{i-1} + \beta \Delta t^2 \ddot{u}_i \end{aligned} \quad (4)$$

An estimation of the longitudinal displacement of hanger 5 due to the previous freight train passage is presented in Figure 6. Except of a few high oscillations during the entrance of the train on the bridge, the peak displacement is about 3.5 mm. For all other instrumented hangers, the peak displacement is estimated during the initial free vibration phase, presented in Table 5.

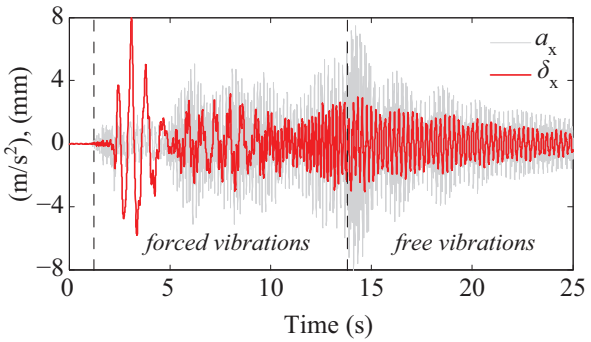

Figure 6. Acceleration and estimated displacements of hanger 5 during passage of a freight train.

Table 5. Estimated peak displacements of the hangers during passage of a freight train.

Hanger	δ_x (mm)	δ_y (mm)
2	1.6	2.9
3	2.4	4.4
4	3.5	3.6
5	8.0	2.9

4 FINITE ELEMENT ANALYSIS

4.1 *2D-model*

The dynamic behavior of the bridge has been simulated using FE-models. A detailed 3D model has been presented in Andersson & Malm (2004) and Malm & Andersson (2005). In the following, a simplified 2D model is instead studied, only accounting for the longitudinal motions.

The FE-model is created using the commercial FE-package SOLVIA03. Half of the bridge is included, comprising one arch, one main beam, one stringer and all hangers on one side. All components are modeled using Euler-Bernoulli beam elements, except the cross beams that are modeled as vertical springs. The spring stiffness is calculated to produce the same vertical displacement as a simply supported beam subjected to two point loads. The model is illustrated in Figure 7. The detailed connections of the model are shown in Figure 8. All elements are modeled along its centre line. To obtain the correct length of the hangers, the connection with the main beam is extended using a rigid link, and is considered as fully clamped. The connection with the arch is however considered hinged. This is accomplished by releasing the rotational degree of freedom belonging to the end node of each hanger.

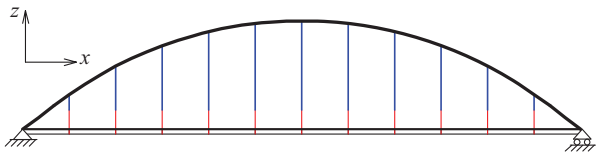

Figure 7. Elevation of the 2D FE-model.

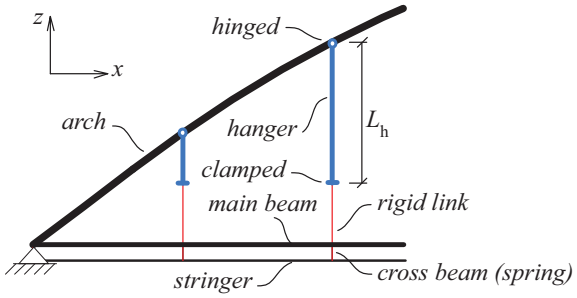

Figure 8. Details of the FE-model.

4.2 *Natural frequencies*

An Eigen-value analysis is performed to calculate the frequencies of the structure. The permanent load is applied prior to the Eigen-value analysis, to account for the axial stress in of the hangers. The results are presented in Table 6.

Table 6. Natural frequencies of the hangers, predicted by the 2D FE-model and a comparison with measured results.

	FEM		FEM / measured	
Hanger	$f_{1,x}$ (Hz)	$f_{2,x}$ (Hz)	$f_{1,x}$ (-)	$f_{2,x}$ (-)
2	16.1	50.5	0.99	0.89
3	7.8	23.8	1.00	0.97
4	7.4	19.8	0.97	0.97
5	4.5	13.4	0.95	1.01
6	4.3	12.7	-	-

Initially, the frequencies for hanger 4 was f_{1x} = 5.4 Hz and f_{2x} = 16.3 Hz, in poor agreement with the measured data. If instead assuming the arch-to-hanger connection as fully clamped, the results in Table 6 was obtained. For sake of comparison, this assumption is used in further analysis. Since the hangers are relatively independent on each other, the corresponding hanger 8 is still assumed hinged.

The two lowest global modes of the bridge are illustrated in Figure 9. The global modes generally excite all hangers, especially if the arch and the main beam are out of phase.

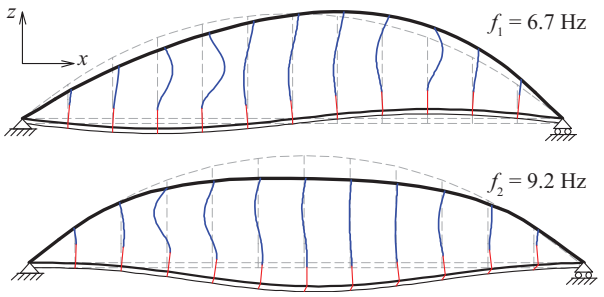

Figure 9. The two lowest global modes of vibration.

4.3 *Dynamic analysis of passing trains*

The 2D FE-model has been used for dynamic analysis of passing trains. The train is modeled as vertical point loads only, travelling along the stringer beam. Since the model only comprises half of the bridge, half of the axle load is applied. The pre-stress of the hangers due to permanent load is accounted for, as well as increased load during train passage. Hence the analysis is considered nonlinear. For this reason, a direct time integration scheme is employed instead of modal superposition. One back draw of the direct time integration is that constant modal damping can not be used. Instead, a frequency dependent material damping according to Equation (5) is used, often denoted as Rayleigh damping. It consists of two components, α for mass proportional damping and β for stiffness proportional damping, Equation (6). For the present case, a critical damping ratio ζ = 0.2% is used, fitted by the frequencies f_n = 4 Hz and f_m = 20 Hz.

$$\begin{Bmatrix}\alpha\\ \beta\end{Bmatrix} = \frac{2\zeta}{\omega_n + \omega_m}\begin{Bmatrix}\omega_n\omega_m\\ 1\end{Bmatrix} \tag{5}$$

$$\mathbf{c} = \alpha\mathbf{m} + \beta\mathbf{k} \tag{6}$$

The train set is composed of one locomotive and 19 wagons. Both the locomotive and the wagons consists of two bogies with two axels in each bogie. For the locomotive (Rc4), the axle distance is 2.7 m, the bogie distance 7.7 m, the total length 15.5 m and the load 195 kN/axle. Standardized freight train wagons are assumed according to load class D2. This corresponds to an axle distance 1.8 m, bogie distance 9.2 m, length 14.0 m and the load 225 kN/axle. The train speed is varied between 60 to 140 km/h in increments of 10 km/h. Time history data is extracted in positions corresponding to the field measurements.

The most pronounced resonance is obtained at 110 km/h. In Figure 10, the longitudinal displacement of hanger 5 is presented. The results from the simplified 2D FE-model agrees reasonably well with the measurements, considering that the train loading is not readily known and that the time integration of measured acceleration may be uncertain.

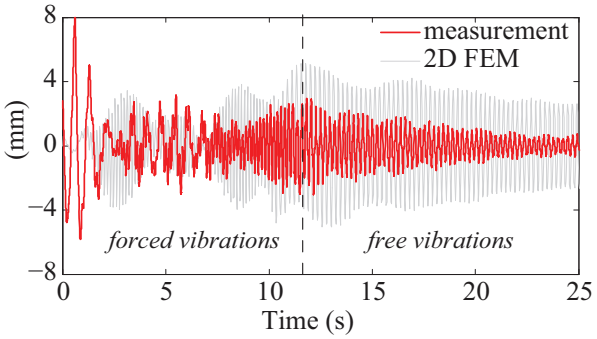

Figure 10. Displacement of hanger 5, comparison of integration of measured acceleration and simulation results from the 2D FE-model.

In Figure 11, the stress components of hanger 6 are presented for the same train passage. Resonance of the hanger causes excessive bending stresses. In the simulation, all wagons are equally loaded and have the same axle configuration. Comparing the axial stress component of Figure 5, the train from the field measurement was likely unevenly loaded.

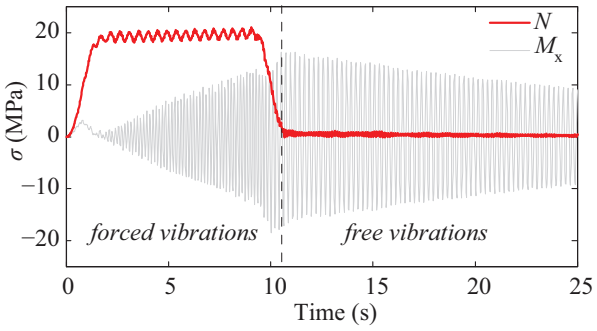

Figure 11. Stress components in hanger 6 during passage of a freight train (type D2 with 19 wagons).

4.4 *Increased hanger damping*

To attenuate the resonant behavior and resulting bending stresses of the hangers, passive dampers was installed on hanger 3 to 9 on each side of the bridge. The installation of the dampers and additional measurements is reported in Hortmanns (2005). The dampers consists of cylindrical shells,

each containing four pendulums partly surrounded by a silicone oil. The diameter of the dampers is 310 mm and the height 350 mm. Based on free vibration tests, the damping ratio was estimated for each hanger. In average, the damping in the longitudinal direction ranged between 1.8 - 6.4 %, with an average of 3.6 %.

The previous 2D FE-model has been updated to account for the increased hanger damping. Since the resulting damping is available, an increased Rayleigh damping using $\zeta = 3.5$ % for all hangers is assumed. The additional mass of the dampers neglected.

In Figure 12, the stress components for hanger 6 calculated with the 2D FE-model is presented, including the updated damping. The bending stresses is attenuated significantly due to the increased damping.

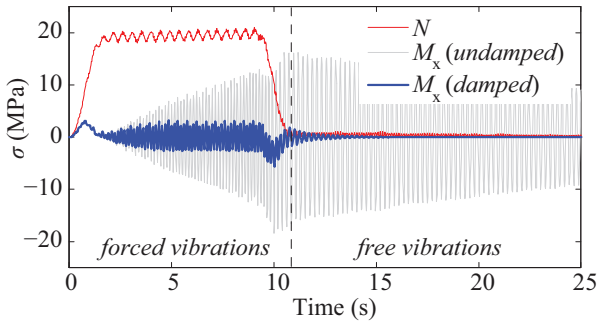

Figure 12. Stress components in hanger 6 during passage of a freight train (type D2 with 19 wagons), influence of increased hanger damping.

5 CONCLUSION

In this paper, the dynamic behavior of a tied arch railway bridge has been analyzed by means of data from field measurements and a 2D FE-model. The measurements showed that the hangers had very low damping, in average 0.2 %. This can be compared to CEN (2003), recommending 0.5 % damping for steel bridges. Resonant behavior was measured, causing excessive increase in bending stresses. Due to the low damping, both the stress magnitude and number of stress cycles affected the fatigue service life. For one hanger, more than 50 % of the fatigue service life was found related to free vibrations.

A 2D FE-model of the bridge was used to compare measured frequencies, displacements and stresses of the hangers. Assuming the hangers to be fully clamped at the connection with the main beam and hinged at the connection with the arch generally produced the best agreement with measured data. For one hanger however, better agreement was found if assuming the upper connection as fixed.

The displacements and stresses estimated by the FE-model was generally in good agreement with the measured data, considering that the train configuration from the field measurements was not known in detail.

To attenuate the resonant behavior, passive dampers were installed in 2005. Based on free vibration tests, the damping ratio after installation was estimated, reported in Hortmanns (2005). The resulting damping was increased to about 2 – 6 %. The FE-model was updated using an average damping of 3.5 %. The result from the model showed that the resonant behaviour was attenuated significantly, especially for the bending stresses.

ACKNOWLEDGEMENTS

The long Life Bridges project is a Marie Curie Industry-Academia Partnerships and Pathways project and is funded by the European Commission 7th Framework Programme (IAPP-GA-2011-286276).

REFERENCES

Andersson, A., Malm R. (2004). *Measurement Evaluation and FEM Simulation of Bridge Dynamics. MSc. Thesis, KTH Royal Institute of Technology*.

Boverket, 2007. Swedish handbook for design of steel structures, BSK 07. *In Swedish*.

CEN (2003). Eurocode 1: Actions on structures – Part 2: Traffic loads on bridge. *EN 1991-2:2003*.

CEN (2005). Eurocode 3: Design of steel structures – Part 1-9: Fatigue. *EN 1993-1-9:2005*.

Hortmanns, M., Schäfer, N. (2005). Ljungan Bridge, Ånge Sweden – Full Scale Measurements. *Tech. report, Prof. Sedlacek & Partner (unpublished)*.

Hortmanns, M. (2005). Ljungan Bridge, Ånge Sweden – Design of dampers for the hangers 3 to 6. *Tech. report, Prof. Sedlacek & Partner (unpublished)*.

Leander, J., Andersson, A., Karoumi, R. (2010). Monitoring and enhanced fatigue evaluation of a steel railway bridge. *Engineering Structures 32, pp. 854-863*.

Malm, R., Andersson, A. (2006). Field testing and simulation of dynamic properties of a tied arch railway bridge. *Engineering Structures 28, pp. 143-152*.

Miner, M. A. (1945). Cumulative damage in fatigue. *Journal of Applied Mechanics, 23(1)*.

Palmgren, A. (1924). Die Lebensdauer von Kugellagern. *VDI Zeitschrift, 68(14)*.

Rychlik, I. (1987). A new definition of the rainflow cycle counting method. *International Journal of Fatigue, 9(2)*.

Paper II.

Semi active damping systems for railway bridges

Andreas Andersson, Raid Karoumi, Alan O'Connor

BCRI 2012, Dublin, Ireland, September 6-7 2012.
(*Conference paper, published*)

Semi-active damping systems for railway bridges

Andreas Andersson[1,2], Raid Karoumi[2], Alan O'Connor[1]
[1]Roughan & O'Donovan Innovative Solutions (RODIS), Arena House, Arena Road, Sandyford, Dublin 18, Ireland
[2]Royal Institute of Technology (KTH), Brinellvägen 23, 100 44 Stockholm, Sweden
email: Andreas.Andersson@rod.ie, Raid.Karoumi@byv.kth.se, Alan.OConnor@rod.ie

ABSTRACT: In this paper, a semi-active control system for vibration mitigation of railway bridges is presented. The real time frequency response is estimated using a short-time Fourier transform, employing curve fitting to relevant peaks for increased accuracy. A control algorithm developed in MATLAB® is linked to a commercial FE-software, facilitating application on arbitrary structures. A numerical study of an existing tied arch railway bridge is presented. From earlier field measurements and numerical analysis, resonance of several hangers during train passage was observed. This was shown to significantly reduce the fatigue service life of the hangers and for the most critical section about 50% of the cumulative damage was related to free vibrations. A system of passive dampers was later installed and the increase in resulting damping was measured. Within the present study, the previous results are reanalysed and compared with a semi-active approach. The natural frequencies of the hangers vary as a result of the variation in axial force. A semi-active control system has the potential to improve the vibration response of the structure when compared to the installed passive system.

KEY WORDS: Bridge dynamics; railway bridge; semi-active damping; finite element method.

1 INTRODUCTION

There is a constant demand on the railway authorities to increase both the allowable axle loads and the allowable speed on existing railway lines. An increased utilization of bridges can sometimes be justified based on refined capacity assessments and field measurements.

In design of railway bridges, dynamic effects are most often accounted for by dynamic amplification factors (DAF) of the static response. This does not account for resonant behaviour and for bridges on high-speed lines separate dynamic calculations are required.

A refined dynamic assessment of a tied arch railway bridge is presented. The project was initiated since excessive vibrations of several hangers were detected. Based on field measurements and numerical simulations, the remaining fatigue service life of the hangers was estimated, as presented in [1],[7]. An existing stabilizing system was later replaced with passive dampers, mounted on the longer hangers, [5],[6].

In this paper, some of the previous field measurement have been reanalysed and employed in updating a simplified 2D finite element model of the bridge. The model is used for estimating the effect of increased damping measured by [5] after installation of the passive dampers. Further, a semi-active damping system is proposed and its potential performance is compared with the passive system, based on numerical simulations.

1.1 The Bridge

The bridge was built in 1959 and is designed as a single span tied arch railway bridge. A photo of the bridge is presented in Figure 1. The mid-support is a remnant from the previous bridge and is not utilized.

Figure 1. View of the Ljungan railway bridge.

The deck is designed as an unballasted steel grillage consisting of main beams, cross beams and stringers. Wooden sleepers are supported directly by the stringers. A cross-section of the deck is illustrated in Figure 2. The distance between the cross beams is 3.75 m, which is the same for the hangers. The hangers consists of solid steel rods with a diameter of 80 mm at the threaded section. The arch has a circular shape with a radius of 31.9 m and a height of 8.9 m, measured from the top of the main beam to the arch centre line.

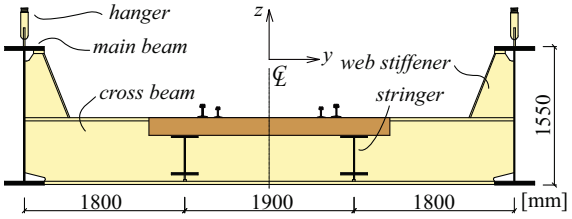

Figure 2. Cross-section of the grillage deck.

Due to excessive vibration of the hangers, a system of diagonal RHS-beams was installed in the 1980's as an attempt to stabilize the hangers. These beams can be seen in Figure 1.

2 FIELD MEASUREMENTS

2.1 *Instrumentation*

Field measurements were carried out in June 2003, comprising 16 strain gauges and 12 accelerometers, mounted on hangers 2 to 5. During the measurements, the stabilizing system of RHS-beams was removed. The position of the gauges and details of the hangers are presented in Figure 3. The total length L_h and distance L_a to the accelerometers are given by Table 1. At each position, three accelerometers are mounted together, measuring in *xyz*-directions. Also, four strain gauges are instrumented at the distance z_1 = 100 mm above the threaded section, spaced 90° apart along the perimeter of the hanger.

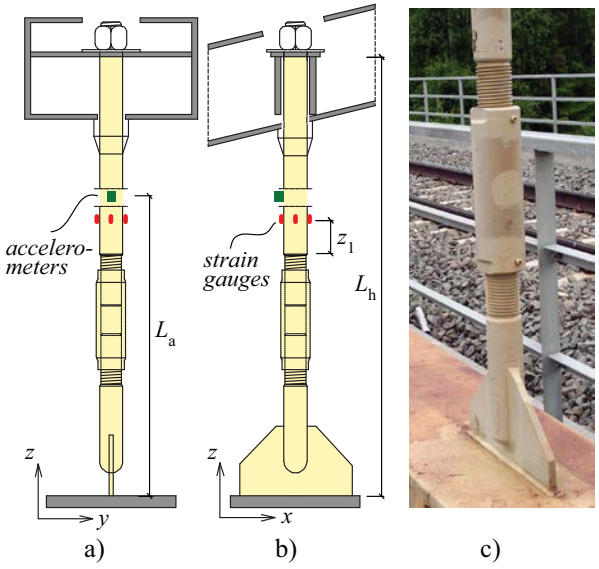

Figure 3. Detail of the hangers, a) section across the bridge, b) section along the bridge, c) photo of the turn buckle.

Table 1. Length of the hangers L_h (according to original drawings) and position of accelerometers L_a, rounded to 5 cm.

Hanger:	1	2	3	4	5	6
L_h (m):	1.30	3.54	5.20	6.30	6.95	7.15
L_a (m):	-	1.55	1.90	2.15	2.30	-

2.2 *Natural frequencies and damping*

The natural frequencies and damping ratios of the hangers were estimated based on free vibration tests. Each hanger was exited by a swift knock in each direction. Based on a Maximum Likelihood estimate of the free decay of motion, the results in Table 2 and Table 3 were obtained. The results show good agreement with similar measurements in [5].

Table 2. Estimated natural frequencies, based on free vibration measurements.

Hanger:	$f_{1,x}$ (Hz)	$f_{2,x}$ (Hz)	$f_{1,y}$ (Hz)	$f_{2,y}$ (Hz)
2	16.0	44.9	10.9	34.0
3	7.9	23.1	6.1	18.9
4	7.2	19.2	6.0	16.5
5	4.3	13.5	3.6	11.4

The average difference on estimated frequency was about 0.1%. The difference of individual damping ratio scatters significantly, but the average for all hangers is 0.2%, both from [5] and Table 3.

Table 3. Estimated damping ratios, based on free vibration measurements.

Hanger:	$\zeta_{1,x}$ (%)	$\zeta_{2,x}$ (%)	$\zeta_{1,y}$ (%)	$\zeta_{2,y}$ (%)
2	0.33	0.18	0.14	0.46
3	0.16	0.22	0.42	0.16
4	0.09	0.08	0.14	0.19
5	0.15	0.05	0.30	0.24

3 FINITE ELEMENT ANALYSIS

3.1 *2D model*

A 2D FE-model of the bridge is created using the commercial FE-software SOLVIA03. Half of the bridge is included, comprising one arch, one main beam, one stringer and all hangers on one side. All components are modelled using Euler-Bernoulli beam elements, except the cross beams that are modelled as vertical springs. The spring stiffness is calculated to produce the same vertical displacement as a simply supported beam subjected to two point loads. The model is illustrated in Figure 4. The detailed connections of the model are shown in Figure 5. All elements are modelled along their centre line. To obtain the correct length of the hangers, the connection with the main beam is extended using a rigid link, and is considered as fully clamped. The connection with the arch is however considered hinged. This is accomplished by releasing the rotational degree of freedom belonging to the end node of each hanger.

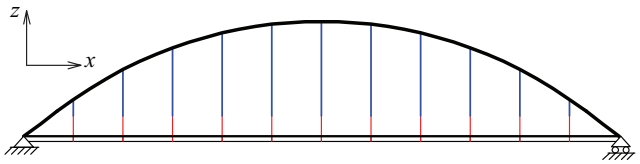

Figure 4. Elevation of the FE-model.

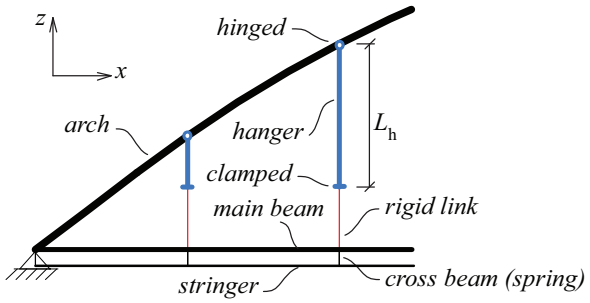

Figure 5. Details of the FE-model.

3.2 *Natural frequencies*

An Eigen-value analysis is performed to calculate the frequencies of the structure. The permanent load is applied prior to the Eigen-value analysis, to account for the axial stress in of the hangers. The results are presented in Table 4.

Table 4. Natural frequencies of the hangers, predicted by the 2D FE-model and a comparison with measured results.

	FEM		FEM / measured	
Hanger:	$f_{1,x}$ (Hz)	$f_{2,x}$ (Hz)	$f_{1,x}$ (-)	$f_{2,x}$ (-)
2	16.1	50.5	0.99	0.89
3	7.8	23.8	1.00	0.97
4	7.4	19.8	0.97	0.97
5	4.5	13.4	0.95	1.01
6	4.3	12.7	-	-

Initially, the frequencies for hanger 4 was f_{1x} = 5.4 Hz and f_{2x} = 16.3 Hz, in poor agreement with the measured data. The model was modified at this location, assuming the arch-to-hanger connection as fully clamped, with the result in Table 4.

For the sake of comparison, this assumption is used in further analysis. Since the hangers are relatively independent on each other, the corresponding hanger 8 is still assumed hinged. The two lowest global modes of the bridge are illustrated in Figure 6. The global modes generally excite all hangers, especially if the arch and the main beam are out of phase.

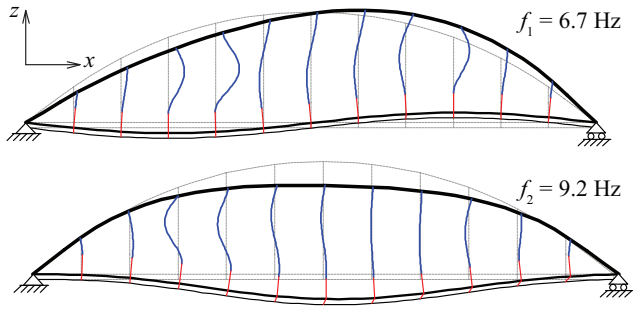

Figure 6. The two lowest global modes of vibration.

3.3 *Dynamic analysis of passing trains*

The 2D FE-model has been used for dynamic analysis of passing trains. The train is modelled as vertical point loads only, travelling along the stringer beam. Since the model only comprises half of the bridge, half of the axle load is applied. The pre-stress of the hangers due to permanent load is accounted for, as well as increased load during train passage. Hence the analysis is considered nonlinear. For this reason, a direct time integration scheme is employed instead of modal superposition. One drawback of the direct time integration is that constant modal damping can not be used. Instead, a frequency dependent material damping according to Equation (1) is used, often denoted as Rayleigh damping. It consists of two components, α for mass proportional damping and β for stiffness proportional damping, Equation (2). For the present case, a critical damping ratio ζ = 0.2% is used, fitted by the frequencies f_m = 4 Hz and f_n = 20 Hz.

$$\begin{Bmatrix}\alpha\\ \beta\end{Bmatrix} = \frac{2\zeta}{\omega_m + \omega_n}\begin{Bmatrix}\omega_m\omega_n\\ 1\end{Bmatrix} \quad (1)$$

$$\mathbf{c} = \alpha\mathbf{m} + \beta\mathbf{k} \quad (2)$$

The train set is composed of one locomotive and 19 wagons. Both the locomotive and the wagons consists of two bogies with two axels in each bogie. For the locomotive (Swedish Rc4), the axle distance is 2.7 m, the bogie distance 7.7 m, the total length 15.5 m and the load 195 kN/axle. Standardized freight train wagons are assumed according to load class D2. This corresponds to an axle distance 1.8 m, bogie distance 9.2 m, length 14.0 m and the load 225 kN/axle. The train speed is varied between 60 to 140 km/h in increments of 10 km/h. Time history data is extracted in positions corresponding to the field measurements.

3.4 *Increased hanger damping*

To attenuate the resonant behaviour and resulting bending stresses of the hangers, passive dampers were installed on hanger 3 to 9 on each side of the bridge. The installation of the dampers and additional measurements is reported in [6]. The dampers consists of cylindrical shells, each containing four pendulums partly surrounded by a silicone oil. The diameter of the dampers is 310 mm and the height 350 mm. Based on free vibration tests, the damping ratio was estimated for each hanger. In average, the damping in the longitudinal direction ranged between 1.8 – 6.4%, with an average of 3.6%. The 2D FE-model has been updated to account for the increased hanger damping. Since the resulting damping is available, an increased Rayleigh damping using ζ = 3.5% for all hangers is assumed. The additional mass of the dampers is neglected.

3.5 *Influence of axial force*

It may be noted that all the estimates presented above of natural frequencies and damping is based on free vibrations of the unloaded bridge. During train passage, increased tensile force in the hangers will result in increased frequency. For an Euler-Bernoulli beam, the relation between natural frequency f_n, flexural rigidity EI and axial force N follows Equation (3). For the bi-pinned case, $\mu_n = n\pi$. For the pinned-clamped case, $\mu_1 \approx 1.25\pi$ is an approximation for the first mode of vibration. Based on the 2D FE-model, the axial force in hanger 5 is estimated as 20 kN due to permanent load and additional 120 kN due to vertical train load type D2. This results in an increase in natural frequency from 4.5 Hz to about 7 Hz using Equation (3) [4].

$$f_n = \frac{\mu_n^2}{2\pi}\sqrt{\frac{EI}{mL^4} + \frac{N}{mL^2\mu_n^2}} \quad (3)$$

The existing passive damping system is tuned based on free vibrations and its properties during train passage are not readily known. Approximating this behaviour with an increased material damping may overestimate its damping characteristics outside of the tuned frequency range.

4 PASSIVE AND SEMI-ACTIVE CONTROL

In the field of external damping for dynamic mitigation, the tuned mass damper (TMD) is one of the most common systems. In its simplest form, it consists of a sprung mass tuned to the frequency of the structure it is mounted on. Regarding the structure as a single degree of freedom (SDOF) system, the combined response with the TMD can be regarded as a 2DOF system, as illustrated in Figure 7.

A passive TMD has fixed properties that can not be altered. It often has a narrow efficient bandwidth and may be highly inefficient outside that range, e.g. due to changed frequency of either the structure, the forced vibrations or the TMD itself. This may partially be overcome using a semi-active system, that has the ability to change in either stiffness or viscous damping due to a control input, usually voltage. Analyses of a semi-active tuned mass damper (SATMD) is performed based on a variable stiffness $k_d(\theta)$. The control input θ is assumed proportional to the stiffness k_d. Damping is introduced to the systems by dashpots c and c_d with constant values.

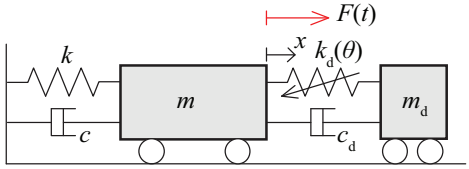

Figure 7. 2DOF model of a TMD/SATMD.

The success in minimizing the dynamic response of the main structure depends on the choice of objective function. In the present study, the stiffness is tuned to the frequency of highest energy.

4.1 Simple TMD model

The potential of dynamic mitigation of hanger 5 is studied for both a passive TMD and semi-active SATMD. Based on the natural frequencies and displacement according to Equation (4), the modal mass and stiffness is found according to Equation (5). A harmonic load according to Equation (6) is used. The steady state response can then be expressed according to Equation (7) [3].

$$\omega_{SDOF} = \sqrt{\frac{k}{m}},\ \omega_{beam} = \sqrt{\frac{EI}{m_{beam}L^4}},\ \delta_{beam} = \frac{FL^3}{48EI} \tag{4}$$

$$m = \frac{48m_{beam}L}{\pi^4},\ k = m\left(2\pi f_1\right)^2,\ c = 2\zeta\sqrt{k\cdot m} \tag{5}$$

$$F(t) = F_0\sin\left(\omega t\right),\ F_0 = kx_{static} \tag{6}$$

$$R_d = \frac{1}{\sqrt{\left[1-\left(\frac{\omega}{\omega_n}\right)^2\right]^2+\left[2\zeta\left(\frac{\omega}{\omega_n}\right)\right]^2}} \approx \frac{1}{2\zeta},\ \zeta < 0.1 \tag{7}$$

For hanger 5 the modal mass is m = 135 kg. Further, using f_1 = 4.3 Hz and ζ = 0.15% results in k = 100 kN/m and c = 11 Ns/m. Due to the low damping, the dynamic amplification factor at resonance is about 300 times the static response. From field measurements, the magnitude of dynamic displacement was estimated as 5 mm, based on integrating the acceleration. The duration of the train passage was only 10 s, thus the time required to reach resonance is more than one minute. To obtain a dynamic displacement of 5 mm after 10 s, a harmonic load with F_0 = 4.5 N is required. At steady state, this corresponds to a displacement of about 15 mm.

The optimal damped mass m_d is estimated based on a univariable analysis of the steady state response. Results for different damping ratios are presented in Figure 8. In further analysis, m_d = 1 kg is used, resulting in k_d = 0.6 kN/m.

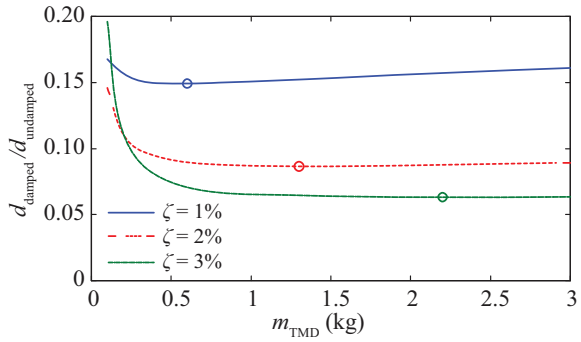

Figure 8. Influence of the TMD mass and damping ratio on the dynamic amplification of the displacement, circles denotes maximum vibration mitigation.

The steady state response is shown in Figure 9. Introducing the TMD attenuates the natural frequency of the structure but introduces two new frequencies, governed by the 2DOF system. For no additional damping, the new peaks are of similar magnitude to the case without the TMD. Due to the low existing damping of the present structure, even very low additional damping of the TMD attenuates the peaks significantly. However, the system is sensitive to mismatch in frequency and a TMD with 5% detuned frequency shows a significant disimprovement.

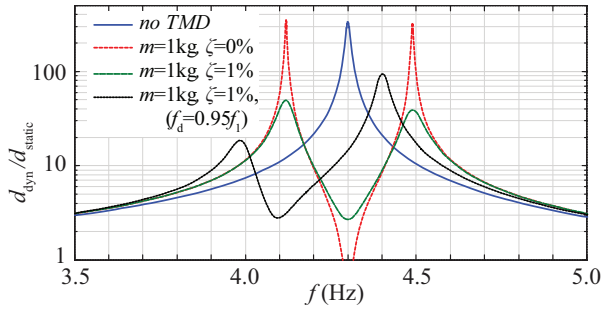

Figure 9. Steady state response for the passive TMD model.

4.2 Simple SATMD model

A simple semi-active control algorithm is developed where the frequency of the TMD is controlled by means of a variable stiffness $k_d(\theta)$. The algorithm is programmed in MATLAB® and uses the solver of the same FE-software as the bridge has been modelled in. The variable stiffness is modelled as a truss element with temperature dependent stiffness properties. Applying a stationary variable temperature load facilitates direct control of the stiffness in incremental dynamic analyses.

The value of the stiffness is determined based on estimates of the governing frequency of the system at the present time. This is accomplished by studying a short part of the signal with duration Δt prior to present time. The frequency content of the short time signal may be estimated using either a Short Time Fourier Transform (STFT) or Wavelet Transform (WT). In the current study, the STFT method is used. The time signal is multiplied with a window function before performing the Fast Fourier Transform available in MATLAB®. Since the frequency resolution is proportional to the time duration, poor estimates are obtained for small values of Δt. This may partially be improved either by zero-padding the signal or applying a curve-fit of the dominant frequency peak.

Recalling Equation (7), the shape of the steady state response is recognized as a 4th order polynomial. This has shown to be successful in estimating frequencies of known signals. Increasing Δt results in less rapid estimates of changing frequencies but is more successful in identifying close modes. The rate of finding changes in frequency can partially be improved by overlapping the time signal. This is accomplished by forwarding the analysis by an increment $t_{incr} < \Delta t$ and analysing the previous Δt of time.

The developed SATMD is tested on the same model as the passive TMD. The influence of changing the initial TMD frequency f_d and forced vibration frequency f_F in comparison with the natural frequency f_1 is studied according to Table 5.

Table 5. Studied configurations of frequencies.

Model:	f_1 (Hz)	f_d (Hz)	f_F (Hz)
a)	4.3	f_1	f_1
b)	4.3	f_1	$0.95f_1$
c)	4.3	$0.95f_1$	f_1
d)	4.3	$0.95f_1$	$0.95f_1$

Tuning the SATMD to the frequency of highest energy may cause it to be detuned if either of the resulting frequencies of the 2DOF system is higher than f_1. This may partially be overcome by choosing a suitable time increment. For the current study, using $\Delta t = t_{incr} = 4$ s was found to give reliable results. Further, all analyses are based on $m_d = 1$ kg and $\zeta_d = 1\%$. The forced vibration has a duration of 10 s.

A summary of peak responses from the different models are presented in Table 6. For the SDOF-model without TMD, a peak displacement of ~5 mm and acceleration of ~3.6 m/s^2 is obtained. Using a passive TMD reduces the responses by a factor ~10. This extreme attenuation is a result of the low existing damping of the structure. Similar results are obtained with the SATMD. Shifting the load frequency by 5% according to model b), the response of the passive TMD increases by a factor 3 while the SATMD remains relatively unchanged. It is noted that the passive TMD shows even higher response than the SDOF-model for the same load. Shifting the TMD frequency by 5% according to model c) results in an increase by a factor ~2 using the passive TMD and about 40% using the SATMD. A potential improvement of the SATMD may be possible by changing either the incremental time or the objective function. In model d), both the load and the TMD are detuned 5% compared to the structure, hence the TMD is perfectly tuned to the load instead of the structure. For this case, the SATMD is not working optimally, likely due to same reasons as for model c).

Table 6. Summary of peak responses of the primary mass from the 2DOF-model.

	Displacement (mm)			Acceleration (m/s^2)		
Model:	SDOF	TMD	SATMD	SDOF	TMD	SATMD
a)	4.98	0.53	0.53	3.64	0.39	0.39
b)	0.88	1.50	0.48	0.61	1.00	0.34
c)	4.98	1.13	0.75	3.64	0.84	0.55
d)	0.88	0.48	0.97	0.61	0.33	0.68

4.3 *TMD and SATMD on the 2D bridge model*

The SATMD algorithm is implemented on the 2D-model of the bridge previously presented in Figure 4. From the model without external damping, resonance of hanger 5 was found at 90 km/h for train load model D2. A comparison of the measured response and the simple 2D-model is presented in Figure 10, for the case of no external damping system. The displacement is obtained from time integration of the measured acceleration, introducing some uncertainties. During integration, a high-pass filter is applied and only the relative motion of the hanger is obtained. For comparison, the same filtering is performed on the displacements predicted by the FE-model. The FE-model generally shows larger response, likely caused by being closer to resonance and subjected to a passing train of equal load and axle distance. Further, no motion in the transverse direction is possible.

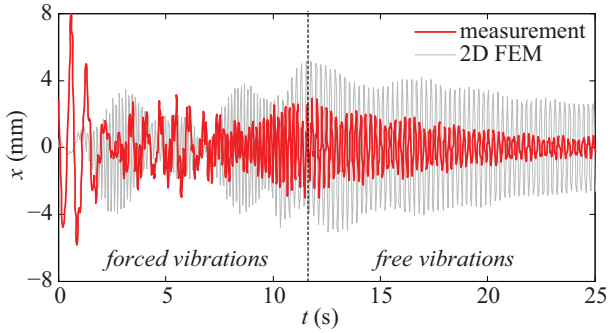

Figure 10. Displacement of hanger 5, comparison of measured response (time integrated from acceleration) and 2D FE-model without external damping.

The SATMD on the bridge model is detailed in Figure 11, positioned at the midpoint of hanger 5. The variable spring stiffness is modelled similar to the previously presented 2DOF model. The damped mass is lumped at two nodes, connected with a rigid link. Both masses are constrained in the vertical direction to follow the motion of the connecting node of the hanger. In further analysis, $m_d = 1$ kg and $\zeta = 3.5\%$ is used. The time increment $\Delta t = t_{incr} = 1$ s was found to give reliable results. The same model is also used for analysis of a passive TMD, by setting a constant damper stiffness. Both the TMD and the SATMD are initially tuned to the first mode of vibrations, $f_1 = 4.5$ Hz.

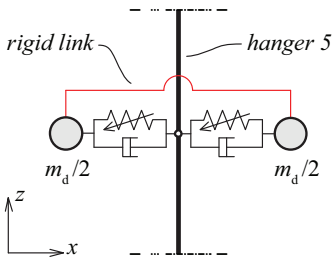

Figure 11. Detail of the SATMD on hanger 5.

Figure 12 presents the time history for displacement of hanger 5. The TMD is found efficient in attenuating the free vibrations, but show little reduction during forced vibrations. The SATMD on the other hand successfully attenuates both the forced and free vibrations.

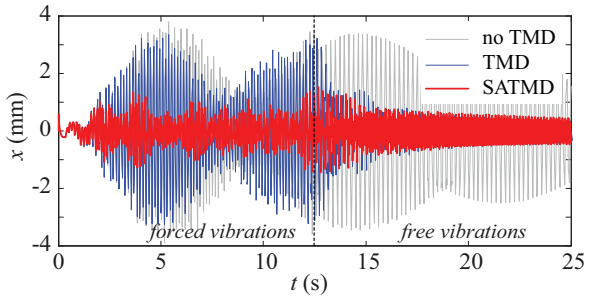

Figure 12. Displacements of hanger 5 predicted by the FE-model during train passage.

The difference of the TMD and the SATMD is further illustrated by studying the frequency content in Figure 13. The unloaded and loaded natural frequency is found at 4.5 Hz and 6.9 Hz respectively (4.3 Hz and 6.3 Hz from the measurements). Without external damping, both peaks show high energy content, as a result of the high magnitude in Figure 12. The passive TMD successfully attenuates the unloaded peak, but is out of range to affect the loaded peak. The SATMD on the other hand attenuates both peaks as result of the control algorithm.

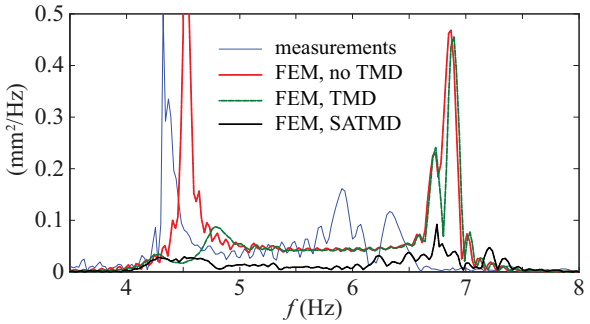

Figure 13. Frequency content from displacement of hanger 5 during train passage.

5 CONCLUSIONS

In this paper, the dynamic behaviour of a tied arch railway bridge has been analyzed. Based on field measurements, very low damping of the hangers was found, on average 0.2%. As comparison, a damping ratio of 0.5% is often used for design of steel bridges [2]. Resonant behaviour of several hangers was observed from field measurements of passing trains. Similar behaviour was obtained by means of a simple 2D FE-model.

The resonant behaviour has earlier been found to decrease the fatigue service life [1],[7] and a system of passive dampers was later installed [5],[6]. The natural frequencies of the hangers change as a result of increased axial force during train passage. Theoretical studies of a semi-active damping system to account for the frequency variation is presented and compared with a corresponding passive system. The results show that a passive damper is sensitive to small changes in frequency, causing inefficient vibration mitigation. Using a simple semi-active control incrementally tuned to the dominant frequency is generally shown to improve the vibration mitigation significantly.

6 FURTHER RESEARCH

Although the current semi-active algorithm was shown to attenuate the dynamic response significantly, several areas for improvement has been identified.

Separating closely spaced modes using the Short Time Fourier Transform method is often a trade off between frequency resolution and incremental response time. If instead wavelet transforms are employed, variable frequency resolutions can be obtained by scaling, potentially improving the accuracy in estimated frequency and facilitate a shorter response time.

In the current algorithm, the damper is tuned to the frequency of highest energy. The choice of another objective function may be called for, especially if the dynamic response is governed by several simultaneous frequencies.

In the present study, only the stiffness of the damper is modified. In many applications, the viscous properties are instead altered, e.g. by using magnetorheological dampers.

The results for the studied bridge are based on a simple 2D-model. From the field measurements, significant transverse vibration of the hangers was found [1],[7]. Due to different boundary conditions, different natural frequencies in each direction was estimated, Table 2. This may be accounted for using a 3D-model. Introducing semi-active dampers in two directions may call for a modification of the current algorithm.

The present study mainly focus on attenuating the dynamic displacement of the hangers. A factor of greater importance is however the mitigation of stresses, to improve the fatigue service life. Cumulative fatigue damage is highly non-proportional to the stress range and the choice of optimizing the damper for either forced or free vibration is not obvious.

Finally, verification of the developed routines by physical testing may be of interest, both experimentally and in-situ.

ACKNOWLEDGMENTS

The field measurements in 2003 were commissioned by the Swedish Transport Administration (former Banverket) and performed by KTH. Development of the semi-active routines and models were performed within the Long Life Bridges project, funded by the European Union 7th framework programme and coordinated by ROD. All funding and support mentioned above is greatly acknowledged.

REFERENCES

[1] Andersson, A., Malm, R. (2004). Measurement Evaluation and FEM Simulation of Bridge Dynamics. *MSc Thesis, KTH Royal Institute of Technology, Sweden*.

[2] CEN (2003). Eurocode 1: Actions on structures – Part 2: Traffic loads on bridges. *EN 1991-2:2003*.

[3] Chopra, A.K. (2001). Dynamics of Structures, Theory and Application of Earthquake Engineering. *Prentice-Hall Inc, 2nd Edition*.

[4] Géradin, M., Rixen, D. (1997). Mechanical Vibrations, Theory and Application to Structural Dynamics. *John Wiley & Sons, 2nd Edition*.

[5] Hortmanns, M., Schäfer, N. (2005). Ljungan Bridge, Ånge Sweden – Full Scale Measurements. *Technical report, Prof. Sedlacek & Partner (unpublished)*.

[6] Hortmanns, M. (2005). Ljungan Bridge, Ånge Sweden – Design of dampers for the hangers 3 to 6. *Technical report, Prof. Sedlacek & Partner (unpublished)*.

[7] Malm, R., Andersson, A. (2006). Field testing and simulation of dynamic properties of a tied arch railway bridge. *Engineering Structures 28, pp. 854-863*.

Paper III.

Vibration mitigation of railway bridges using adaptive damping control

Andreas Andersson, Raid Karoumi, Alan O'Connor

IABSE 2013, Rotterdam, The Netherlands, May 6-8 2013.
(*Conference paper, accepted*)

Vibration mitigation of railway bridges using adaptive damping control

Andreas ANDERSSON
Ph.D., Researcher
Royal Institute of Technology (KTH), Stockholm, Sweden
adde@kth.se

Raid KAROUMI
Professor
Royal Institute of Technology (KTH), Stockholm, Sweden
raidk@kth.se

Alan O'CONNOR
Associate Professor
Trinity College Dublin, Roughan & O'Donovan Innovative Solutions
Dublin, Ireland
oconnoaj@tcd.ie

Summary

In this paper, the advantage of an adaptive damping system is presented. A damper with variable stiffness is tuned based on estimates of the real-time frequency response, facilitating optimal vibration mitigation. The performance of the developed routines is investigated on an existing tied arch railway bridge. Based on previous field measurements, resonant behaviour of several hangers was found. In combination with low structural damping, the induced stresses resulted in a reduced fatigue service life. Passive dampers are currently installed on the longer hangers, each tuned to the fundamental natural frequency of the individual hanger. However, increased axial force during train passage results in a significant variation in natural frequency, with an apparent risk of detuning the passive dampers. The predicted performance of an adaptive damping system to account for this variation in dynamic behaviour is presented and its potential application is discussed.

Key words: Railway bridge dynamics; tuned mass damper; adaptive control; finite element method.

1. Introduction

There is a constant demand on the railway authorities to increase both the allowable axle loads and the allowable speed on existing railway lines. An increased utilization factor of the bridges can often be justified based on refined capacity assessment and field measurements. For bridges susceptible to high dynamic amplification or resonance, a moderate increase in speed or axle load may result in a significant increase in utilization. For cases of excessive vibrations, external damping systems may be called for. Such systems often have a rather narrow bandwidth, making them sensitive to any mismatch in tuning frequency. This is especially pronounced for cases of low structural damping, which is often the reason for installing damper systems in the first place. Even a small change in either structural frequency or loading frequency may result in a significant disimprovement in vibration mitigation. In some cases a detuned damper may even result in a magnified dynamic response compared to the case of no external damping system. The bandwidth may be widened either by increasing the damping ratio or by installing multiple dampers with different tuning frequencies. Another, often more efficient alternative, is to use a damper with variable properties that via a control system analyses the real-time response to retune the damper.

2. Tuned mass damper systems

One of the most established methods for external damping systems is the tuned mass damper (TMD). The concept is to add a suspended mass to an existing structure and tune the natural frequency of the suspended mass to the dominant frequency of the main structure. If the vibration of the suspended mass is out of phase compared to the main structure, a counteracting inertia force will attenuate the vibration of the resulting system. The theory of the TMD was first established by [7] and much research has been devoted to find configurations for optimal vibration mitigation. The most decisive parameters are the mass ratio $\gamma = m_{\mathrm{TMD}}/m_{\mathrm{structure}}$ and the damping ratio of the TMD. A

mass ratio of a few percent often results in sufficient vibration mitigation. For global damping of large structures, e.g. bridges or buildings, this may still result in rather large dampers.

2.1 SDOF and MDOF models

Structures dominated by a single frequency may be simplified to a single degree of freedom (SDOF) system, Fig. 1a. The natural frequency and viscous damping of the SDOF-system is given by Eq. (1). For the case of a simply supported beam, Eq. (2), the equivalent stiffness k_1 and modal mass m_1 are governed by Eq. (3). Including the TMD results in a 2DOF-system illustrated in Fig. 1b and the equation of motion can be expressed according to Eq. (4). This simple system is suitable for parametric studies and for finding optimal damping parameters. The parameters are often evaluated based on the steady-state response. For the 2DOF-model in Fig. 1b, a closed solution can be found in [9]. For more complicated systems the equilibrium equation for each circular frequency ω can be solved using Eq. (5), implemented in many commercial finite element packages.

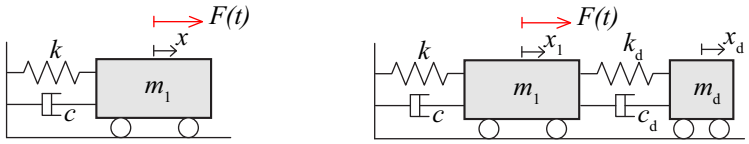

Fig. 1: a) SDOF-model, b) 2DOF model of the same system with a TMD.

$$f_{\mathrm{SDOF}} = \frac{1}{2\pi}\sqrt{\frac{k}{m_1}}\,,\; c = 2\zeta\sqrt{m_1 k} \tag{1}$$

$$f_{\mathrm{beam}} = \frac{\pi}{2}\sqrt{\frac{EI}{m_{\mathrm{beam}}L^4}}\,,\; \delta_{\mathrm{beam}} = \frac{qL^3}{48EI}\,,\; q = m_{\mathrm{beam}}gL \tag{2}$$

$$q = k\cdot\delta \rightarrow k = \frac{48EI}{L^3}\,,\; f_{\mathrm{SDOF}} = f_{\mathrm{beam}} \rightarrow m_1 = \frac{48m_{\mathrm{beam}}L}{\pi^4} \tag{3}$$

$$\begin{bmatrix} m_1 & 0 \\ 0 & m_{\mathrm{d}} \end{bmatrix}\begin{Bmatrix} \ddot{x}_1 \\ \ddot{x}_{\mathrm{d}} \end{Bmatrix} + \begin{bmatrix} c+c_{\mathrm{d}} & -c_{\mathrm{d}} \\ -c_{\mathrm{d}} & c_{\mathrm{d}} \end{bmatrix}\begin{Bmatrix} \dot{x}_1 \\ \dot{x}_{\mathrm{d}} \end{Bmatrix} + \begin{bmatrix} k+k_{\mathrm{d}} & -k_{\mathrm{d}} \\ -k_{\mathrm{d}} & k_{\mathrm{d}} \end{bmatrix}\begin{Bmatrix} x_1 \\ x_{\mathrm{d}} \end{Bmatrix} = \begin{Bmatrix} F(t) \\ 0 \end{Bmatrix} \tag{4}$$

$$\left(-\omega^2\mathbf{M} + i\omega\mathbf{C} + \mathbf{K}\right)\mathbf{x} = \mathbf{F} \tag{5}$$

A precursor of the TMD is the pendulum damper, depicted in Fig. 2. It is often based on the same concepts as the TMD, i.e. to create a vibrating mass phase-shifted to the primary system. The natural frequency of the classical pinned pendulum is given by Eq. (6). If the mass of the rod is negligible compared to the mass of the bob, the frequency depends solely on the length of the pendulum. For the clamped pendulum, the natural frequency is obtained by considering a cantilever beam with a lumped end mass, resulting in Eq. (7). Damping can be added to the pendulum based on an SDOF approach, Eq. (8). It shall be noted that for the MDOF-system in Fig. 2b, the motion of the pendulum depends on the motion of the primary system. Not accounting for this may cause the damper to be partly detuned. In numerical simulations of pendulum motions, a nonlinear analysis is normally required.

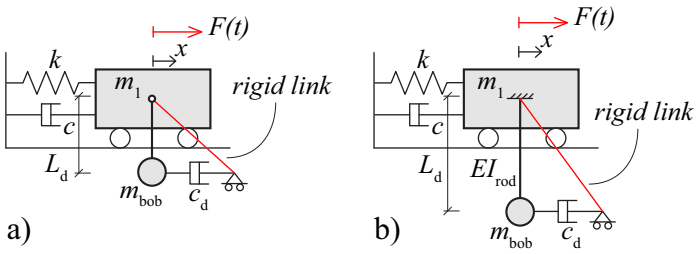

Fig. 2: Pendulum damper models, a) pinned pendulum, b) clamped pendulum.

$$f_{\mathrm{p,pinned}} = \frac{1}{2\pi}\sqrt{\frac{g}{L_{\mathrm{d}}}}\sqrt{\frac{m_{\mathrm{bob}}}{m_{\mathrm{bob}} + m_{\mathrm{rod}}/3}} \tag{6}$$

$$f_{\mathrm{p,clamped}} = \frac{1}{2\pi}\sqrt{\frac{3EI_{\mathrm{rod}}}{m_{\mathrm{bob}}L_d^{\,3} + \frac{48m_{\mathrm{rod}}L_d^{\,3}}{\pi^4}\left(3-\frac{8}{\pi}\right)}} \tag{7}$$

$$c_{\mathrm{d}} = 2\zeta\sqrt{m_{\mathrm{d}}k_{\mathrm{d}}}\,, \quad k_{\mathrm{d}} = m_{\mathrm{d}}\omega_{\mathrm{d}}^{\,2}\,, \quad m_{\mathrm{d}} = m_{\mathrm{bob}} \tag{8}$$

2.2 Adaptive and semi-active control

Vibration control systems are often divided in passive systems, adaptive/semi-active control and active control. A passive system is not able to change properties and is most suitable for time-invariant loading. An adaptive control system can change properties of the damper but with a significantly narrower bandwidth than the vibration system, i.e. a relatively slow change in properties compared to the dynamics of the structure. A semi-active system however has a significantly higher bandwidth and can change properties several times during a single period of vibration, [4]. In a fully active system, a force control is obtained by a load actuator. One of the benefits of the adaptive and semi-active systems is that they need only a fraction of the energy input compared to a fully active system.

Some adaptive systems are based on stiffness control, with the objective to retune the frequency of the TMD for optimal vibration mitigation. In practical applications, the variable stiffness component often consists of non-trivial mechanical devices with multiple moving parts and a rather limited frequency range. In comparison, semi-active systems are often based on damping control. This can be accomplished by magnetorheological devices, which are able to rapidly change properties due to a small controllable electrical current. Semi-active and active control systems originate from the use of shock absorbers but can also be implemented for TMD applications. The principle of controllable shock absorbers is to create a force that at any increment of time counter-acts the motion of the structure. In comparison, a TMD produces a force based on its natural frequency, which counteracts the corresponding frequency of the structure due to its phase shift.

Variable stiffness control is based on incremental update of the present dominant frequencies. The two most common time-frequency estimators are the Short Time Fourier Transform (STFT) and the Short Time Wavelet Transform (STWT). Both operate on a short time signal prior to present time and the performance of the system depends on how rapidly and accurately the frequency content can be estimated. The frequency resolution of the STFT method can be increased by zero-padding or copying the signal, without adding additional information in the signal. Using wavelets, arbitrary frequency resolution can be obtained by scaling. However, the accuracy in both methods is still limited to the information contained in the studied signal. The final performance is therefore a trade-off between response time and frequency resolution.

3. Case study bridge

The use of passive and adaptive damping systems are studied on an existing railway bridge by means of numerical simulations. The bridge has earlier been the subject of dynamic assessments and its dynamic behaviour has been verified by field measurements [1,5]. The objective of this paper is to illustrate the potential of an adaptive damping system for vibration mitigation.

3.1 Bridge properties

The bridge is located approximately 110 km West of Sundsvall, a municipality in central Sweden. It is part of the Northern main line and is important for ore transports as well as commuter trains. It was built in 1959 and is designed as a single span single track tied arch railway bridge. The span is 45 m. A photo of the bridge is presented in Fig. 3a. The mid support is a remnant from the previous bridge and is not utilized. The deck is designed as an unballasted steel grillage consisting of main beams, cross beams and stringers. Wooden sleepers are supported directly by the stringers. A cross-section of the deck is shown in Fig. 3b. The distance between the cross beams is 3.75 m which is the same for the hangers. The hangers consist of solid steel rods with a diameter of 80 mm. The arch has a circular shape with a radius of 31.9 m and height of 8.9 m, measured from the top of the main beam to the arch centre line.

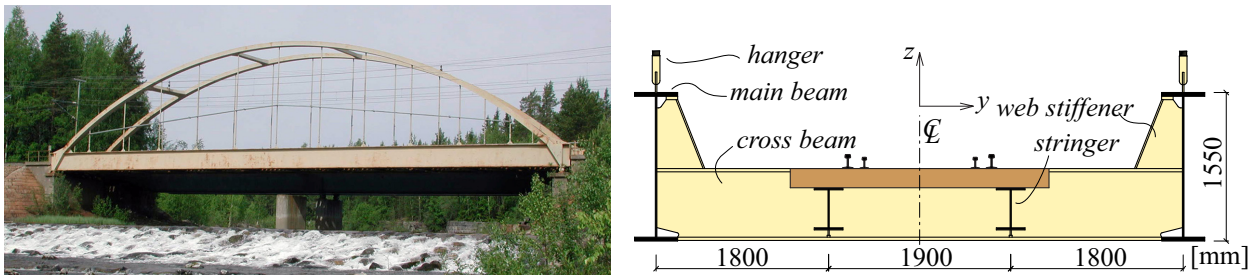

Fig. 3: The Ljungan bridge, a) view, b) cross-section of the steel beam grillage.

During train passage, resonant vibration of several hangers was observed, resulting in a significant decrease in estimated fatigue service life. The most critical section was found to be a threaded turn buckle connection at the lower part of the hanger, depicted in Fig. 4a-c.

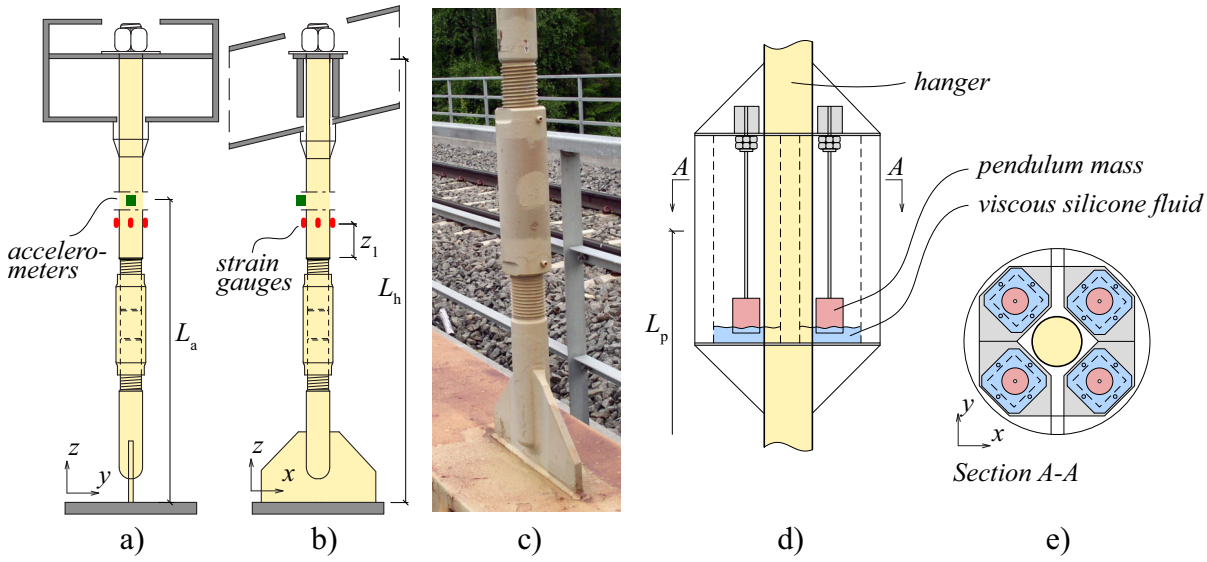

Fig. 4: Hanger details, a)-c) instrumentation without damper systems, d-e) current pendulum dampers on hanger 3-9, reproduced from [3].

The response was evaluated both by field measurements and numerical simulations. Resonant loading in combination with low damping showed that more than 50% of the cumulative fatigue damage of the longer hangers were related to free vibrations [1,5]. In 2005, a system of external pendulum dampers was installed on the hangers, illustrated in Fig. 4d-e [2,3]. The pendulum dampers are tuned to the natural frequencies of the unloaded bridge and based on free vibration measurements the average damping ratio was increased from 0.2% to 3.5% [3]. Due to the boundary conditions of the hangers, different frequencies in the longitudinal and transverse direction are obtained. The hangers are numbered 1 to 6 with a length from 1.30 m to 7.15 m.

3.2 Finite element models

Although the dynamic behaviour of the bridge is three-dimensional, the essential response can be illustrated using a 2D approach. A 2D FE-model of the bridge is illustrated in Fig. 5, constituting a symmetric half of the bridge. All components are modelled as Euler-Bernoulli beam elements. The hangers are assumed rigidly connected to the main beam but hinged to the arch. This has shown to give a good fit of natural frequencies compared to the field measurements. The dynamic response from passing trains is modelled as vertical point loads applied directly on the stringer beam. The cross beams are modelled as vertical springs with a stiffness calculated on basis of a simply supported beam subjected to two point loads. During train passage, the increase in axial force of the hangers results in a significant change in natural frequency. This is accounted for by a geometrically nonlinear analysis. As a consequence, modal superposition is not applicable and a direct time integration scheme is used. A structural damping of 0.2% is included and the resulting damping matrix is based on Rayleigh damping.

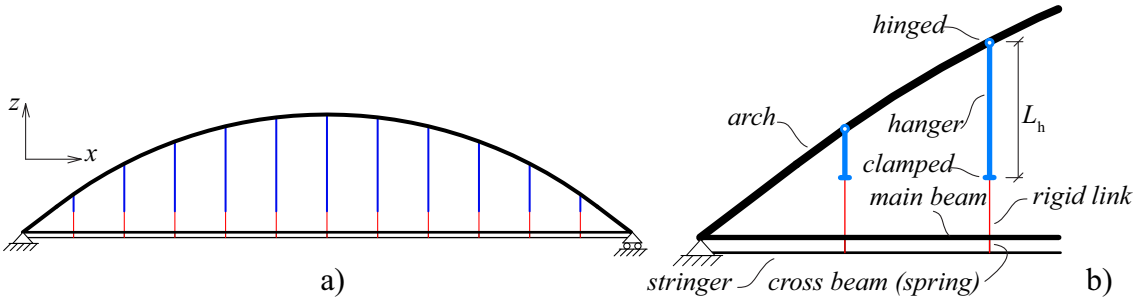

Fig. 5: 2D FE-model of the bridge, a) elevation, b) details and connections.

External dampers are modelled as illustrated in Fig. 6. The damper mass m_d is modelled as a lumped nodal mass. The TMD-model is connected to the hanger by springs and dashpots in the longitudinal direction and is fully constrained to follow the motion of the hanger in vertical direction. The relative motion between the two nodal masses is also constrained. For the pendulum model, the nodal mass is connected by a beam element with stiffness EI_d, which at the upper end is rigidly connected to the hanger, hence acting as a clamped pendulum. An additional viscous damping is included by a horizontal damper c_d.

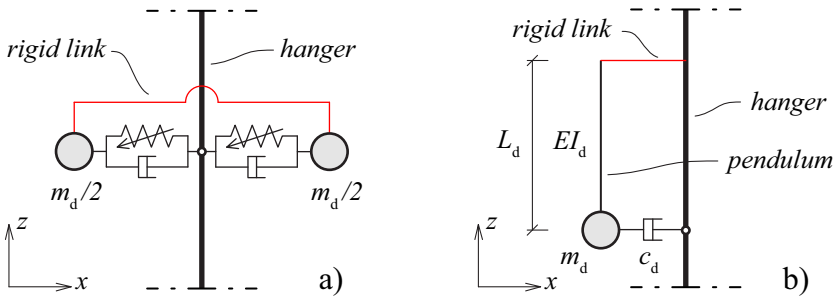

Fig. 6: Detail of dampers in the 2D-model, a) variable stiffness TMD, b) clamped pendulum.

The properties of the damper models are determined by Eq. (1), Eq. (7) and Eq. (8). When modelling the adaptive TMD, the stiffness matrix is incrementally updated to account for the change in spring stiffness. The analysis is performed using the commercial FE-package SOLVIA03 [8] and an adaptive scheme is automated by routines developed in MATLAB [6].

4. Simulation results

In this paper, simulations of the dynamic behaviour of hanger 5 are presented. The length of the hanger is 6.95 m and from field measurements the first longitudinal natural frequency was estimated at 4.3 Hz with an appertaining damping of 0.15%.

4.1 MDOF-models, transient dynamics

Assuming the hanger to be simply supported, Eq. (3) results in m_1 = 135 kg and k = 100 kN/m. Further, Eq. (1) gives c = 11 Ns/m. Due to the low damping, the steady state response is about 300 times the static response. From field measurements, the magnitude of dynamic longitudinal displacement was estimated as 5 mm based on time integrated accelerations. The duration of the train passage was about 10 s. Using the MDOF-models, a harmonic load block with duration of 10 s is used in a transient dynamic analysis. The influence of frequency detuning is investigated by a parametric study according to Table 1, where f_1 is the natural frequency, f_d the frequency of the damper and f_F the frequency of the load. The magnitude of the load is adjusted to produce a displacement of 5 mm for the SDOF-model. For both the TMD and pendulum models, a mass m_d = 1 kg and damping ratio ζ_d = 1% is used.

The results in terms of peak displacements are presented in Fig. 7. Due to the low structural damping, the resonance peak of the SDOF-model is rather narrow and a detune of the load frequency results in an off-resonance response and a reduction by a factor of 5, case b) and d). For a perfectly tuned TMD, the initial response is reduced by a factor of ~10, case a). However, a detune of either the load frequency or the damper frequency show a significant disimprovement, worse than the detuned SDOF-system. The peak displacement is obtained during the forced vibration and detuning both the damper and the force frequency, case d) results in a force-tuned TMD with similar performance to the perfectly tuned case. However, the following free vibrations will still experience significant oscillation. Comparison of the pendulum dampers show that they both perform similarly to the TMD, except for the detuned pinned pendulum. For the adaptive variable stiffness TMD, frequency estimators based on STFT and STWT are compared. For the perfectly tuned case, all models perform similarly to the passive TMD. In detuning however, the STWT routine performs slightly better and is comparable to the perfectly tuned TMD for all studied cases.

Table 1: Set of parameter studies for frequency variation of the MDOF models.

case	f_1 (Hz)	f_d (Hz)	f_F (Hz)
a)	4.30	f_1	f_1
b)	4.30	f_1	$0.95f_1$
c)	4.30	$0.95f_1$	f_1
d)	4.30	$0.95f_1$	$0.95f_1$

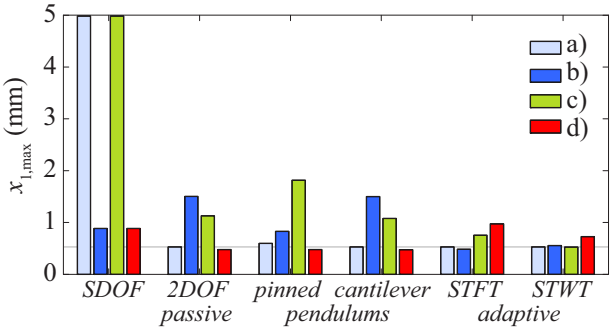

Fig. 7: Peak displacement of the primary structure due to a transient loading block, influence of frequency variation for different TMD models.

4.2 2D-model, dynamics of passing trains

The dynamic response of the bridge during train passage is analysed using the 2D FE-model. A freight train consisting of one locomotive and 19 wagons is used. For the locomotive (Swedish Rc4), the axle distance 2.7 m, bogie distance 7.7 m, the total length 15.5 m and the load 195 kN/axle are used. Standardized freight train wagons are assumed according to load class D2. This corresponds to an axle distance 1.8 m, bogie distance 9.2 m, length 14.0 m and an axle load of 225 kN/axle. A similar train passage was recorded during the field measurements, although the exact specifications were not known. The stress components in hanger 5 during the train passage are presented in Fig. 8. The measured response is found to be comparable with the simple 2D-model, although the transverse bending component σ_{Mx} is not accounted for. Comparing the axial stresses indicate that not all wagons of the real train have the same specifications regarding axle load and/or axle distances. Both the measured response and the FE-model demonstrate excessive bending stresses due to resonant loading. It shall be noted that due to the low structural damping, the response may change significantly for a small change in load frequency, e.g. due to different train speed or axle distance. Also, due to different frequencies in the longitudinal and transversal direction, resonance in either direction may be dominant for different speeds.

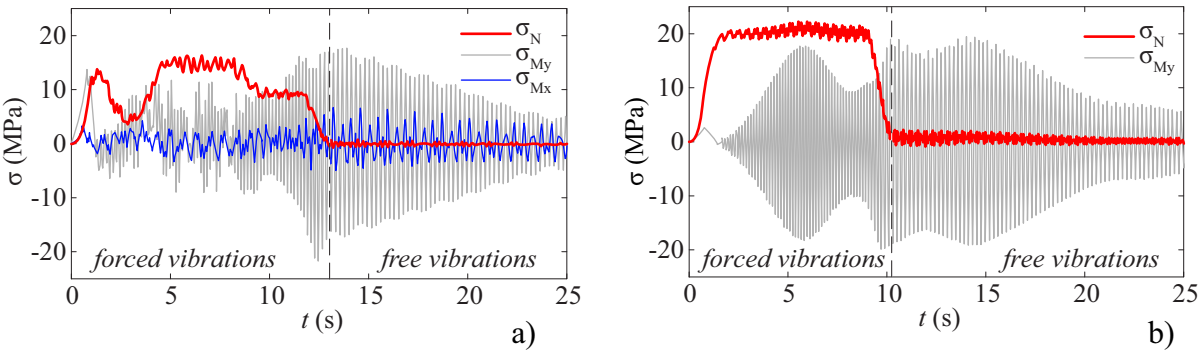

Fig. 8: Stress components in hanger 5 during train passage, a) from field measurements, b) from 2D FE-model, v = 115 km/h. Results without external dampers.

During train passage, the increased axial force in hanger 5 results in an increase in natural frequency from 4.3 Hz to about 6.5 Hz. This will cause a passive damper system to be almost completely detuned during the train passage, if tuned based on the unloaded hanger frequency. A comparison of different damper systems is presented in Fig. 9, all based on the 2D FE-model. For clarity, envelopes of the bending stresses are shown. The light shaded area represents the undamped response, as in Fig. 8b.

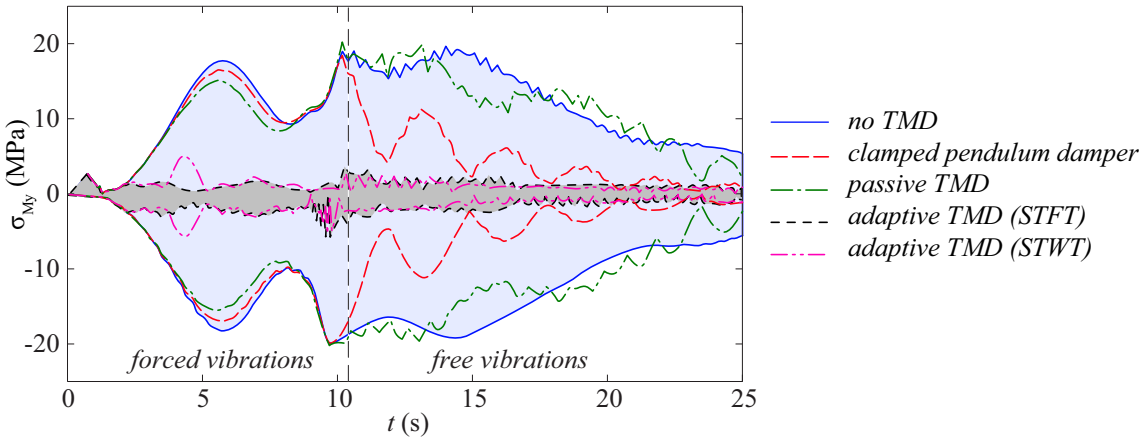

Fig. 9: Bending stress in hanger 5, results from the 2D-model with different damping systems.

Both the pendulum damper and the passive TMD show little improvement during the forced vibrations. During free vibrations, the pendulum damper performed significantly better than the passive TMD. The darker shaded area represents the working range of the adaptive TMD, proving an overall significant vibration mitigation for both forced and free vibrations.

5. Conclusions

In this paper, the use of passive and adaptive damping systems for mitigation of railway bridge dynamics is studied, by means of numerical simulations. Based on MDOF-models, it is shown that a passive TMD is sensitive to detuning, which can be greatly improved by an adaptive variable stiffness TMD. The application of the damper systems is further illustrated for a case study bridge, proven to be susceptible to resonant loading. During train passage, the frequency of vertical hangers change due to increased axial force. Numerical simulations show that passive systems tuned to the frequency of the unloaded bridge will have little influence on the forced vibration but significant influence on the free vibrations. For such configurations, the initial free vibrations have rather high amplitude, affecting the possible vibration mitigation. Using an adaptive system however, the forced vibration is attenuated significantly, causing initially lower amplitudes during free vibration and hence lower amplitudes during both forced and free vibration.

Acknowledgements

The field measurements in 2003 were commissioned by the Swedish Transport Administration (former Banverket) and performed by KTH. Additional analysis and the development of routines for adaptive vibration damping were performed within the Long Life Bridges project, a Marie Curie Industry-Academia Partnerships and Pathways project funded by the European Commission 7th Framework Programme (IAPP-GA-2011-286276). All funding and support mentioned above is greatly acknowledged.

References

[1] ANDERSSON, A., MALM R., “Measurement Evaluation and FEM Simulation of Bridge Dynamics”, *MSc Thesis, KTH Royal Institute of Technology, Sweden*, 2004.

[2] HORTMANNS, M., SCHÄFER, N., “Ljungan Bridge, Ånge Sweden – Full Scale Measurements”, *Technical report (unpublished), Prof. Sedlacek & Partner, 2005.*

[3] HORTMANNS, M., “Ljungan Bridge, Ånge Sweden – Design of dampers for the hangers 3 to 6”, *Technical report (unpublished), Prof. Sedlacek & Partner, 2005.*

[4] LIEDES, T., “Improving the performance of the semi-active tuned mass damper”, *PhD-Thesis, University of Oulu, Finland*, 2009.

[5] MALM, R., ANDERSSON, A., “Field testing and simulation of dynamic properties of a tied arch railway bridge”, *Engineering Structures 28(1)*, 2006.

[6] MATLAB, “MATLAB 2009b Reference manual”, *The MathWorks Inc*, 2009.

[7] ORMONDROYD, J., DEN HARTOG, J.P., ”The theory of the dynamic vibration absorber”, *ASME, Journal of Applied Mechanics 50*, 1928.

[8] SOLVIA, “SOLVIA-PRE for Stress Analysis, User Manual”, *Report SE 03-1, SOLVIA Finite Element Systems Version 03*, 2008.

[9] TSAI, H.-C., LIN, G.-C., “Explicit formulae for optimum absorber parameters for force-excited and viscously damped systems”, *Journal of Sound and Vibration 176(5)*, 1994.

Paper IV.

Passive and Adaptive Damping Systems for Vibration Mitigation and Increased Fatigue Service Life of a Tied Arch Railway Bridge

Andreas Andersson, Raid Karoumi, Alan O'Connor

(*Journal paper. submitted to ASCE Journal of Bridge Engineering, February 2013*)

Passive and Adaptive Damping Systems for Vibration Mitigation and Increased Fatigue Service Life of a Tied Arch Railway Bridge

Andreas Andersson[1,2,3], Raid Karoumi[2], Alan O'Connor[1]

[1]Roughan & O'Donovan Innovative Solutions (ROD-IS), Arena House, Arena Road, Sandyford, Dublin 18, Ireland
[2]Royal Institute of Technology (KTH), Brinellvägen 23, SE-100 44 Stockholm, Sweden
[3]The Swedish Transport Administration (Trafikverket), Solna Strandväg 98, SE-171 54 Solna, Sweden
email: Andreas.Andersson@byv.kth.se, Raid.Karoumi@byv.kth.se, Alan.OConnor@rod.ie

Abstract: In this paper, the use of external damping systems for vibration mitigation of railway bridge dynamics is studied. Theoretical analysis and numerical simulations are presented based on both passive and adaptive tuned mass dampers (TMD). Routines for a variable stiffness TMD in combination with incremental frequency estimates are developed and its performance under different loadings is studied. The potential of the dampers are studied on a tied arch railway bridge by means of numerical simulations. The bridge has earlier been the subject of extensive dynamic assessments and available field measurements of the response during train passage are reanalyzed and used for model calibration. Both field measurements and numerical simulations show resonant behavior of several hangers during train passage. Due to low structural damping, the resulting stresses are shown to significantly reduce the fatigue service life. A system of passive pendulum dampers was installed in 2005, proving an increased damping ratio due to free vibrations. Its performance during train passage was however not measured. The dynamic response is studied for different damping models based on a calibrated 3D finite element model. The response is highly sensitive to the train speed due to the risk of resonance. Fragility curves are adopted to estimate the extent of cumulative damage under mixed traffic loads at variable speeds.

Keywords: Railway bridge dynamics; tuned mass damper; adaptive control; finite element method; fatigue; fragility curve.

Introduction

Internationally, there is an increasing demand on railway authorities to increase both the allowable axle load and allowable speed on existing railway lines. An increased utilization of the bridges can sometimes be justified based on refined capacity assessment and field measurements.

In the design of railway bridges, dynamic effects are usually accounted for by a dynamic amplification factor of the static response. This factor does not account for resonant behavior and only for railway bridges on high-speed lines a full dynamic analysis is normally required.

In this paper, a bridge on a non high-speed railway line is investigated with emphasis on its dynamic behavior during train passage. The bridge is found susceptible to resonant behavior due to structural members with low natural frequencies and low structural damping, resulting in a reduced fatigue service life. Vibration mitigation using external damping systems is investigated, with an emphasis on passive and adaptive control to account for variation in dynamic characteristics and to optimize the resulting damping. Estimating the fatigue service life under the influence of resonant loading is afflicted with great uncertainties due to the large difference at resonance and off resonance. Fragility curves are demonstrated as a tool for estimating the extent of cumulative fatigue damage and in the extent the remaining fatigue service life.

Case study Bridge

The bridge presented in this paper is located approximately 110 km West of Sundsvall, a municipality in central Sweden. It is part of the Northern main line and is important for ore transports as well as commuter trains. The dynamic behavior of the bridge has been the subject of previous studies, e.g. (Andersson & Malm, 2004), (Malm & Andersson, 2005) comprising both numerical analysis and field measurements and comprising field measurements and installation of passive damper systems, (Hortmanns & Schäfer, 2005), (Hortmanns, 2005).

Bridge properties

The bridge was built in 1959 and is designed as a single span single track tied arch railway bridge. A photo of the bridge is presented in Fig. 1. The mid-support is a remnant from the previous bridge and is not utilized.

Fig. 1. View of the Ljungan railway bridge.

The deck is designed as an unballasted steel grillage consisting of main beams, cross beams and stringers. Wooden sleepers are supported directly by the stringers. A cross-section of the deck is illustrated in Fig. 2. The distance between the cross beams is 3.75 m, which is the same for the hangers. The hangers consist of solid steel rods with a diameter of 80 mm above the threaded section. The arch has a circular shape with a radius of 31.9 m and a height of 8.9 m, measured from the top of the main beam to the arch centre line.

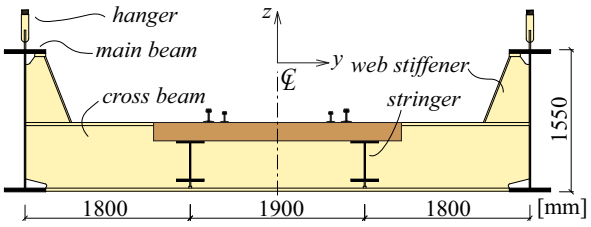

Fig. 2. Cross-section of the grillage deck.

The dimensions of the beams are presented in Table 1. In addition, secondary bracing systems with profile $L90\times90\times9$ connects to the upper flange of the stringers and with profile $L140\times140\times13$ to the lower flange of the main beams and cross beams. Due to excessive vibration of the hangers, a system of diagonal RHS-beams was installed in the 1980's as an attempt to stabilize the hangers. This system was replaced by individual pendulum dampers in 2005.

Table 1
Beam cross-sectional properties. The arch has a rectangular hollow section; all I-beams are doubly symmetric.

(mm)	h	b_f	t_f	t_w
main beam	1550	450	40	16
cross beam	750	300	34	18
stringer	440	300	22	12
arch	350	600	16	20

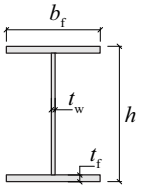

Field measurements

Field measurements were carried out in June 2003, comprising 16 strain gauges and 12 accelerometers, mounted on hangers 2 to 5. During field measurements, the stabilizing system of RHS-beams was removed. The position of the gauges and details of the hangers are presented in Fig. 3. The total length of L_h and distance L_a to the accelerometers are given by Table 2. At each position, three accelerometers are mounted together, measuring in *xyz*-directions. Also, four strain gauges are instrumented at the distance z_1 = 100 mm above the threaded section, spaced 90° apart along the perimeter of the hanger. Gauge e_1, e_5, e_9, e_{13} are closest to the track.

Table 2
Length of the hangers L_h (according to original drawings) and position of accelerometers L_a, rounded to 5 cm. L_p is the position of installed passive pendulum dampers.

hanger	h_1	h_2	h_3	h_4	h_5	h_6
L_h (m):	1.30	3.54	5.20	6.30	6.95	7.15
L_a (m):	–	1.55	1.90	2.15	2.30	–
L_p (m):	–	–	3.12	3.67	4.00	4.10

Two different data acquisition systems were used; a HBM MGC*Plus* for the strain gauges and a Sony PC216AX with a UNO-MWL006 amplifier for the accelerometers. The sampling frequency was set to 2 kHz for the strain gauges and 6 kHz for the accelerometers. To avoid signal overloading, an analogue 20 Hz low-pass filter (PC-848) was used for the accelerometers. To synchronize the signals, strain gauge e_1, e_2, e_{15}, e_{16} were connected to both systems.

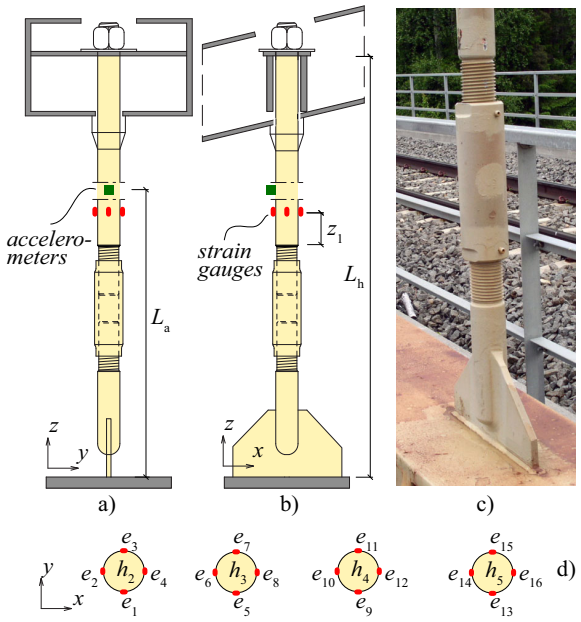

Fig. 3. Detail of the hangers and instrumentation, a) section across the bridge, b) section along the bridge, c) photo of the turn buckle, d) position of strain gauges on hanger 2 to 5.

Natural frequencies and damping estimates

The natural frequencies and damping ratios of the hangers were estimated based on free vibration tests of the unloaded bridge. Each hanger was excited by a swift knock in each direction. Based on a Maximum likelihood estimate of the free decay of motion, the results in Table 3 were obtained. A significant difference in frequency for the *x*- and *y*-direction is observed, mainly due to different boundary conditions in the longitudinal and transversal direction. The results show good agreement with similar measurements presented in (Hortmanns & Schäfer, 2005).

Table 3
Estimated natural frequencies (Hz) and damping (%), based on free vibration tests of the unloaded bridge.

hanger	$f_{1,x}$	$f_{2,x}$	$f_{1,y}$	$f_{2,y}$	$\zeta_{1,x}$	$\zeta_{2,x}$	$\zeta_{1,y}$	$\zeta_{2,y}$
h_2	16.0	44.9	10.9	34.0	0.33	0.18	0.14	0.46
h_3	7.9	23.1	6.1	18.9	0.16	0.22	0.42	0.16
h_4	7.2	19.2	6.0	16.5	0.09	0.08	0.14	0.19
h_5	4.3	13.5	3.6	11.4	0.15	0.05	0.30	0.24

Installed pendulum dampers

Analysis performed by (Andersson & Malm, 2004) and (Malm & Andersson, 2005) showed that the threaded section of the hanger turnbuckle was susceptible to fatigue, due to excessive vibration of the hanger. Simulations including the stabilizing RHS-beams indicated increased stresses in the transverse direction, causing more hangers to vibrate rather than acting as a stabilizer. A system of passive pendulum dampers were installed in 2005, developed by (Hortmanns & Schäfer, 2005), (Hortmanns, 2005). The objective was to attenuate the vibration of the longer hangers that had been shown most critical to resonance. A sketch of the pendulum dampers is provided in Fig. 4. The pendulum dampers are

mounted on hanger h_3 to h_9 on each side of the bridge, at a distance L_p from the upper flange of the main beam, Table 2.

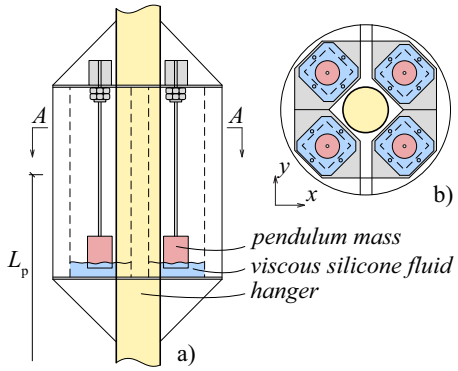

Fig. 4. Sketch of the installed passive pendulum dampers, a) cross-section, b) plane section *A-A*, reproduced from (Hortmanns, 2005).

Each damper box contains four individual pendulums, tuned to the first natural frequency of the corresponding hanger. The pendulum mass is partly suspended in a viscous silicone fluid, increasing the resulting damping. The upper connection of the pendulum rod is fastened with a bolted backing and is considered fully clamped.

Free vibration measurements were performed before and after installation of the pendulum dampers, reported in (Hortmanns, 2005). The average total structural damping was 3.6% in the longitudinal direction and 4.4% in the transverse direction. The appertaining coefficients of variation were 0.4 and 0.2 respectively. No additional measurement of resulting stresses in the hangers or the response during train passage was reported.

Tuned mass damper systems

In the field of vibration mitigation, the tuned mass damper (TMD) is one of the most established methods. The concept is to add a suspended mass to an existing structure and tune the natural frequency of the suspended mass to the dominant frequency of the main structure. If the vibration of the suspended mass is out of phase compared to the main structure, a counteracting inertia force will attenuate the vibration of the resulting system. The theory of the TMD was first established by (Ormondroyd & Den Hartog, 1928) and much research has been devoted to find configurations for optimal vibration mitigation.

SDOF-model of a simply supported beam

Structures dominated by a single frequency may be simplified to a single degree of freedom (SDOF) model, Fig. 5. The natural frequency and viscous damping of the SDOF-system is given by Eq. (1). Fitting the stiffness k and mass m_1 to the first natural frequency of a simply supported beam, Eq. (2), results in the stiffness according to Eq. (3) and modal mass according to Eq. (4). Assuming a harmonic forced vibration $F(t)$ according to Eq. (5), the steady state response is governed by Eq. (6) (Clough & Penzien, 2003). At resonance, when $\omega/\omega_1 = 1$, the dynamic amplification for low damping is approximately $1/2\zeta$.

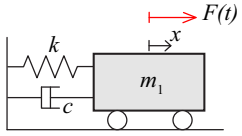

Fig. 5. SDOF-model.

$$f_{\text{SDOF}} = \frac{1}{2\pi}\sqrt{\frac{k}{m_1}}\,,\quad c = 2\zeta\sqrt{m_1 k} \tag{1}$$

$$f_{\text{beam}} = \frac{\pi}{2}\sqrt{\frac{EI}{m_{\text{beam}}L^4}}\,,\quad \delta_{\text{beam}} = \frac{qL^3}{48EI}\,,\quad q = m_{\text{beam}}gL \tag{2}$$

$$q = k\cdot\delta \rightarrow k = \frac{48EI}{L^3} \tag{3}$$

$$f_{\text{SDOF}} = f_{\text{beam}} \rightarrow m_1 = \frac{48m_{\text{beam}}L}{\pi^4} \tag{4}$$

$$F(t) = F_0\sin(\omega t),\quad F_0 = kx_{\text{static}} \tag{5}$$

$$R_{\text{d}} = \frac{1}{\sqrt{\left[1-\left(\frac{\omega}{\omega_1}\right)^2\right]^2 + \left[2\zeta\left(\frac{\omega}{\omega_1}\right)\right]^2}} \tag{6}$$

Pendulum model

Pendulum dampers are often designed according to the same principle as tuned mass dampers. For the classical pinned pendulum, Fig. 6a, the natural frequency depends mainly on the length of the rod L_d. Accounting for the total mass of the rod m_{rod} however, results in Eq. (7). The case of the clamped pendulum, Fig. 6b, can be regarded as a cantilever beam with a lumped end mass, resulting in a natural frequency according to Eq. (8) (Irvine, 2011). Additional damping due to the pendulum can be approximated by a viscous damper c_d, where k_d, m_d and ω_d are related to the dynamics of the pendulum, considered as an SDOF-system. It shall be noted that for the MDOF-system depicted in Fig. 6b, the motion of the pendulum depends on the motion of the primary system. Not accounting for this may cause the pendulum to be detuned.

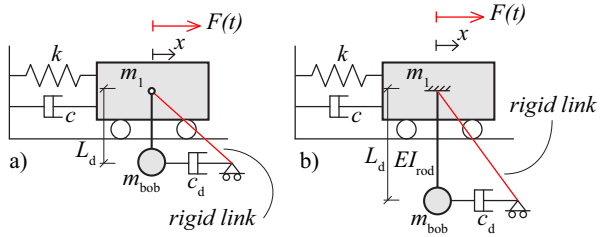

Fig. 6. MDOF-system of a pendulum damper, a) pinned pendulum, b) clamped pendulum.

$$f_{\text{p,pinned}} = \frac{1}{2\pi}\sqrt{\frac{g}{L_{\text{d}}}}\sqrt{\frac{m_{\text{bob}}}{m_{\text{bob}} + m_{\text{rod}}/3}} \tag{7}$$

$$f_{\text{p,clamped}} = \frac{1}{2\pi}\sqrt{\frac{3EI_{\text{rod}}}{m_{\text{bob}}{L_d}^3 + \frac{48m_{\text{rod}}{L_d}^3}{\pi^4}\left(3-\frac{8}{\pi}\right)}} \tag{8}$$

$$c_{\text{d}} = 2\zeta\sqrt{m_{\text{d}}k_{\text{d}}}\,,\quad k_{\text{d}} = m_{\text{d}}{\omega_{\text{d}}}^2\,,\quad m_{\text{d}} = m_{\text{bob}} \tag{9}$$

Passive TMD-model

The principle of a passive TMD is illustrated by extending the SDOF-model in Fig. 5 to a 2DOF-model according to Fig. 7. The equation of motion follows Eq. (10) using Eq. (11) and Eq. (12) (Chopra, 2001).

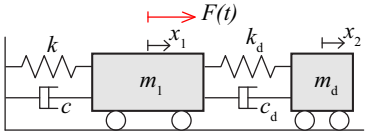

Fig. 7. 2DOF-system of a passive tuned mass damper.

$$\mathbf{M}\{\ddot{x}\}+\mathbf{C}\{\dot{x}\}+\mathbf{K}\{x\}=\{F\} \tag{10}$$

$$\mathbf{M}=\begin{bmatrix} m_1 & 0 \\ 0 & m_d \end{bmatrix}, \mathbf{K}=\begin{bmatrix} k+k_d & -k_d \\ -k_d & k_d \end{bmatrix}, \mathbf{C}=\begin{bmatrix} c+c_d & -c_d \\ -c_d & c_d \end{bmatrix} \tag{11}$$

$$\{x\}=\begin{Bmatrix} x_1 \\ x_2 \end{Bmatrix}, \{F\}=\begin{Bmatrix} F(t) \\ 0 \end{Bmatrix} \tag{12}$$

The objective is to attenuate the vibration of the primary structure by suitable values for m_d, k_d and c_d. The steady-state response of the primary structure was derived by (Tsai & Lin, 1994) and is presented in Eq. (13), with auxiliary equations Eq. (14). For a perfectly tuned TMD at resonance, $f = 1$ and $g = 1$, result in Eq. (15). Setting $m_d = 0$ reduces to Eq. (6). It shall be noted however, that the peak magnitude for a TMD with low damping occurs at one of the resulting natural frequencies of the combined 2DOF-model. Those frequencies can be determined from an Eigen value analysis of Eq. (10).

According to (Den Hartog, 1947) and (Brock, 1946), the optimal tuning frequency and damping of the TMD is governed by Eq. (16), provided an undamped primary structure. For non-zero damping of the primary structure, optimal parameters for the TMD are often estimated based on numerical min-search of Eq. (13).

$$R_{d,2DOF}=\frac{\sqrt{A_1}}{\sqrt{A_2+A_3}}=\frac{x_{1,dyn}}{x_{1,stat}} \tag{13}$$

$$A_1=\left(f^2-g^2\right)^2+\left(2gf\zeta_d\right)^2 \tag{14a}$$

$$A_2=\left(gf^2g^2-\left(g^2-1\right)\left(g^2-f^2\right)+4\zeta\zeta_d fg^2\right)^2 \tag{14b}$$

$$A_3=4g^2\left(\zeta_d f\left(g^2+\gamma g^2-1\right)+\zeta\left(g^2-f^2\right)\right)^2 \tag{14c}$$

$$f=\frac{\omega_d}{\omega}, g=\frac{\omega}{\omega_1}, \gamma=\frac{m_d}{m_1} \tag{14d}$$

$$R_{d,2DOF}\left(f=1,g=1\right)=\frac{2\zeta_d}{\sqrt{\left(\gamma+4\zeta\zeta_d\right)^2+\left(2\zeta_d\gamma\right)^2}} \tag{15}$$

$$f_{opt}=\frac{1}{1+\gamma}, \zeta_{opt}=\sqrt{\frac{3\gamma}{8(1+\gamma)}}, \zeta=0 \tag{16}$$

Adaptive variable stiffness TMD-model

Most optimizations of the passive TMD are based on the steady state response of a single harmonic time-invariant load. Small changes in either the forced vibration or the primary structure may however cause the TMD to be detuned. Even a small detune can lead to a significant disimprovement in vibration mitigation and may even result in a greater response than without the TMD. For many real structures, both the forced vibration and the characteristics of the primary structure changes over time; either to long term effects, e.g. temperature or material behavior or short term effects, e.g. vehicle loading. For many structures several modes contribute to the total vibration level, depending on the position and frequency of the loading.

One way to account for variation in frequency is to install multiple TMDs with different tuning frequencies. This does however increase the total damped mass to obtain the same performance as a perfectly tuned TMD, and also the cost of installation. Another option is a TMD with variable properties that via a control system analyses the real-time response and is able to retune the TMD to an optimal configuration.

Vibration control systems are often divided in passive systems, adaptive/semi-active control and active control. A passive system is not able to change properties and is most suitable for time-invariant loading. An adaptive control system can change properties of the damper but with a significantly narrower bandwidth than the vibration system, i.e. a relatively slow change in properties compared to the dynamics of the structure. A semi-active system however has a significantly higher bandwidth and can change properties several times during a single period of vibration, (Liedes, 2009). In a fully active system, a force control is obtained by a load actuator.

Some adaptive systems are based on stiffness control, with the objective to retune the frequency of the TMD for optimal vibration mitigation. In practical applications, the variable stiffness component often consists of non-trivial mechanical devices with multiple moving parts and a rather limited bandwidth. In comparison, semi-active systems are often based on damping control. This can be accomplished by magneto-rheological devices, which are able to rapidly change properties due to a small controllable electrical current. Semi-active and active control systems originate from applications on shock absorbers but can also be implemented for TMD applications. The principle of controllable shock absorbers is to create a force that at any increment of time counteracts the motion of the structure. In comparison, a TMD produces a force based on its natural frequency, which counteracts the corresponding frequency of the structure due to its phase shift.

Incremental time-frequency estimators

The tuning of a variable stiffness TMD is based on real time estimates of the frequency response of the structure. The two most common methods to accomplish this are the short time Fourier transform (STFT) and the short time wavelet transform (STWT). In both cases, the objective is to estimate the frequency response of a short time signal with duration t_w prior to the present time.

The STFT algorithm is based on a discrete Fourier transform, Eq. (17), facilitating the fast Fourier transform *FFT* available in Matlab (Matlab, 2009). Prior to Fourier transformation, the time signal is subjected to a Hann-window, Eq. (18) and then zero padded. Windowing will narrow the frequency content to a shorter time period and

improve continuity of the Fourier transform. Zero padding will increase the number of frequency line without adding additional information to the signal. This is useful in estimating the peak frequency but can optionally be performed by curve fitting of relevant peaks in frequency domain.

$$X(k)=\sum_{j=1}^{N} x(j)\omega_N^{(j-1)(k-1)},\ \omega_N=\mathrm{e}^{-2\pi i/N} \tag{17}$$

$$w(n)=\sin^2\left(\frac{\pi n}{N-1}\right) \tag{18}$$

The continuous wavelet transform is governed by Eq. (19), operating on the signal $x(t)$, * denotes the complex conjugate of the wavelet function. In this study, a Morlet wavelet is chosen as the mother wavelet, Eq. (20). The wavelet is modulated by a scaling parameter a and translation parameter b. Scaling can be seen as frequency modulation; lower scales compress the wavelet to obtain better resolution for higher frequencies, higher scales dilates the wavelet to obtain better resolution for lower frequencies. The translation parameter relates to time modulation. The time integral is normalized with $|a|^{-1/2}$ to produce the same energy for all scales. In further analysis, the 1-D continuous wavelet parameters are calculated by using the function *cwt* available in Matlab.

$$X_{\mathrm{w}}(a,b)=\frac{1}{\sqrt{|a|}}\int_{-\infty}^{\infty} x(t)\psi^*\left(\frac{t-b}{a}\right)dt \tag{19}$$

$$\psi(t)=C\mathrm{e}^{-x^2}\cos(5x) \tag{20}$$

The scale is not directly related to frequency but can be translated to pseudo-frequencies f_{w} by using the centre frequency f_{c} of the wavelet, the scale a and the sampling period Δt according to Eq. (21). This is performed by using the function *scal2frq* available in Matlab.

$$f_{\mathrm{w}}=\frac{f_{\mathrm{c}}}{a\Delta t} \tag{21}$$

Similar to the STFT method, the STWT operates on a short time signal prior to the present time to estimate the tuning frequency of the TMD. Although scaling the wavelet results in arbitrary frequency resolution, the accuracy still depends on the amount of data processed within the time window t_{w}. Increasing t_{w} results in better frequency estimation but is a trade-off on how rapid a change in frequency can be detected. To obtain a running frequency estimate, the above process is updated every dt increment of time to obtain one new tuning frequency based on the previous t_{w} period of time, $dt < t_{\mathrm{w}}$.

Numerical analysis of bridge dynamics

In this section, the numerical analysis of the case study bridge is presented, concerning the dynamic response during train passages. Firstly, the performance of the TMD-systems are demonstrated, both by calculating the steady state response and the transient response corresponding to a train passage. The routines for adaptive control and signal processing are developed in Matlab, the structural models are modeled and analyzed in the commercial FE-package SOLVIA03 (SOLVIA, 2008).

MDOF models, steady state

The potential of tuned mass dampers is demonstrated on hanger 5 of the case study bridge, using MDOF models. Assuming the hanger to be simply supported, the modal mass for the first mode of vibration is calculated using Eq. (4), resulting in m_1 = 135 kg. Further, using f_1 = 4.3 Hz and ζ = 0.15% results in k = 100 kN/m and c = 11 Ns/m. Due to the low damping, the resonant response is about 300 times greater than the static response.

The steady state response of the 2DOF model is shown in Fig. 8, based on Eq. (13). Introducing the TMD attenuates the frequency of the SDOF model but introduced two adjacent frequencies. For the case of no additional damping, these peaks are of about the same magnitude as the SDOF-model and the TMD results in a frequency shift without significant vibration attenuation. Due to the low existing damping of the primary structure, even a very low additional damping of the TMD attenuates the peaks significantly. The system is however sensitive to mismatch in frequency and a TMD with 5% detuned frequency shows a significant disimprovement. The steady state response of the pendulum models is identical to the 2DOF-model, provided that the frequency shift for the cantilever pendulum is accounted for.

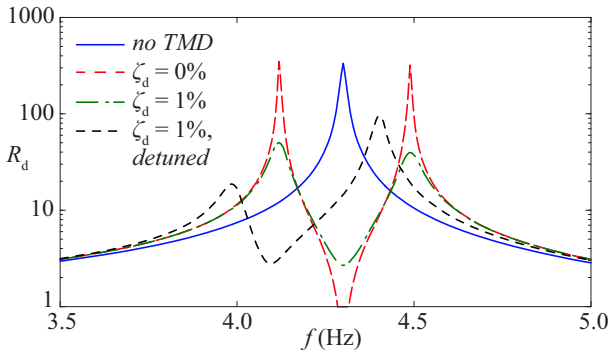

Fig. 8. Steady-state response of a passive 2DOF TMD damper, for detuned TMD: $f_{\mathrm{d}} = 0.95 f_1$.

The influence of the TMD mass ratio γ and damping ratio ζ_{d} are illustrated in Fig. 9 and Fig. 10, using Eq. (13). For low damping ratios, the mass ratio has moderate influence on the results and the steady state response is dominated by two peaks as in Fig. 8. For increased damping however, the response at f_1 will gradually increase while the adjacent peaks are attenuated. At a transition point, in the present study about 5% damping, the adjacent peaks will diminish and the response resembles the SDOF system. Beyond that point, the TMD gradually contributes in additional mass rather than a traditional TMD.

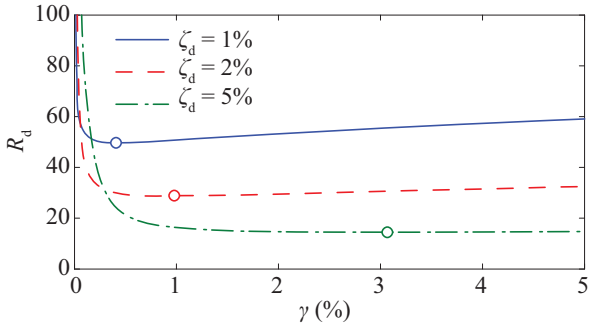

Fig. 9. Min-search for optimal damper mass ratio γ for different damping ratios, peak steady state response.

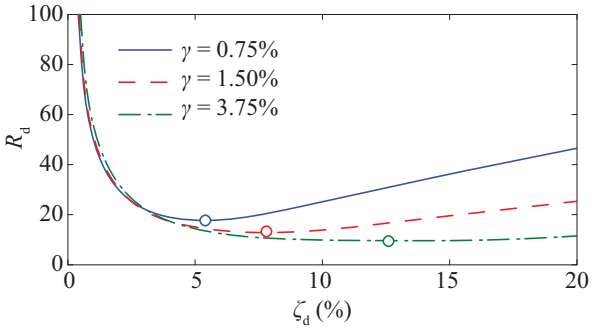

Fig. 10. Min-search for optimal damping ratio ζ_d for different mass ratios, peak steady state response.

MDOF models, transient dynamics

From field measurements, the magnitude of dynamic displacement of hanger 5 was estimated to 5 mm based on time integrated acceleration (Andersson & Malm, 2004), (Malm & Andersson, 2005). The duration of the train passage was only 10 s but the time to reach resonance is more than one minute. To obtain a dynamic displacement of 5 mm after 10 s, a harmonic load with F_0 = 4.5 N is required. At steady state, this corresponds to a displacement of about 15 mm. The MDOF-models are subjected to a harmonic loading with magnitude and duration as above and the response during both forced vibration and free vibration is studied. The analyses are performed by means of direct time integration using the solver in SOLVIA03. All models are verified by assuring that the steady state response calculated with SOLVIA03 produces the result as Eq. (13) for all cases presented in Fig. 8.

An adaptive TMD is modeled based on the 2DOF system in Fig. 7. The tuning frequency is estimated based on the displacement of the primary structure and is taken as the frequency of highest magnitude. The short time frequency content is estimated with both the STFT and STWT methods. The stiffness k_d is recalculated based on the new tuning frequency and the stiffness matrix updated correspondingly. For relatively low TMD damping, the highest frequency peak may correspond to a detuned state, since the preferable frequency is at a minimum, see Fig. 8. Depending on the loading frequency, the optimal tuning frequency may be difficult to determine. This may be worked around by using a time window and incremental update time that produces a sufficiently smooth frequency response. For the 2DOF models, setting both of these parameters to 4 s was found to produce the most reliable results. In addition, the Hann-window used in the STFT method is squared, producing a narrower band similar to a Chebychew window. It should be noted that the presented parameters were determined deterministically from a set of uni-variable analyses; other configurations may produce similar results.

The different TMD models are subjected to a transient loading block of a 10 s harmonic load. The influence of detuning and the performance of the adaptive algorithms are analyzed. Four cases are studied, denoted a) to d) in Table 4, f_1, f_d and f_F are the natural frequencies of the primary structure, the TMD and the load respectively. For all models, a mass m_d = 1 kg and damping ratio ζ_d = 1% are used for the TMD.

Table 4
Set of parameter studies for frequency variation of the MDOF models.

case	f_1 (Hz)	f_d (Hz)	f_F (Hz)
a)	4.30	f_1	f_1
b)	4.30	f_1	$0.95f_1$
c)	4.30	$0.95f_1$	f_1
d)	4.30	$0.95f_1$	$0.95f_1$

The peak displacement of the primary structure is presented in Fig. 11 for the studied models and cases. For the SDOF model, the target displacement of 5 mm is reached when f_1 = f_F, i.e. case a). A shift in load frequency by 5% results in a decreased response by more than a factor 5.

For a perfectly tuned TMD, the response is reduced by a factor of ~10. This extreme attenuation is a result of the low damping of the primary structure. If the load frequency is detuned by 5%, case b), a significant disimprovement is found and the response is about 70% larger than the corresponding SDOF model. Detuning the frequency of the TMD, case c), results in approximately a 30% larger response than case b) of the SDOF model. If the frequency of both the load and the TMD is detuned by the same amount, a response similar to a perfectly tuned TMD is obtained. This can be realized by comparing the steady state response in Fig. 8.

The cantilever pendulum model shows similar response to the 2DOF model for all studied cases. For the pinned pendulum however, a significant difference for case b) and c) is found, despite the resemblance at steady state. The cause for this is believed to be due to the nonlinear nature of pendulum dampers. For the transient dynamics, second order displacements must be accounted for to describe the dynamics of the pendulum. The pinned pendulum undergoes relatively larger motions than its cantilever counterpart and may be more susceptible to nonlinearities.

The adaptive routine is implemented on the 2DOF model and the performance using either the STFT or the STWT method for predicting the tuning frequency is studied. For case a) no tuning is needed and both adaptive models give the same result as the passive model. For a detuned load or damper frequency, case b) and c), the adaptive routines provide a significant improvement compared to the passive model. The STWT method is shown to produce the best tuning frequency with results comparable to the passive perfectly tuned case. For case d), the current adaptive routines are triggered to retune the frequency, resulting in higher vibration levels than the passive case.

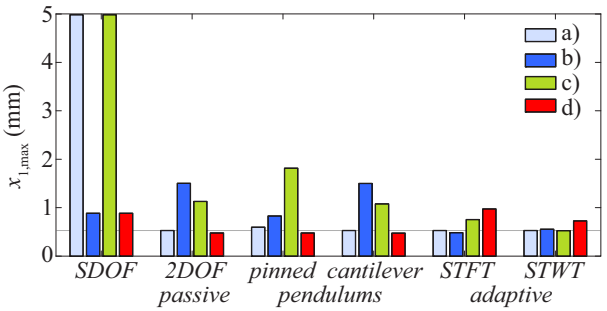

Fig. 11. Peak displacement of the primary structure for a transient loading, influence of frequency variation for different TMD models.

Bridge models

Both 2D and 3D FE-models of the case study bridge have been created, modeled in SOLVIA03. A view of the 3D-model is presented in Fig. 12. All structural components are modeled as Euler-Bernoulli beam elements, detailed in Fig. 13a. The upper end of the hanger is only constrained to the arch in translation, creating a pinned connection. The lower part of the hanger is rigidly connected to the main beam. All other intersections are modeled as fully rigid. The entire beam grillage is modeled in the same plane; the cross-sections are however defined with an offset to comply with the geometry of Fig. 2.

The existing pendulum dampers are modeled as detailed in Fig. 13b. Four nodal masses m_d are each lumped to the end of a beam element with stiffness EI_{rod}. The upper end of the pendulum rod is rigidly connected to the hanger, hence acting as cantilever pendulums. Additional damping is added via viscous dashpots c_d. When modeling the adaptive TMD, the lumped masses are instead connected to the hanger directly via spring elements in the xy-plane and following the vertical motion of the hanger.

A corresponding rationale 2D-model of the bridge is created, consisting of a symmetric half bridge in the y-direction. The cross beams are then modeled as vertical springs, with stiffness calculated on basis of a simply supported beam subjected to two point loads.

Passing trains are modeled as moving point loads applied directly to the stringer beams. In the 2D-model, only half the train load is applied, since only half the bridge is modeled.

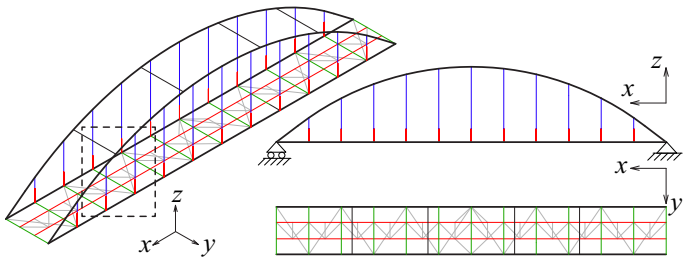

Fig. 12. View of the 3D-model of the bridge.

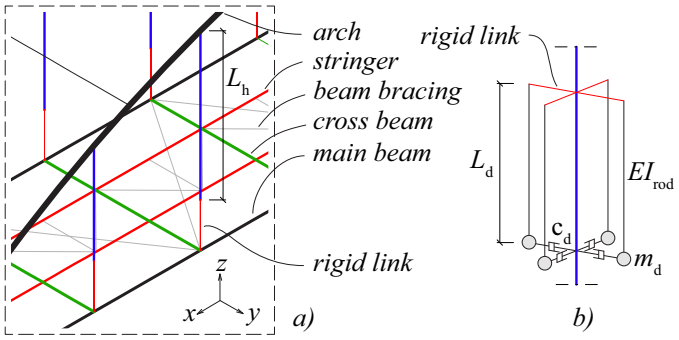

Fig. 13. Details of the 3D-model, a) beam components, b) detail of the pendulum damper.

Natural frequencies

The natural frequency of cables and hangers highly depend on the tensile force. For an Euler-Bernoulli beam, the relation between natural frequency f_n, flexural rigidity EI, mass m and axial force N follows Eq. (22), (Géradin & Rixen, 1997). For the pi-pinned case, $\mu_n = n\pi$, for the pinned-clamped case $\mu_1 = 1.25\pi$ is an approximation for the first mode of vibration.

Based on the 2D-model, the axial force in hanger 5 is about 20 kN due to permanent load and additional 120 kN due to a vertical train load with 225 kN/axle. This results in an increase in natural frequency from 4.5 Hz to about 7 Hz using Eq. (22).

$$f_n = \frac{\mu_n^2}{2\pi}\sqrt{\frac{EI}{mL^4}+\frac{N}{mL^2\mu_n^2}} \tag{22}$$

The natural frequencies of the bridge are calculated using an Eigen-value analysis. Forces due to permanent load are accounted for by a static analysis prior to the Eigen value extraction. Results from the 2D-model are presented in Table 5. Initially, the calculated frequencies for hanger 4 were $f_{1,x} = 5.4$ Hz and $f_{2,x} = 16.3$ Hz, which were in poor agreement with the measured data. The model was modified at this location, assuming the arch-to-hanger connection as fully clamped, with the result in Table 5. For the sake of comparison, this assumption is used in further analysis of the 2D-model. The corresponding hanger 8 of the same length is however unaltered. The two first global modes predicted by the 2D-model are presented in Fig. 14. The global modes excite several hangers simultaneously.

Table 5
Natural frequencies of the hangers due to permanent load, predicted by the 2D-model and a comparison with measured results.

	FEM		*FEM / measurements*	
Hanger	$f_{1,x}$ (Hz)	$f_{2,x}$ (Hz)	$f_{1,x}$ (–)	$f_{2,x}$ (–)
2	16.1	50.5	0.99	0.89
3	7.8	23.8	1.00	0.97
4	7.4	19.8	0.97	0.97
5	4.5	13.4	0.95	1.01
6	4.3	12.7	–	–

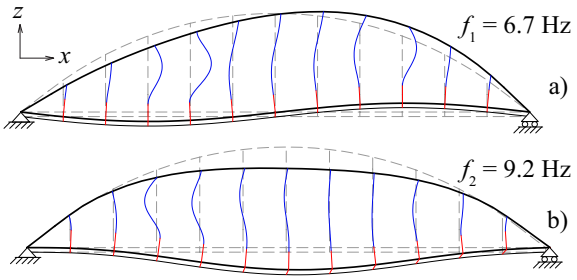

Fig. 14. The two lowest global modes of vibration, from the 2D FE-model.

For the corresponding 3D-model, the hanger frequencies are presented in Table 6. The results are generally in good agreement with the measured results in Table 3, the largest deviation is still found for hanger 4. In further analysis of the 3D-model, the boundary conditions of hanger 4 are not altered to fit measured data. The model gives about 300 modes in the range up to 50 Hz, of which about 100 modes are dominated by individual hangers. About 30 global modes are found, often exciting all hangers in different directions. The first global mode has a frequency of 2.1 Hz and consists of transverse bending of the arch. The first longitudinal bending mode of the bridge is found at 6.1 Hz, comparable with Fig. 14a. About 170 modes are mainly related to the secondary bracing system and are of little interest for the present study.

Table 6
Natural frequencies of the hangers due to permanent load, predicted by the 3D-model.

Hanger	$f_{1,x}$ (Hz)	$f_{2,x}$ (Hz)	$f_{1,y}$ (Hz)	$f_{2,y}$ (Hz)
2	16.6	50.1	11.5	40.9
3	8.1	24.2	5.8	19.4
4	5.7	16.6	5.6	16.6
5	4.7	13.4	3.5	11.2
6	4.5	13.0	3.4	10.6

Dynamic response from passing trains

The dynamic response from passing trains is modeled by means of vertical moving point loads applied directly to the stringer beams. The variation in tensile hanger force is accounted for by means of geometric nonlinearity. For this reason, a direct time integration using Newmarks method is adopted instead of modal superposition. Structural damping is included by using Rayleigh damping according to Eq. (23), assuming ζ = 0.15% at f_m = 4 Hz and f_n = 20 Hz. The final damping matrix is a linear combination of the mass- and the stiffness matrix, Eq. (24).

$$\begin{Bmatrix}\alpha\\ \beta\end{Bmatrix} = \frac{2\zeta}{\omega_m + \omega_n}\begin{Bmatrix}\omega_m\omega_n\\ 1\end{Bmatrix} \tag{23}$$

$$\mathbf{C} = \alpha\mathbf{M} + \beta\mathbf{K} \tag{24}$$

In a reference model, a freight train composed of one locomotive and 19 wagons is studied. Both the locomotive and the wagons consist of two axles per bogie. For the locomotive (Swedish Rc4), the axle distance is 2.7 m, the bogie distance 7.7 m, the total length 15.5 m and the load 195 kN/axle. Standardized freight train wagons are assumed according to load class D2. This corresponds to an axle distance 1.8 m, bogie distance 9.2 m, length 14.0 m and the load 225 kN/axle.

Due to the risk of resonance, the dynamic response highly depends on the speed of the train. Because of the low structural damping, the resonance peaks are expected to be very narrow. The speed of the train is varied from 30 km/h to 200 km/h in increments of 1 km/h. Near resonance, additional speed increments are introduced to assure that the peak response is captured. The allowable speed on the bridge is currently 110 km/h for freight trains and 140 km/h for commuter trains.

The influence of the train speed is illustrated in Fig. 15, comparing the peak to peak bending stress of hanger 5. There is a significant difference in response when comparing the longitudinal bending from the 2D and 3D-model, although the natural frequencies are similar. The resonance speed can be expressed as a function of the natural frequency f_0 and the load distance d according to Eq. (25). The load distance can be any of the distance between the axles, bogies, intermediate bogies or wagons, depending on the studied structural component. The resonance speed of 116 km/h from the 2D model is likely related to the global bending mode at 6.7 Hz, using the intermediate bogie distance of 4.8 m. An STFT-analysis of the time response at that speed also confirms that the forced vibration is dominated by the frequency at 6.7 Hz, dropping to 4.5 Hz during free vibrations. Similar analysis of the other hangers shows the same frequency during the loaded bridge, confirming the hypothesis that the global mode of the bridge is excited. Still, the stresses in adjacent hangers 4 and 6 are significantly lower than in hanger 5. One reason may be that the additional axial force during train passage increases the frequency of hanger 5 close to the load induced frequency, hence magnifying the response correspondingly. Similar understanding for the 3D-model is clearly more complicated due to significantly more combination of interacting modes.

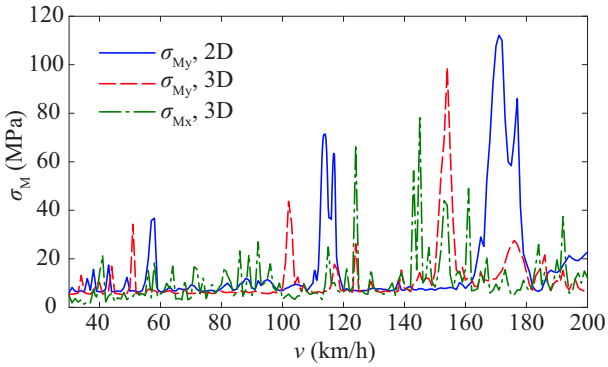

Fig. 15. Peak to peak bending stress in hanger 5 as function of the train speed, results from 2D and 3D model without external damping system.

$$v_i = f_0\lambda_i,\ \lambda_i = d/i,\ \ i = 1, 2, 3, \ldots \tag{25}$$

Fatigue assessment

Stress components

The excessive vibrations of the hangers constitute an increased risk of fatigue failure and the most critical part is the threaded section of the turn buckle, illustrated in Fig. 3. For threaded bolts and rods, a detail category $C = 50$ is to be used according to EN 1993-1-9 (CEN, 2005). This corresponds to a theoretical fatigue service life of 2×10^6 stress cycles at a constant stress range of 50 MPa. The detail category shall be multiplied with a stress intensity factor k_s according to Eq. (26) for rods of a diameter larger than 30 mm. It is also stated in EN 1993-1-9 that the stresses shall be increased by a safety factor $\gamma_{Mf} = 1.35$. In addition, the nominal diameter of the threaded section is 74 mm compared to the plain diameter of 80 mm. Since the total stress is composed of both axial force and bending moments, the corresponding stress concentration factors $k_{s2,N}$ and $k_{s2,M}$ are used according to Eq. (27).

For the case of bi-axial bending, it is not obvious which combination of axial force and bending moment result in the most critical stresses. Navier's equation for plane stress can be used to calculate the stresses along the perimeter of the hanger, in Eq. (28) also including the stress concentration factors for the threaded section.

$$k_s = (30/d)^{0.25} \tag{26}$$

$$k_{s2,N} = (d_{plain}/d_{nom})^2,\ k_{s2,M} = (d_{plain}/d_{nom})^3 \tag{27}$$

$$\sigma(\theta) = k_{s2,N}\frac{N}{A} \pm k_{s2,M}\frac{M_x}{I} r\sin(\theta) \pm k_{s2,M}\frac{M_y}{I} r\cos(\theta) \tag{28}$$

Eq. (28) has also been used to calculate the stress components from measured strain, instrumented according to Fig. 3d. The measured response of hanger 5 during passage of a freight train with 19 wagons is shown in Fig. 16. The results refer to nominal stresses without increase due to the threaded section. As a comparison, the corresponding response from the 3D-model is presented in Fig. 17. For the numerical model, all wagons are assumed fully loaded. Comparing the axial stress with the measured response indicates that several wagons were less loaded. For both cases, the stresses are dominated by transverse bending. Recalling Fig. 15 however indicates opposite proportions at different speeds. The stress magnitude is also found to differ significantly for small variation in train speed, owing to the resonant behavior and low structural damping.

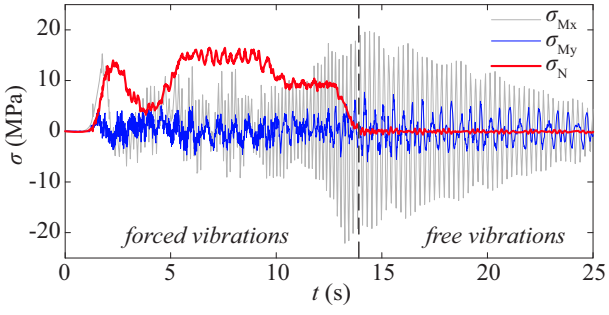

Fig. 16. Stress components in hanger 5 during a freight train passage, based on measured strains.

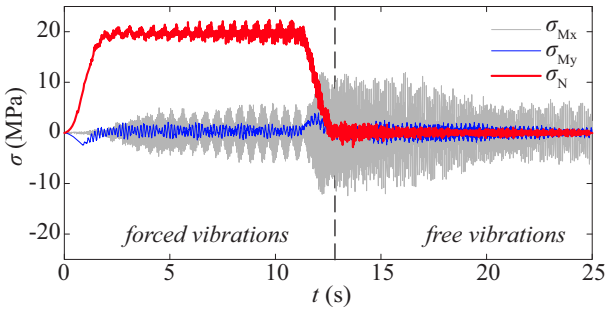

Fig. 17. Stress components in hanger 5 during a freight train passage, based on the 3D-model, $v = 92$ km/h.

Cumulative damage

The risk of fatigue is estimated based on Palmgren-Miners cumulative damage rule (Palmgren, 1924), (Miner, 1945), according to Eq. (29), where n_{Ei} is the number of stress cycles with a stress range $\Delta\sigma_{Ri}$ and N_{Ri} is the maximum number of stress cycles until failure for a constant stress range. According to the hypothesis of Palmgren-Miner, fatigue failure is obtained when $D_d = 1$.

The fatigue strength is governed by Eq. (30) according to EN 1993-1-9. For $N > 10^8$, the fatigue limit $\Delta\sigma_L$ is used. The stress collective is calculated using a Rainflow counting algorithm according to (Rychlik, 1987).

$$D_d = \sum_{i=1}^{n}\frac{n_{Ei}}{N_{Ri}} \tag{29}$$

$$\begin{aligned} &\Delta\sigma_R^m N_R = \Delta\sigma_C^m 2\times10^6, \quad m = 3, \qquad N \le 5\times10^6 \\ &\Delta\sigma_R^m N_R = \Delta\sigma_D^m 5\times10^6, \quad m = 5, \ 5\times10^6 \le N \le 10^8 \\ &\Delta\sigma_D = 0.4^{1/3}\Delta\sigma_C, \ \Delta\sigma_L = 0.05^{1/5}\Delta\sigma_D \end{aligned} \tag{30}$$

The cumulative damage is calculated as a function of the angle along the perimeter of the hangers. For the train passage related to Fig. 16 and Fig. 17, a polar representation of the cumulative damage is presented in Fig. 18. For hanger 2, the stresses are dominated by the axial force, resulting in a rather evenly distributed damage. For hanger 5 however, the damage is clearly dominated by the transverse bending.

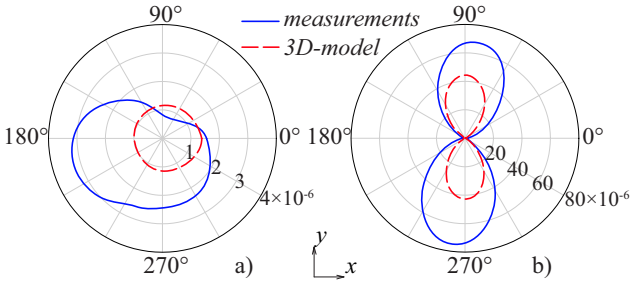

Fig. 18. Cumulative damage distribution along the perimeter of a) hanger 2, b) hanger 5, during one freight train passage. Note the different scales of damage.

Fragility curves

Recalling Fig. 15, the bending stresses were found to be highly sensitive to the train speed due to resonant behavior. Estimations of the cumulative damage depend on the stresses

to the power of 3 or 5, Eq. (30) and is consequently significantly more sensitive to the train speed than the stresses. To deal with this uncertainty, fragility curves are adopted.

Fragility curves describe the conditional probability of reaching a certain limit state. If the limit state *LS* is a continuous function of a demand x, the probability can be expressed as a convolution integral according to Eq. (31), where $F(x)$ is the fragility function and $g(x)$ is the hazard function. $F(x)$ is on the form of a cumulative distribution function and $g(x)$ as a probability density function. (Lee & Rosowsky, 2005)

$$P[LS] = \int_0^\infty F(x)g(x)dx \tag{31}$$

The fatigue service life depends on the variation in both loading and resistance. The fatigue strength is assumed constant and the Palmgren-Miners hypothesis is adopted, hence the resistance is regarded as deterministic. Further, the variation in loading is regarded only due to variation in train speed, keeping all other parameters constant. The same freight train is used that produced the response in Fig. 17.

In (Leander et al., 2010), the variation of the train speed at a bridge with predominantly commuter trains was estimated based on an extreme value distribution. A noticeable part of the trains were found to travel at a significantly lower speed than allowed, possibly due to traffic congestions. Also, several trains were estimated to run faster than the allowable speed. To account for these events, a tri-linear probability density function (PDF) is constructed according to Eq. (32), illustrated in Fig. 19. The main reason for including the lower tail of the distribution is that the FE-models predict resonance peaks at even low speeds, as seen in Fig. 15. The proportions of the PDF are selected to a similar shape as in (Leander et al., 2010). The maximum allowable speed at the location of the bridge is 110 km/h for freight trains and 140 km/h for commuter trains. In further analysis, a = 30 km/h, b = 60 km/h, c = 110 km/h, d = 120 km/h and p_{ab} = 5% is used.

$$g(x|a,b,c,d) = \begin{cases} 0 & x < a \\ p_1 \dfrac{x-a}{b-a} & a \le x \le b \\ p_1 + (p_2 - p_1)\dfrac{x-b}{c-b} & b < x \le c \\ p_2 \dfrac{x-d}{c-d} & c < x \le d \\ 0 & d < x \end{cases} \tag{32a}$$

$$p_1 = \frac{2}{b-a} p_{ab}, \quad p_2 = \frac{2}{b-a}\frac{a-b-p_{ab}(a-c)}{b-d}, \quad p_{ab} = p(x \le b) \tag{32b}$$

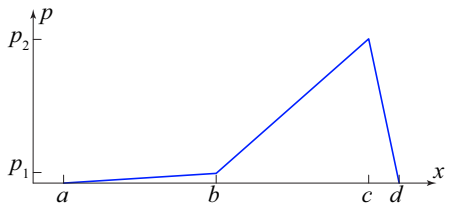

Fig. 19. Tri-linear probability density function for the train speed.

Fragility curves are calculated as the cumulative sum of the damage at different speeds multiplied with its probability of running at that speed.

Results based on the 2D-model are shown in Fig. 20, presented as damage per train passage. The steep slope of the fragility curves in Fig. 20a shows that the damage is relatively insensitive to the train speed for P<0.8 and that the shorter hangers are more prone to fatigue. For P>0.8 however, the damage increases rapidly due to the influence of resonant behavior and Fig. 20b shows the largest risk of fatigue for the longer hangers.

The effect of different damping systems and the resulting cumulative damage is studied for hanger 5 in Fig. 21. For all models, m_d = 1 kg and ζ_d = 1% is used. The pendulum damper and the passive TMD produce comparable results. The dampers are tuned to the first natural frequency of the unloaded hanger. During train passage, the natural frequency of the hangers increase due to increased tensile force. In addition, global frequencies of the bridge influence the hangers. This causes the passive systems to be detuned and the reduction in vibration is mainly due to the free vibrations. For the adaptive TMD however, a significant reduction is obtained both off resonance, Fig. 21a, and near resonance, Fig. 21b.

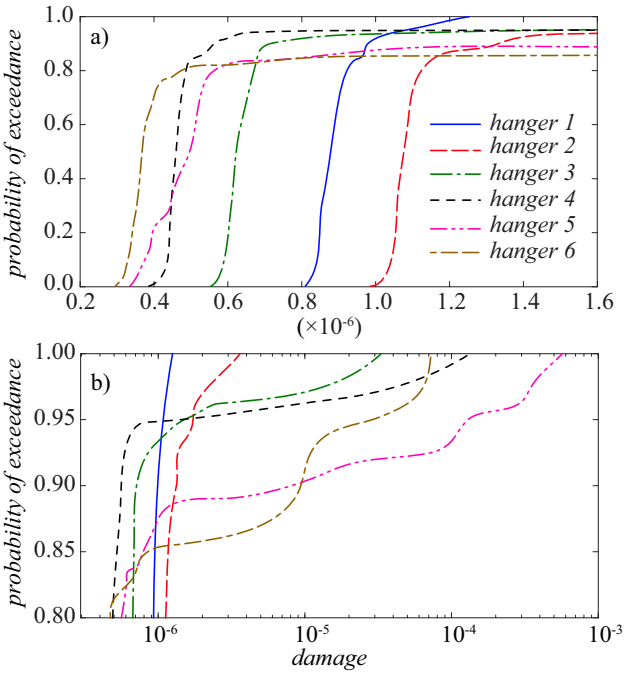

Fig. 20. Fragility curves for cumulative damage, 2D-model without damping systems, a) range 0<P<1, b) range 0.8<P<1 (log scale).

As was illustrated in Fig. 18, biaxial bending causes different cumulative damage at different angles along the perimeter of the hanger. When producing fragility curves based on stresses from the 3D-model, individual curves for different angles are calculated. The results for hanger 5 are presented in Fig. 22. The results are clearly influenced by transverse bending and a 45° angle appears to be most critical. The fatigue service life is assumed to be governed by the first crack and the resulting fragility curve is calculated as the envelope of fragility curves at different angles.

The resulting fragility envelopes are presented in Fig. 23. Similar to the 2D-model, the cumulative damage increases rapidly beyond a certain probability threshold, Fig. 23a. For hanger 4 and hanger 6, this threshold occurs at a lower probability of exceedance, i.e. shows a greater risk of fatigue. These hangers also show the greatest extremes, Fig. 23b.

Both the 2D-model and the 3D-model show great scatter in estimated rate of cumulative fatigue damage. For non-resonant loading, the fatigue damage is generally low and the remaining service life is significant. For resonant loading however, the immense increase in fatigue damage show a total service life corresponding to only a few thousand train passages.

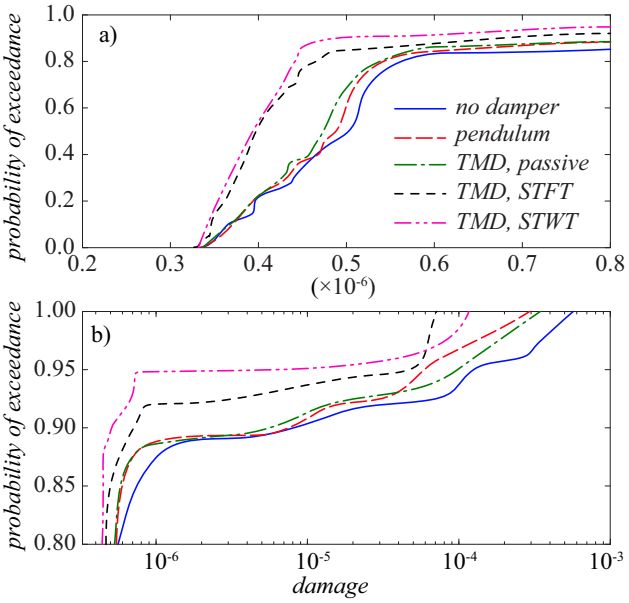

Fig. 21. Fragility curves for cumulative damage in hanger 5, 2D-model with different damping systems, a) range $0<P<1$, b) range $0.8<P<1$ (log scale).

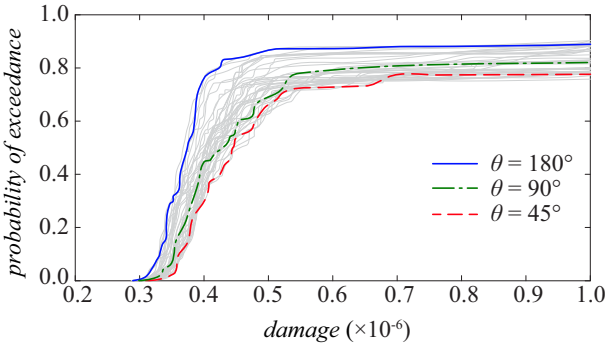

Fig. 22. Fragility curves for cumulative damage in hanger 5, 3D-model without damping systems.

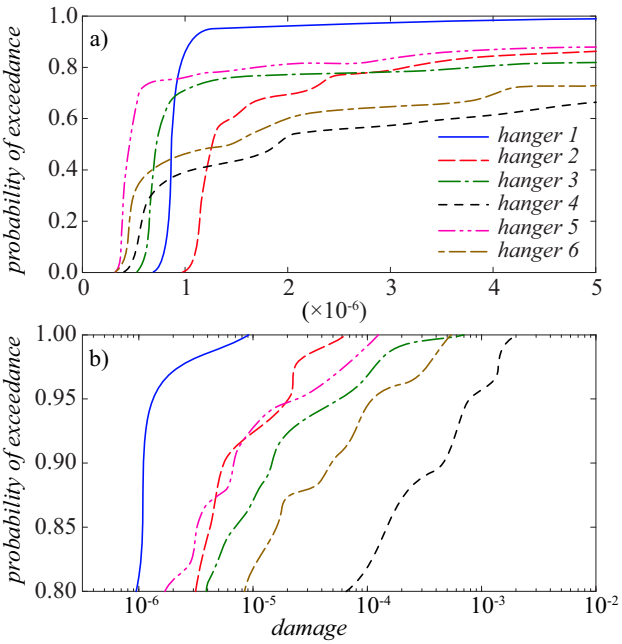

Fig. 23. Fragility curves for cumulative damage, 3D-model without damping systems, a) range $0<P<1$, b) range $0.8<P<1$ (log scale).

Conclusions

In the present paper, the use of passive and adaptive damping systems for mitigation of railway bridge dynamics have been studied using numerical simulations. Passive dampers are often sensitive to detuning and even a small change in either load frequency or natural frequency may result in a significant disimprovement. Based on MDOF-models, a variable stiffness TMD is demonstrated to significantly improve the performance during off-tuned conditions.

The performance of different damping systems is further studied on a case study bridge. The bridge is prone to resonance during train passage and excessive stresses result in a reduced fatigue service life. The behavior has been partly confirmed with field measurements. During train passage, the increased axial force in tensile members results in a change in natural frequency. In addition, the resulting stresses are highly influenced of both longitudinal and transversal bending, each having different natural frequencies. As a consequence, the dynamic response is very sensitive to the loading and the train speed. A probability density function for the train speed is assumed and the resulting cumulative damage is presented by means of fragility curves. The results show that for a probability of exceedance $P<0.8$, the fatigue damage is generally low, resulting in a sufficient remaining fatigue service life. For $P>0.8$ however, extreme increases in fatigue damage is obtained, allowing for only a few thousand train passages.

The use of passive dampers tuned to the frequency of the unloaded bridge is shown to have moderate influence on the vibration mitigation. The main reason is that the dampers are partly detuned during forced vibrations, initially starting at a high level of free vibration. The vibration mitigation is greatly improved using an adaptive damper, being able to work efficiently during both forced and free vibrations. As a result,

the initial level of free vibration is lower compared to the case of the passive damper reducing the overall fatigue damage.

Acknowledgements

The field measurements in 2003 were commissioned by the Swedish Transport Administration (former Banverket) and performed by KTH. Additional analysis and the development of routines for adaptive vibration damping were performed within the Long Life Bridges project, a Marie Curie Industry-Academia Partnerships and Pathways project funded by the European Commission 7th Framework Programme (IAPP-GA-2011-286276). All funding and support mentioned above is greatly acknowledged.

References

Andersson, A., Malm, R. (2004). Measurement Evaluation and FEM Simulation of Bridge Dynamics. *MSc Thesis, KTH Royal Institute of Technology, Sweden*.

Brock, J.E. (1946). ASME A, 284. A note on the damped vibration absorber.

CEN (2005). Eurocode 3: Design of steel structures – Part 1-9: Fatigue. *EN 1993-1-9:2005*.

Chopra, A.K. (2001). Dynamics of Structures, Theory and Application of Earthquake Engineering. *Prentice-Hall Inc, 2nd Edition*.

Clough, R.W., Penzien, J. (2003). Dynamics of Structures. *Computers & Structures, Inc, 3rd edition*.

Den Hartog, J.P. (1947). Mechanical Vibrations. *McGraw-Hill, 3rd edition*.

Géradin, M., Rixen, D. (1997). Mechanical Vibrations, Theory and Application to Structural Dynamics. *John Wiley & Sons, 2nd edition*.

Hortmanns, M., Schäfer, N. (2005). Ljungan Bridge, Ånge Sweden – Full Scale Measurements. *Technical report, Prof. Sedlacek & Partner (unpublished)*.

Hortmanns, M. (2005). Ljungan Bridge, Ånge Sweden – Design of dampers for the hangers 3 to 6. *Technical report, Prof. Sedlacek & Partner (unpublished)*.

Irvine, T. (2011). Bending frequencies of beams, rods and pipes. *Vibrationdata Publications, Rev. P*.

Leander, J., Andersson, A., Karoumi, R. (2010). Monitoring and enhanced fatigue evaluation of a steel railway bridge. *Engineering Structures 32(3)*.

Lee, K.H., Rosowsky, D.V., (2005). Fragility assessment for roof sheathing failure in high wind regions. *Engineering Structures 27(6)*.

Liedes, T. (2009). Improving the performance of the semi-active tuned mass damper. *PhD-Thesis, University of Oulu, Finland*.

Malm, R., Andersson, A. (2006). Field testing and simulation of dynamic properties of a tied arch railway bridge. *Engineering Structures 28(1)*.

Matlab (2009). MATLAB 2009b Reference manual. *The MathWorks, Inc*.

Miner, M.A. (1945). Cumulative damage in fatigue. *Journal of Applied Mechanics, 23(1)*.

Ormondroyd, J., Den Hartog, J.P. (1928). The theory of the dynamic vibration absorber. *ASME, Journal of Applied Mechanics 50*.

Palmgren, A. (1924). Die Lebensdauer von Kugellagern. *VDI Zeitschrift, 68(14)*.

Rychlik, I. (1987). A new definition of the rainflow cycle counting method. *International Journal of Fatigue, 9(2)*.

SOLVIA (2008). SOLVIA-PRE for Stress Analysis, User Manual. *Report SE 03-1, SOLVIA Finite Element Systems Version 03*.

Tsai, H.-C., Lin, G.-C. (1994). Explicit formulae for optimum absorber parameters for force-excited and viscously damped systems. *Journal of Sound and Vibration 176(5)*.

Paper V.

Development and Testing of a Bi-directional Multi-Passive Tuned Mass Damper

Andreas Andersson, Alan O'Connor, Raid Karoumi

(Journal paper. submitted to ASCE Journal of Structural Engineering, February 2013)

Development and Testing of a Bi-directional Multi-Passive Tuned Mass Damper

Andreas Andersson[a,c,d], Alan O'Connor[a,b], Raid Karoumi[c]

[a]*Roughan & O'Donovan Innovative Solutions (ROD-IS), Arena House, Arena Road, Sandyford, Dublin 18, Ireland*
[b]*Trinity College Dublin (TCD), Department of Civil, Structural and Environmental Engineering, Dublin, Ireland*
[c]*Royal Institute of Technology (KTH), Brinellvägen 23, SE-100 44 Stockholm, Sweden*
[d]*The Swedish Transport Administration (Trafikverket), Solna Strandväg 98, SE-171 54 Solna, Sweden*
email: Andreas.Andersson@byv.kth.se, Alan.OConnor@rod.ie, Raid.Karoumi@byv.kth.se

Abstract: This paper presents the development and testing of a bi-directional multi-passive tuned mass damper (bi-MTMD). A prototype of the damper has been built and tested under laboratory conditions. The damper was developed for application to a vertical hanger on an existing tied-arch railway bridge. During train passage, resonance has been observed in several hangers, resulting in a reduction in the predicted fatigue service life. The objective of the damper is to mitigate the vibrations to reduce the resulting stresses and consequently to extend the life of the hanger. The hanger has different natural frequencies for longitudinal and transversal bending. In addition, a significant difference in natural frequency is obtained for the loaded and unloaded bridge, due to the increase in axial force in the hangers. The developed damper accounts for both scenarios and is tuned based on previous field measurements. The results from the laboratory experiments are compared with a 3D FE-model of the damper.

Keywords: Tuned mass damper; Bi-directional damper; experimental testing; frequency response function; railway bridge.

Introduction

Vibration mitigation by the use of external damping systems may be a feasible solution for structures subjected to excessive dynamic response and loading. For railway bridges, the combination of heavy trains and equally spaced axles may induce resonance that for bridges with low structural damping can result in excessive vibrations and stresses.

One of the most common systems of external damping is the tuned mass damper (TMD). The theory of the TMD was first established by (Ormondroyd & Hartog, 1928) and much research has been devoted since to finding configurations for optimal vibration mitigation. The concept of a TMD is to suspend a mass on an existing structure. The inertia force of the suspended mass will counteract the motion of the main structure due to a frequency phase shift. The TMD will only operate efficiently if properly tuned to a relevant frequency of the structure. A detuned damper may cause larger vibrations than the corresponding case without any damper. The effective bandwidth of the damper may be increased by the use of multiple tuned mass dampers (MTMD). Studies by (Igusa & Xu, 1994) concludes that a MTMD-system can be optimally designed for wide-band input if the dampers are distributed over a frequency range centered at the main oscillator natural frequency. Introducing viscous damping to the TMD may also improve the vibration mitigation. In (Jangid, 1999), numerical search techniques were used to find optimal parameters of a MTMD-system. It was concluded that the optimal damping ratio decreases with the number of dampers and increases with the mass ratio. It was also concluded that the optimum bandwidth increases with both the mass and number of dampers. MTMD-systems can also be used to suppress several modes of vibration, as shown by (Luu et al., 2012) for applications on high-speed railway bridges. It can also be used as a combination of several wide-band dampers, as shown in (Yau & Yang, 2004). A more extensive summary of MTMD-systems can be found in (Varadarajan, 2005).

If vibrations are expected in different directions, bi-directional TMDs may be an alternative to MTMD-systems. Studies by (Lin et al., 2010) conclude that it is easier to find the optimal parameters for a bi-directional TMD compared to a MTMD. In (Ankireddi & Yang, 2000), the performance of uni-directional, bi-directional and tri-directional TMDs is compared. It is found that the bi-directional and tri-directional TMD is independent of the excitation direction and have a better control performance than a single uni-directional damper.

Theoretical models and analysis

Background

The damper presented in this paper was developed for a specific bridge that has previously been found to be susceptible to resonance. The bridge is designed as a tied arch railway bridge to carry a single track. During train passages, several vertical hangers were found to experience resonance. Due to very low structural damping, the resulting stress collective has been shown to significantly decrease the fatigue service life. From field measurements, as much as 50% of the cumulative damage was related to free vibrations after train passages (Malm & Andersson, 2006). The developed damper has been tuned to one of the hangers shown to experience significant resonant behavior, denoted hanger 5. From free vibration tests, the first natural frequency of the hanger was estimated to 4.3 Hz for the longitudinal bending (x-direction) and 3.6 Hz for the transverse bending (y-direction). The corresponding damping was estimated to be about 0.2%. During train passage, the natural frequency increased by about 50% in both directions, due to increased axial force. More details of the bridge and previous studies are reported in (Malm & Andersson, 2006), (Andersson et al., 2013) and (Andersson & Malm, 2004).

FE-model of the bi-MTMD

To mitigate the vibrations and reduce the stress ranges in fatigue critical sections, a bi-directional multi-passive tuned mass damper (bi-MTMD) is proposed. The concept of the damper is to account for both longitudinal and transverse vibrations, for both the unloaded and loaded hanger.

A 3D FE-model of the damper is illustrated in Fig. 1. The model and analysis is performed using the commercial FE-software SOLVIA03 (SOLVIA Engineering, 2008). The mass consists of two steel rings, suspended by wires and connected in series. The rings and wires are modeled with Euler-Bernoulli beam elements. In the FE-model, the mass was connected to the hanger via lateral springs and dashpots, as well as via the upper rigid links. For comparison with experimental tests, a base plate with mass m_b, stiffness k_b and damping c_b was included in the FE-model. The dynamic properties of the base plate were determined from experiments and are described by Eq. (1), where ζ_b is the damping ratio of the base plate.

Each ring has a weight of 2.3 kg. The outer diameter is 170 mm, the inner diameter 150 mm and the height 50 mm. The free suspended length is L = 110 mm. The length is chosen to be sufficiently long so as not to cause significant coupled modes between the two rings. The wires consist of a 2 mm nylon string, modeled with a Young's modulus of 2 GPa. Due to the wire suspension, the damper is essentially a combination of a regular tuned mass damper and a pendulum damper. The lower ring is tuned to the fundamental natural frequencies of the unloaded hanger. The upper hanger is tuned to the loaded bridge conditions, assuming a 50% increase in the natural frequency of hanger 5.

$$k_b = m_b \omega_b^{\,2}, \quad c_b = 2\zeta_b \sqrt{k_b m_b} \tag{1}$$

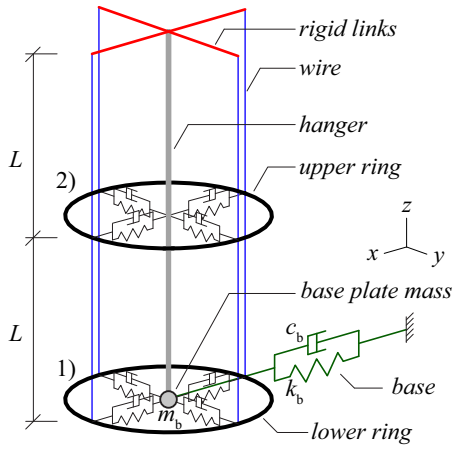

Fig. 1. 3D FE-model of the damper.

Frequency domain methods

The dynamic characteristics of the damper depend both on the lateral motion and the pendulum motion. Both rings are also slightly coupled. The stiffness for each component of the damper is initially estimated as being similar to Eq. (1), followed by a numerical iteration using an Eigen-value analysis. The four translational modes of vibration are illustrated in Fig. 2.

The equation of motion can be expressed in the form of Eq. (2), where **M**, **C**, **K** are the mass, damping and stiffness matrices respectively and **F** is the force vector. The frequency response function (FRF) is then found by solving for the frequency dependent displacement vector $\mathbf{x}(\omega)$, for each prescribed circular frequency ω (Clough & Penzien, 2003).

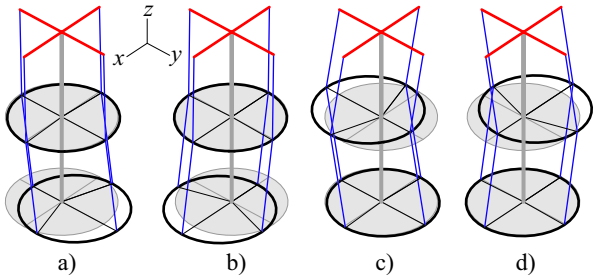

Fig. 2. The first four translational Eigen-modes, based on the FE-model excluding the base plate.

$$\left(-\omega^2\mathbf{M} + i\omega\mathbf{C} + \mathbf{K}\right)\mathbf{x}(\omega) = \mathbf{F} \tag{2}$$

Time domain dynamics

In addition to the FRF, the response to harmonic load blocks is studied. The purpose is to simulate the induced load from passing trains. Each load block is described by Eq. (3a), where the static load is determined from a prescribed steady-state displacement d_{dyn}, Eq. (3b-c), where R_d is the dynamic amplification factor.

$$F(t) = F_0 \sin \omega t \tag{3a}$$

$$F_0 = k_b d_{stat} = k_b d_{dyn} R_d^{\,-1} \tag{3b}$$

$$R_d = \frac{1}{2\zeta_b \sqrt{1-\zeta_b^{\,2}}} \approx \frac{1}{2\zeta_b} \tag{3c}$$

The dynamic analysis is performed using direct time integration according to Newark's scheme, Eq. (4) (Chopra, 2001). In addition, large displacements are accounted for, resulting in a nonlinear dynamic analysis. This is solved using a Newton-Raphson iteration at each time increment. In nonlinear dynamics, abrupt forced vibration at resonance frequency may cause transient response and convergence problems. This is attenuated by applying a smooth transition at the start and the end of the load block. The transition zone is set to 0.2 s and follows a √x curve. Additional numerical damping is introduced by using the Hilber-Hughes-Taylor α-method, Eq. (5) (Chopra, 2001). In the analysis, α = –0.05 is employed.

$$\begin{aligned} \dot{u}_i &= \dot{u}_{i-1} + (1-\gamma)\Delta t \ddot{u}_{i-1} + \gamma \Delta t \ddot{u}_i \\ u_i &= u_{i-1} + \Delta t \dot{u}_{i-1} + (1/2-\beta)\Delta t^2 \ddot{u}_{i-1} + \beta \Delta t^2 \ddot{u}_i \end{aligned} \tag{4}$$

$$\gamma = (1-2\alpha)/2\,, \quad \beta = (1-\alpha)^2/4\,, \quad \alpha \in [-1/3, 0] \tag{5}$$

Damping estimators

Several methods for estimating damping exist. In this study, the Half-Power Bandwidth method (HPB) is used. The HPB-method operates on the frequency domain, and a

bandwidth Δf is calculated for a 3dB decrease of the frequency response, corresponding to $Q/\sqrt{2}$ in Fig. 3 (De Silva, 2007). The frequency lines are in direct proportion to the time length of the signal. For short signals, the frequency resolution may result in poor estimation of both frequencies and damping. The resolution in frequency domain may be increased by zero-padding. A more accurate estimate of the damping may also be obtained by curve fitting of the resonance peak. The damping is given by Eq. (6).

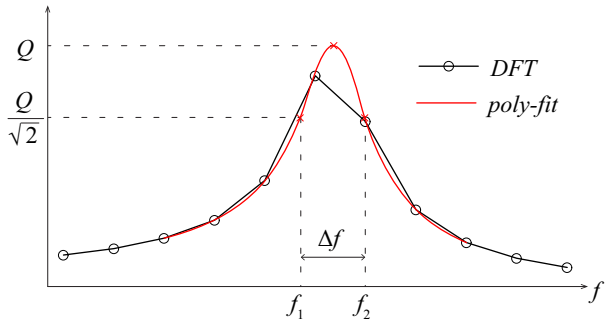

Fig. 3. Illustration of the HPB-method.

$$\zeta = \frac{f_2 - f_1}{f_2 + f_1} \tag{6}$$

Experimental work

Experimental setup and instrumentation

The development and experimental verification of the damper was performed at Trinity College Dublin, Department of Civil, Structural and Environmental Engineering. A photo of the damper and the experimental setup is presented in Fig. 4. Each steel ring (mass) is suspended by nylon wires and mounted to a hollow steel tube which is an accurate representation of the hanger. The steel tube is fastened to a sliding base plate and connected to a load shaker. The total mass of the base plate and the steel tube is 5.3 kg. Accelerometers a_1 and a_2 are mounted on the lower and upper steel rings respectively. The base plate is instrumented with a load cell F, accelerometer a_b and displacement transducer d_b. The sensor specifications are given by Table 1.

Table 1
Sensor specifications.

sensor:	*make:*	*range:*
a_1 ,a_2	*Entran EGCS-A2*	±2g
a_b	*Sensotec 060-F482-02*	±5g
F	*Vishay, Model 615*	±50 kg
d_b	*Sangamo DC25 LVDT*	±25 mm

The laboratory equipment consists of the following:

- *LDS V455 Electro-dynamic shaker.*
- *LDS PA1000L Linear Power Amplifier.*
- *Tektronix TDS 210 Oscilloscope.*
- *TGA1241 waveform generator.*
- *Vishay 7000-32-SM data acquisition system (24 bit).*

The load shaker is powered by the linear power amplifier; the load is controlled by the oscilloscope and the waveform generator. All sensors were connected to the same data acquisition system. The data logger has an input voltage of ±10V and all sensors have an output voltage of ±5V. Data is collected with a sampling frequency of 200 Hz.

A schematic section of a half ring is illustrated in Fig. 5. The coil springs are connecting to the steel ring by vertical steel plates in one end and to a hose clamp in the other end. The hose clamp is then tightened to the hanger. The coil springs are made of 0.9 mm steel wires and coiled to specific requirements to obtain the target frequencies. A foam material is placed between the ring and the hanger in the x-direction and is only fixed in place by the intersecting coil spring.

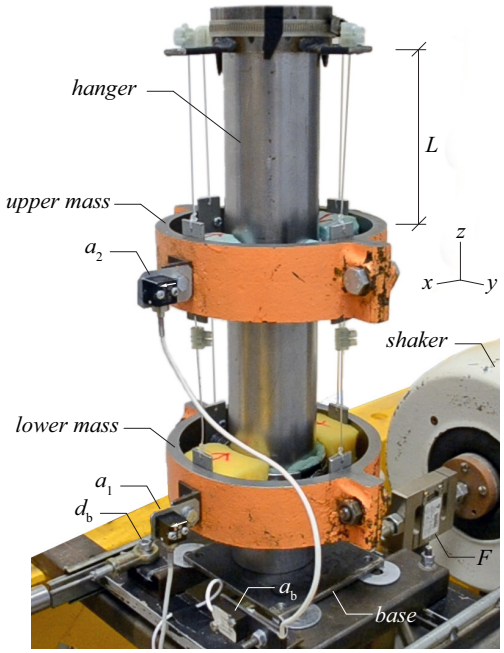

Fig. 4. View of the prototype damper and instrumentation.

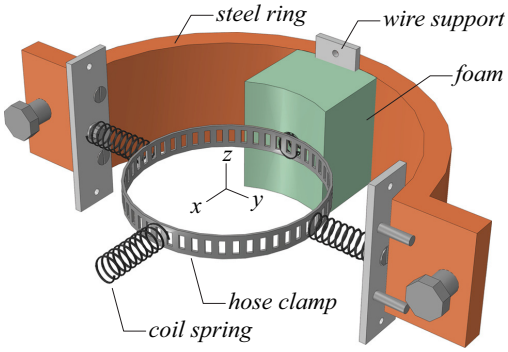

Fig. 5. Sketch of the model, detail of a half ring.

Signal quality

The quality of the measured signal depends both on the level of electrical disturbances and the effective data resolution. Electrical disturbances are often dominated by specific narrow-band frequencies, e.g. 50 Hz AC-current, and can often be successfully removed by stop-pass filtering. For the current case, only frequencies in the range

1 – 10 Hz are of interest, and all signals are therefore subjected to a corresponding band-pass filter. The main reason for removing lower frequencies is due to the performance of the load shaker in that frequency range.

The effective data resolution depends on the ratio between the input and output voltage. The signal quality due to data resolution may also be improved by filtering, similar to averaging. For a bipolar voltage range, the data resolution is governed by Eq. (7) and the corresponding effective bit-resolution is given by Eq. (8) (Lockhart, 2009).

The signal quality is evaluated based on ambient vibrations in the laboratory environment. The effective resolution and standard deviation is presented in Table 2. The effective resolution is estimated based on unique data increments of the measured signal. The quality is considered to be sufficient for further data processing and analysis.

$$Q = \frac{v_{\text{in}}}{v_{\text{out}}\, 2^{\text{n}-1}} E \tag{7}$$

$$n_{\text{eff}} = -\ln\left(\frac{v_{\text{out}}}{v_{\text{in}}} \frac{Q_{\text{eff}}}{2E} \right) \ln(2)^{-1} \tag{8}$$

v_{in} = *full-scale input voltage range of the data logger*,
v_{out} = *full-scale output voltage range of the sensor*,
E = *full-scale output in engineering unit*,
n = *ADC bit-resolution*.

Table 2
Effective data resolution, based on ambient measurements. The standard deviation is based on a signal subjected to a 1–10 Hz band-pass filter.

sensor:	Q_{eff}*:*	*std:*	n_{eff} (bit)
F (N):	0.24×10^{0}	0.030×10^{0}	17.3
a_1 (m/s^2):	0.40×10^{-3}	0.159×10^{-3}	18.9
a_2 (m/s^2):	0.40×10^{-3}	0.278×10^{-3}	18.9
a_{b} (m/s^2):	1.08×10^{-3}	7.468×10^{-3}	17.5
d_{b} (mm):	0.39×10^{-3}	0.052×10^{-3}	17.6

Results

In the following section, results from both steady-state analysis and harmonic load blocks are presented. The analysis and signal processing has been performed in Matlab (MathWorks, 2009). The results from the laboratory work are used for updating the FE-model, which is subsequently to be employed in a global bridge model.

Time integration

It is of interest to estimate the dynamic displacement of both the base and the damper from the experiments. This is performed by integrating the measured acceleration, using Eq. (4). The parameters $\gamma = 1/2$ and $\beta = 1/4$ are used, corresponding to the trapezoidal rule. When integrating measured signals, the results will drift due to the presence of noise. The drift can be regarded as a low frequency response and is removed by high-pass filtering after each integration. If the trends overlap structural frequencies, difficulties in determining the total displacements occur.

To study the performance of the sensors, a separate test of only the base plate is performed, instrumented with all accelerometers. The response from a 5 Hz constant sine wave with 5V input gain is analyzed. The gauge factor for the load shaker is about 1 mm/V. The steady-state response of the base plate is presented in Table 3. For a measured acceleration amplitude A = 5 m/s^2 at 5 Hz, a displacement of $A/\omega^2 \approx 5$ mm is expected. The integrated acceleration of each individual accelerometer is within 2% of the expected displacement. The acceleration can be obtained by differentiating the measured displacement of the LVDT, without any need of filtering. The acceleration can also be obtained from the load cell, provided a known mass of the base plate. The standard deviation refers to the amplitude at steady-state.

The dynamic characteristics of the base plate are studied by applying a variable frequency sine sweep load. With a base mass of 5.3 kg, a resonant frequency at 9 Hz with 32% damping is estimated. The dynamics of the load shaker may be more accurately described using electro-mechanical models, e.g. (Ricci et al., 2009). In (Kraaij, 2008), dynamic parameters for the same load shaker as the present study are determined from experiments.

Table 3
Comparison of output response, 5 Hz sine wave with 5V input gain, all sensors mounted on the base plate, with the damper removed.

	peak:	*std:*		*peak:*	*std:*
a_1 (m/s^2):	5.38	0.36	$\iint a_1$ (mm):	5.35	0.03
a_2 (m/s^2):	5.62	0.38	$\iint a_2$ (mm):	5.60	0.04
a_{b} (m/s^2):	5.23	0.35	$\iint a_{\text{b}}$ (mm):	5.21	0.05
$\text{d}^2/\text{dt}^2\, d_{\text{b}}$ (m/s^2):	5.43	0.32	d_{b} (mm):	5.44	0.29
F/m_{b} (m/s^2):	5.16	0.39			

Frequency response function

The dynamic characteristics of the damper can be studied by the frequency response function (FRF) of the measured response. An input load with linearly variable frequency and constant amplitude is sent to the load shaker via the oscilloscope and the linear power amplifier. A 10 min sweep is performed with a 3V input gain and a frequency range from 2 to 10 Hz and then back to 2 Hz. Near resonance, the contributing mass of the damper influences the response of the load shaker, resulting in nonlinear variation of both the input force and the base displacement. To account for this, all results are normalized with respect to a unit base displacement. The corresponding transfer function is calculated as the time domain response of the single sided Fourier transform of the measured base displacement.

The displacement of the damper is estimated based on time integration of the corresponding acceleration. The FRF is obtained directly from the peaks of the resulting time response. A comparison between the FRF obtained from the experimental data and the FE-model is presented in Fig. 6. The resulting dynamic characteristics estimated from the experiment are summarized in Table 4.

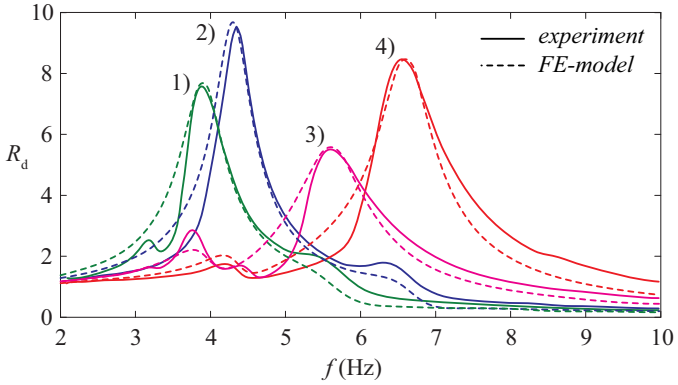

Fig. 6. FRF, comparison between experiment and FE-model.

Similar experimental testing is performed without the foam material. The results are presented in Table 5 and clearly show that the foam contributes to both stiffness and damping in all modes of vibration.

Table 4
Estimated natural frequencies and damping ratio of the complete prototype damper, based on a 10 min sine sweep load.

	(Hz)		(%)		(mm)		(N)
f_{1x}	4.3	ζ_{1x}	5.5	d_{1x}	9.2	F_{1x}	20.4
f_{1y}	3.9	ζ_{1y}	6.5	d_{1y}	7.4	F_{1y}	14.0
f_{2x}	6.6	ζ_{2x}	6.1	d_{2x}	8.4	F_{2x}	35.3
f_{2y}	5.6	ζ_{2y}	7.2	d_{2y}	5.5	F_{2y}	17.2

Table 5
Estimated natural frequencies and damping ratio of the prototype damper without foam material, based on a 10 min sine sweep load.

	(Hz)		(%)		(mm)		(N)
f_{1x}	3.2	ζ_{1x}	2.2	d_{1x}	16.5	F_{1x}	23.9
f_{1y}	3.4	ζ_{1y}	2.4	d_{1y}	15.5	F_{1y}	27.1
f_{2x}	4.9	ζ_{2x}	1.0	d_{2x}	23.1	F_{2x}	49.8
f_{2y}	4.9	ζ_{2y}	1.6	d_{2y}	14.8	F_{2y}	30.7

The FE-model is calibrated based on the experimental data, with the natural frequency and steady-state displacement as the primary objective functions. All calibrated input parameters are given in Table 6, both with and without the foam material. The foam results in a stiffness increase of about a factor of 2 in the x-direction and about 40% in the y-direction. As illustrated in Fig. 5, the foam is only present in the x-direction and the increase in the y-direction is mainly due to shear. The increase in viscous damping is about a factor 2 for both directions of the lower ring, a factor 3 and 4 for the upper ring in the y- and x-direction correspondingly. The large ratio of increase is due to the inherent low damping of the setup with only coil springs.

Table 6
Input parameters for the FE-model of the damper, calibrated based on experimental data.

	Complete damper				*Damper with no foam*			
	(kN/m)		(Ns/m)		(kN/m)		(Ns/m)	
k_{1x}	0.75	c_{1x}	3.65	k_{1x}	0.38	c_{1x}	1.60
k_{1y}	0.61	c_{1y}	4.22	k_{1y}	0.45	c_{1y}	1.81
k_{2x}	1.70	c_{2x}	5.21	k_{2x}	0.80	c_{2x}	1.25
k_{2y}	1.14	c_{2y}	6.43	k_{2y}	0.79	c_{2y}	1.91

Harmonic load blocks

To simulate the working conditions of the damper once installed on the bridge, a set of harmonic load blocks is applied. Each block has duration of 10 s and consists of a single frequency with constant base amplitude. The input gain is set to 3V, with expected base plate amplitude of 3 mm. Examples of time responses are presented in Fig. 7. It is noted that the base displacement in Fig. 7c is about 2 mm. This is likely to be due to the interaction with the load shaker. In the FE-model, the input load is calculated based on a steady-state displacement of 3 mm and using Eq. (3).

A total of four load blocks are studied, causing resonance in each of the dampers modes of vibration. Comparisons between the experimental results and the FE-model are presented in Table 7 to Table 10. The results are evaluated based on the peak response at steady-state, excluding both the initial excitation and the ending free vibration.

In Table 7, results from exciting the lower ring in the y-direction are presented. The input load is higher in the FE-model compared to the experiment, resulting in higher base displacement and base acceleration. The response of the damper is however in good agreement with the experimental results.

In Table 8, results from exciting the lower ring in the x-direction are presented. The input load in the FE-model is in good agreement with the experiments, also resulting in good agreement of the base motion. The motion of the lower ring is underestimated by some 8% while the upper ring is overestimated by some 20%. The absolute motion of the upper ring is however small, since it is off resonance.

In Table 9, results from exciting the upper ring in the y-direction are presented. The base force is slightly overestimated in the FE-model, but still results in good agreement of the base motion. The motion of the upper ring is underestimated by some 10%. The motion of the lower ring is underestimated by 50%, but still experiences off-resonant behavior.

In Table 10, results from exciting the upper ring in the x-direction are presented. Although the input force is lower in the FE-model, good agreement is found for the base motion. The motion of the upper ring is underestimated by some 20%.

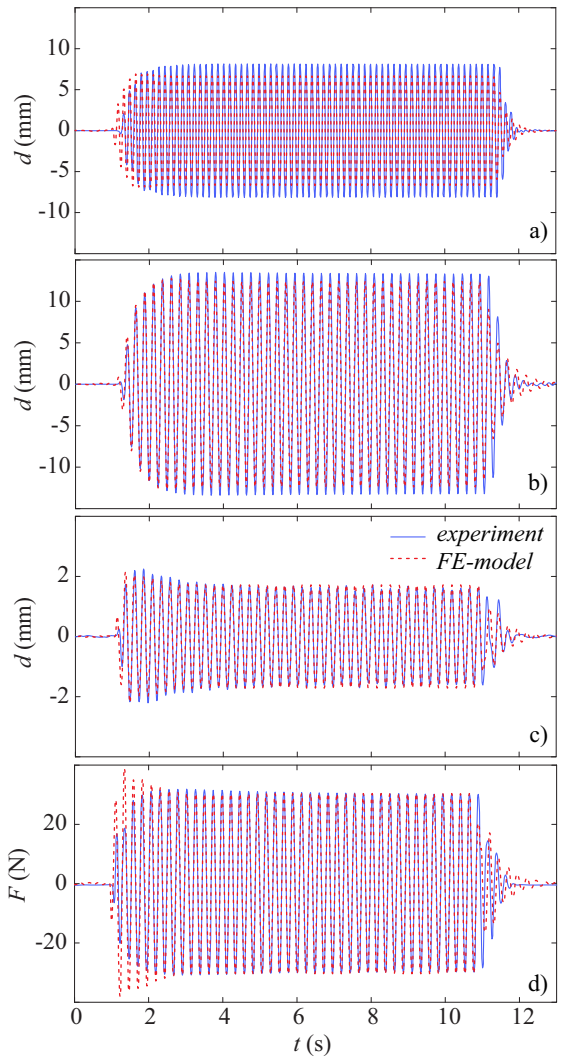

Fig. 7. Displacement from a 10 s harmonic load block, comparison with experiment and FE-model, a) upper ring, f_F = 6.3 Hz, b) lower ring, f_F = 4.2 Hz, c)-d) base, f_F =4.2 Hz.

Table 7
Results from a 10 s harmonic load block, f_F = 3.8 Hz, *y*-direction.

	Experiment:		*FE-model:*		*FEM/Exp.*
	mean	*std*	*mean*	*std*	*mean*
F (N):	23.1	0.125	34.1	0.008	1.48
a_1 (m/s^2):	7.0	0.084	7.0	0.002	1.01
a_2 (m/s^2):	2.4	0.019	2.3	0.001	0.96
a_b (m/s^2):	1.0	0.007	1.1	0.000	1.15
d_1 (mm):	12.2	0.037	12.3	0.003	1.01
d_2 (mm):	4.1	0.044	4.0	0.001	0.98
d_b (mm):	1.6	0.017	1.9	0.000	1.24

Table 8
Results from a 10 s harmonic load block, f_F = 4.2 Hz, *x*-direction.

	Experiment:		*FE-model:*		*FEM/Exp.*
	mean	*std*	*mean*	*std*	*mean*
F (N):	30.3	0.350	30.4	0.009	1.00
a_1 (m/s^2):	9.3	0.087	8.6	0.003	0.92
a_2 (m/s^2):	1.9	0.200	2.2	0.001	1.18
a_b (m/s^2):	1.2	0.017	1.2	0.000	0.99
d_1 (mm):	13.3	0.054	12.4	0.004	0.93
d_2 (mm):	2.7	0.068	3.2	0.001	1.21
d_b (mm):	1.6	0.046	1.7	0.000	1.05

Table 9
Results from a 10 s harmonic load block, f_F = 5.5 Hz, *y*-direction.

	Experiment:		*FE-model:*		*FEM/Exp.*
	mean	*std*	*mean*	*std*	*mean*
F (N):	23.6	0.057	25.8	0.013	1.09
a_1 (m/s^2):	3.4	0.016	1.9	0.001	0.55
a_2 (m/s^2):	9.0	0.064	8.1	0.004	0.90
a_b (m/s^2):	1.7	0.015	1.7	0.001	1.00
d_1 (mm):	2.8	0.010	1.5	0.001	0.54
d_2 (mm):	7.5	0.012	6.8	0.003	0.91
d_b (mm):	1.4	0.015	1.4	0.001	1.02

Table 10
Results from a 10 s harmonic load block, f_F = 6.3 Hz, *x*-direction.

	Experiment:		*FE-model:*		*FEM/Exp.*
	mean	*std*	*mean*	*std*	*mean*
F (N):	33.3	0.164	21.8	0.014	0.66
a_1 (m/s^2):	3.8	0.028	1.9	0.001	0.51
a_2 (m/s^2):	12.9	0.097	10.4	0.006	0.81
a_b (m/s^2):	1.9	0.021	1.8	0.001	0.95
d_1 (mm):	2.4	0.017	1.2	0.001	0.50
d_2 (mm):	8.1	0.018	6.7	0.004	0.82
d_b (mm):	1.2	0.030	1.2	0.001	0.97

Conclusion

In this paper, the development and experimental testing of a bi-directional multi-passive tuned mass damper (bi-MTMD) is presented. The dynamic characteristics of the damper are estimated based on the FRF of the measured response. The frequencies of the damper are governed by a set of coil springs and foam material. The prototype damper was calibrated to specified target frequencies by changing the amount of foam material. The properties of the foam were not measured explicitly, but the effect was estimated based on experiments and FE-analyses with and without the foam. It was found that the foam contributes both to the stiffness and increased structural damping, both in compression and in shear.

The FE-model is calibrated based on the FRF of the measured response, resulting in good agreement. The damper is also tested for a series of constant harmonic load blocks, to simulate real working conditions, corresponding to passing trains. Although the FE-model is able to produce

similar behavior to the experiment, the scatter in results is larger compared to the FRF. One reason may be due to the influence of the load shaker, another reason may be nonlinear behavior of the damper itself or mismatch in model calibration. Still, the FE-model is considered to be sufficiently accurate to describe the dynamic behavior of the TMD.

Although the presented damper is tailor-made for a specific bridge component, the concept may be applicable to a wider range of applications, e.g. stay cables on cable stayed bridges. In the case of non-vertical components, the gravitational component needs to be accounted for.

Future work includes a full-scale testing of the developed damper on the intended railway bridge.

Acknowledgements

The development of the presented multi-passive tuned mass damper was performed within the Long Life Bridges project, a Marie Curie Industry-Academia Partnerships and Pathways project funded by the European Commission 7th Framework Programme (IAPP-GA-2011-286276). The funding is kindly acknowledged.

The experimental work was carried out at Trinity College Dublin, Department of Civil, Structural and Environmental Engineering. A special thank goes to Dr. Kevin Ryan and the laboratory staff at the Department for the help in manufacturing and testing the prototype damper.

References

Ormondroyd J, Den Hartog JP. (1928). The theory of the dynamic vibration absorber. *ASME, Journal of Applied Mechanics 50*.

Igusa T, Xu K. (1994). Vibration control using multiple tuned mass dampers. *Journal of Sound and Vibration 175(4)*.

Jangid RS. (1999). Optimum multiple tuned mass dampers for base-excited undamped system. *Earthquake Engineering and Structural Dynamics, 28*.

Luu M, Zabel V, Könke C. (2012). An optimization method of multi-resonant response of high-speed train bridges using TMDs. *Finite Element in Analysis and Design, 53*.

Yau J-D, Yang Y-B. (2004). A wideband MTMD system for reducing the dynamic response of continuous truss bridges to moving train loads. *Engineering Structures, 26*.

Varadarajan N. (2005). Novel smart variable stiffness tuned mass damper and its real time identification and control using time frequency techniques. *PhD Thesis, Rice University*.

Lin J-L, Tsai K-C, Yu Y-J. (2010). Bi-directional coupled tuned mass dampers for the seismic response control of two-way asymmetric-plan buildings. *Earthquake Engineering and Structural Dynamics, 40*.

Ankireddi S, Yang H. (2000). Directional mass dampers for buildings under wind or seismic loads. *Journal of Wind Engineering, 85*.

Malm R, Andersson A. (2006). Field testing and simulation of dynamic properties of a tied arch railway bridge. *Engineering Structures 28(1)*.

Andersson A, Karoumi R, O'Connor A. (2013). Passive and adaptive damping systems for vibration mitigation and increased fatigue service life of a tied arch railway bridge. *Preprint submitted to ASCE Journal of Bridge Engineering; February 2013*.

Andersson A, Malm R. (2004). Measurement Evaluation and FEM Simulation of Bridge Dynamics. *MSc. Thesis, KTH Royal Institute of Technology; Sweden*.

SOLVIA Engineering (2008). SOLVIA-PRE for Stress Analysis, User Manual. *Report SE 03-1, SOLVIA Finite Element Systems Version 03*.

Clough RW, Penzien J. (2003). Dynamics of Structures. *Computers & Structures, Inc, 3rd edition*.

Chopra AK. (2001) Dynamics of Structures, Theory and Application of Earthquake Engineering. *Prentice-Hall Inc, 2nd Edition*.

De Silva CW. (2007). Vibration Damping, Control, and Design. *CRC Press, Taylor & Francis Group*.

Lockhart RW. (2009). How Much ADC Resolution Do You Really Need? *Technical Note, DATAQ Instruments*.

MathWorks (2009). MATLAB 2009b Reference manual. *The MathWorks, Inc*.

Ricci S, Peeters B, Fetter R, Boland D, Debille J. (2009). Virtual shaker testing for predicting and improving vibration test performance. *IMAC-XXVII, Orlando, USA; February 2009*.

Kraaij, C.S. (2008). A semi-analytical buckling approach: modeling and validation. *MSc Thesis, Eindhoven University of Technology, the Netherlands*.

Paper VI.

External damping of stay cables using adaptive and semi-active vibration control

Andreas Andersson, Raid Karoumi, Alan O'Connor

ICSBOC 2013, Edinburgh, Scotland, 3-5 June 2013

(Conference submitted)

EXTERNAL DAMPING OF STAY CABLES USING ADAPTIVE AND SEMI-ACTIVE VIBRATION CONTROL

Andreas Andersson [1)], Alan O'Connor [2)], Raid Karoumi [3)]

[1] Researcher, Royal Institute of Technology (KTH), Stockholm, Sweden
[2] Associate Professor, Trinity College Dublin (TCD), Dublin, Ireland
[2] Director, Roughan & O'Donovan Innovative Solutions, Dublin, Ireland
[3] Professor, Royal Institute of Technology (KTH), Stockholm, Sweden

Abstract
In this paper, the performances of different external damping systems for stay cables are studied based on numerical simulations. Two types of dampers have been analysed; a near anchorage viscous damper and a tuned mass damper (TMD) mounted near the midspan of the stay cable. For the passive case, both dampers are tuned to the fundamental mode of vibration of the cable. The optimal viscous damping for the near anchorage damper is determined based on well-known equations for a taut string. For the TMD, parametrical studies have been performed to determine the optimal damping ratio as function of the damper mass. The resulting vibration mitigation from the two systems are also studied for higher modes of vibration and the potential increase in performance using an adaptive or semi-active vibration control system is studied.

Keywords: Stay-cable; external damping system, TMD, semi-active control, finite element analysis.

1. Introduction

Stay cables for cable-stayed bridges often have a very low inherent structural damping, making them prone to vibrations. Wind or wind-rain induced vibrations may cause excessive vibrations, that without countermeasures may risk to decrease the fatigue service life of the cable. Forming of longitudinal water rivulets during rain may initiate so-called wet-galloping. One of the first cases of rain-induced cable vibrations was observed on the Meiko-Nishi Bridge in 1986. Large amplitude vibrations were observed at relatively low wind velocities, 5 – 15 m/s, and for higher cable modes in the range of 1 – 3 Hz. On the Great Belt Bridge, cable vibrations with amplitudes of 2 m have been observed, caused by icing. The forming of ice on the cables resulted in a significant change in the aerodynamic force coefficients, causing aerodynamic instability and making them more prone to wind induced vibrations. [1]

Different countermeasures for mitigate cable vibrations are avaiable. The cable surface can be modified with longitudinal channels, dimples or bumps that can disrupt the formation of longitudinal water rivulets and will significantly decrease the risk of galloping and vortex-shedding. Cross ties with stabilising ropes can be used to couple several cables with each other and to change the dynamic system. Mechanical damping systems can be installed, e.g. near anchorage viscous dampers or TMD. Near anchorage dampers can consist of a chock absorber with one end mounted to the bridge deck and the other end connected to the stay cable. The primary vibration mitigation is due to increased structural damping of the stay cable, produced by the chock absorber. Due to geometrical implications, the damper is most often installed relatively close to the anchorage, resulting in a decreased efficiency for longer cables. A TMD works on the principle of disrupting a structural mode of vibration by means of a small suspended mass. For the case of no inherent damping of the TMD, two adjacent modes of vibrations will be obtained with similar magnitude as the undamped structure. Introducing a damping in the TMD will however contribute to the damping of the primary structure. For lightly damped structures as stay cables, a relatively small mass may produce significant vibration mitigation. External dampers are most often designed based on optimal parameters for the fundamental mode of vibration. This may however result in a poor performance for higher modes. Advanced dampers with a variable range of stiffness and/or damping can in combination with a control system be used to improve the vibration mitigation for higher modes.

2. Models of a stay cable with an external damper

The dynamic behaviour of a stay cable is analysed with a 2D FE-model, using the commercial software SOLVIA03 [2]. The cable is modelled with beam elements with negligible flexural stiffness. The inclination and the sag of the cable are neglected, as well as the out-of-plane motion.

Data for the cable is taken from [3], also studied in [4]. The cable has a length L = 93 m, mass m = 114 kg/m, axial stiffness EA = 1615 MN and an axial pre-stress of 5017 kN. The first natural frequency of the undamped cable is f_1 = 1.127 Hz.

The model of the near anchorage damper is illustrated in Figure 1, the distance $x_c = 0.02L$. The model with a TMD is illustrated in Figure 2, in which $x_c = 0.4L$. The position of the TMD is chosen to be able to mitigate vibrations from higher modes. The first four modes of vibration for the undamped cable are presented in Figure 3, based on an eigen-value analysis, accounting for the axial pre-stress.

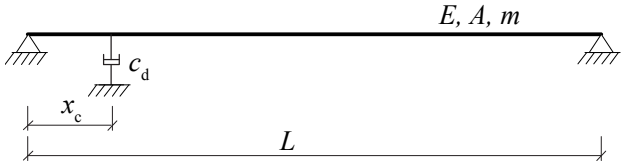

Figure 1: Simplified model of a stay cable with a near anchorage viscous damper.

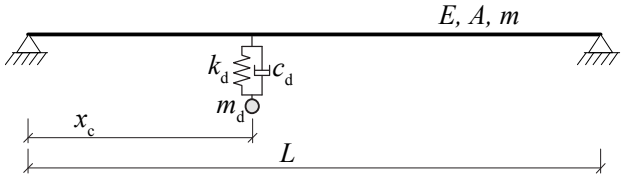

Figure 2: Simplified model of a stay cable with a tuned mass damper.

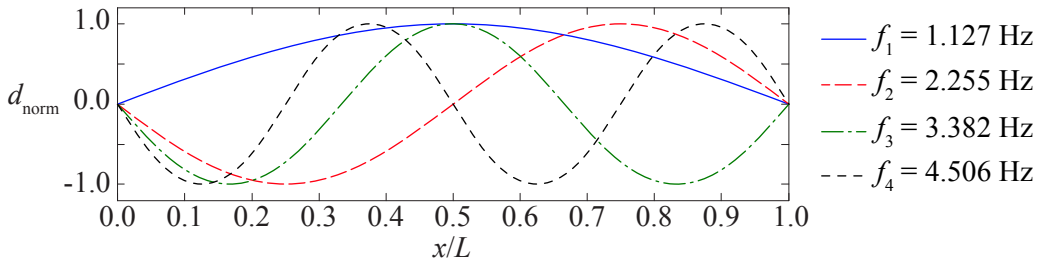

Figure 3: First four modes of vibration, the stay cable without a damper.

3. Methods of analysis

Throughout this paper, the cable is subjected to a vertical harmonic unit load, acting at $x = 0.4L$. The results are based on the vertical displacements at the same location. The results are presented as a dynamic amplification factor $R_d = d_{dyn}/d_{stat}$, where d_{stat} is the static displacement of the unit load and d_{dyn} the corresponding peak dynamic displacement.

For the case of linear and non-varying dampers, the steady state frequency response can be calculated using Eq. (1). **M**, **C**, **K** are the mass, damping and stiffness matrices respectively and **F** is the force vector. The frequency response function (FRF) is then found by solving for the frequency dependent displacement vector $\mathbf{x}(\omega)$, for each prescribed circular frequency ω [5].

$$\left(-\omega^2\mathbf{M} + i\omega\mathbf{C} + \mathbf{K}\right)\mathbf{x}(\omega) = \mathbf{F} \tag{1}$$

For the case of adaptive or semi-active dampers, the damping or the stiffness is incrementally updated in the analysis. A direct time integration scheme is then employed and the load consists of a harmonic force with linearly increasing frequency. The rate of change in frequency is chosen sufficiently long to approximate the steady-state response.

The resulting structural damping due to the dampers is estimated using the Half-Power Bandwidth method, according to Eq.(2). To improve the accuracy of the method, a curve fit using a 4th order polynomial is used, as illustrated in Figure 4.

$$\zeta = \frac{f_2 - f_1}{f_2 + f} \tag{2}$$

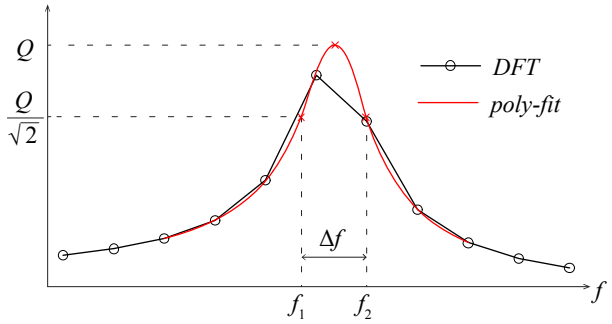

Figure 4: Illustration of the Half-Power Bandwidth method.

4. Optimal damper parameters

For a near anchorage damper, the relation between the viscous damper c_d and the resulting cable damping ζ_i for mode i can be presented in a normalised form according to Figure 5, [7]. The results in Figure 5 are produced based on the steady-state response of the model in Figure 1, varying the viscous damper c_d. For the case study cable, an optimal viscous damping c_d = 376 kNs/m is calculated based on the first mode of vibration. For $x_c = 0.02L$, the optimal damping is about 1%.

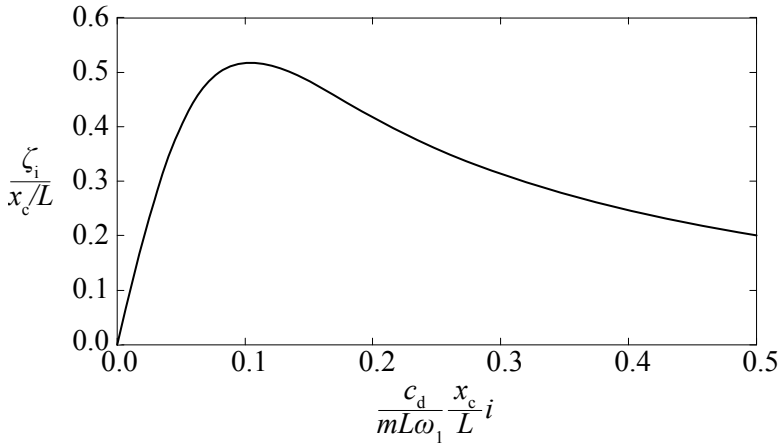

Figure 5: Optimal viscous damping for a near anchorage damper.

For the TMD, the stiffness k_d and viscous damper c_d are calculated according to Eq. (3). The mass of the TMD is often presented as a ratio of the total mass of the cable, $\gamma = m_{TMD} / m_{cable}$.

$$k_d = m_d \omega_d^{\,2}, \quad c_d = 2\zeta_{TMD}\sqrt{k_d m_d} \tag{3}$$

A parametrical study is performed to determine the TMD parameters for the optimal cable damping ζ_{cable}. A series of steady-state analyses are performed using the model in Figure 2 and varying the mass and the damping of the TMD. The results for the first mode of vibration are shown in Figure 6. For low TMD damping ratios, the FRF is characterised by two separate resonance peaks, adjacent to the structural mode of the cable. For increased TMD damping ratios, the two peaks are eventually merged and the optimal damping is found in this transition zone. For low TMD mass ratio, the transition is more distinct, causing a sudden change in estimated total damping. For the present case, $\gamma > 0.7$ results in a moderate increase in total cable damping. For further analysis, $\gamma = 0.9$ is used, corresponding to about 100 kg in TMD mass. The appertaining optimal damping is $\zeta_{TMD} = 9\%$, corresponding to c_d = 127 Ns/m, about 3000 times less than for the near anchorage damper. The resulting cable damping is about 6 %. Similar magnitude of damping has been obtained by [6].

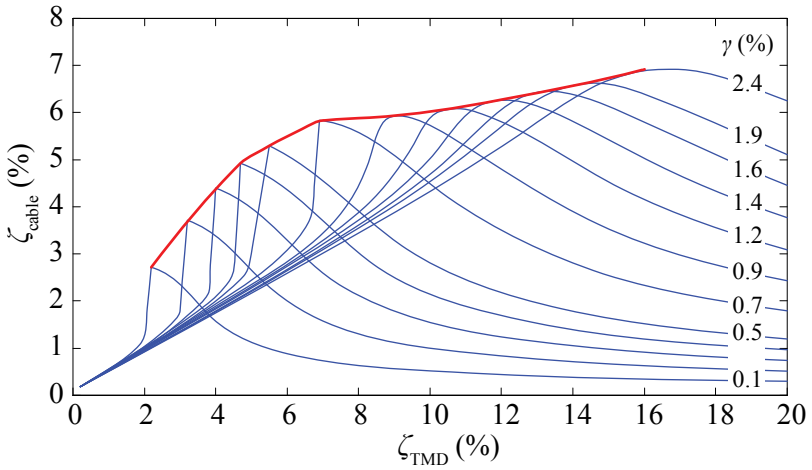

Figure 6: Resulting cable damping due to a TMD, influence of the damping ratio ζ_{TMD} and mass ratio γ.

The performance of the near anchorage damper and the TMD is shown in Figure 7, for the first mode of vibration. An inherent damping $\zeta_{cable} = 0.1\%$ is set for the cable itself, to limit the resonant response. For the case of the undamped TMD, the fundamental mode of vibration for the cable is separated in two adjacent peaks. The response at resonance is reduced by about a factor 2. Using the optimal damping according to Figure 6, no distinct resonance peaks are obtained and the response at resonance is reduced by about a factor 50, compared to the cable with no damper. The near anchorage damper maintains a single fundamental mode of vibration of the cable, but with increased damping. The response at resonance is however about 3 times larger compared to the optimal damped TMD. The TMD performs better than the near anchorage damper mainly due to the location further up along the cable, where the magnitude of vibration is larger.

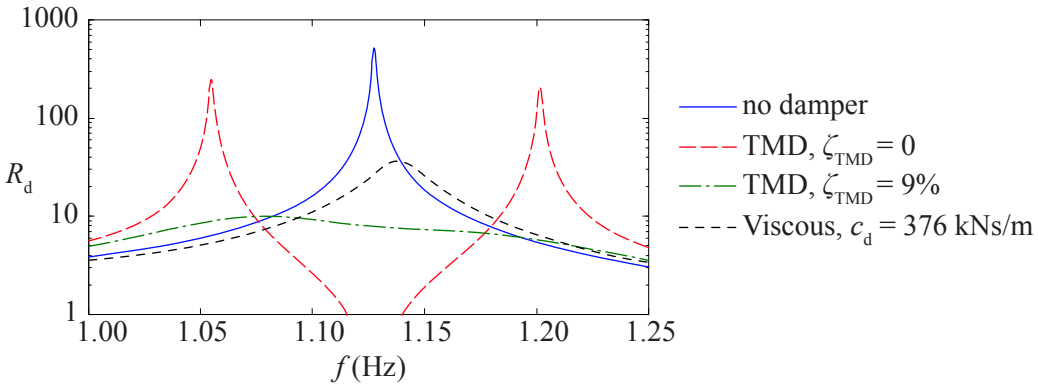

Figure 7: Steady-state response of the first mode of vibration, comparison of a near anchorage damper and a TMD.

5. Adaptive vibration control

In vibration control of damping systems, the damper has time-variant properties that can be controlled by a control system. The physical behaviour of such systems can vary, but is often based on a controllable electrical input current. In this paper, it is assumed that either the stiffness k_d or viscous damping c_d can be controlled independently. One sometimes distinguishes between adaptive systems that can change its property within a few cycles of vibration (seconds) and semi-active systems that can change within a few milliseconds.

A schematic of the control procedure is illustrated in Figure 8. The system of equation is solved using a direct time incrementation. The previous t_{incr} of time response is modulated with a window function and zero-padded to obtain a virtually higher frequency resolution. The modulated signal is subjected to a Fast Fourier Transform and the dominant frequency f_i is estimated. The procedure is often denoted Short Time Fourier Transform (STFT). For the near anchorage damper, the natural frequency closest to f_i is determined and the corresponding optimal viscous damper c_d is calculated according to Figure 5. For the case of the TMD, a new stiffness k_d is instead calculated according to Eq. (3). The damping or stiffness matrix is updated and the analysis is forwarded t_{incr}.

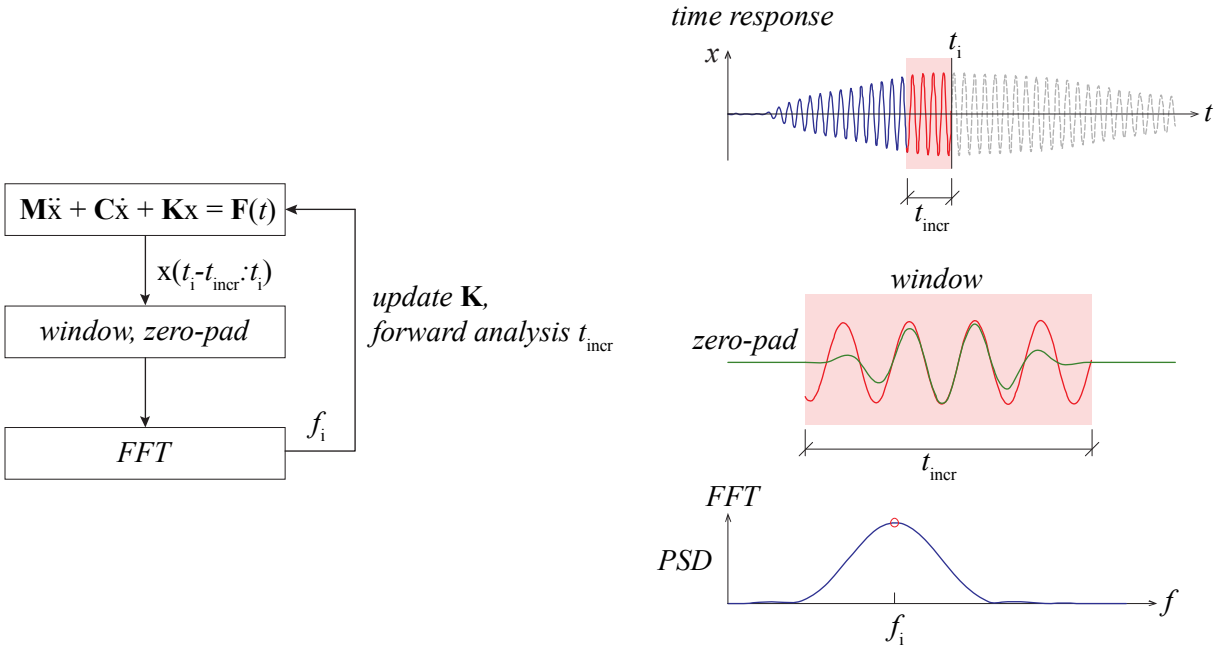

Figure 8: Schematics for the procedure of the adaptive control.

6. Vibration mitigation in higher modes

The performance of the TMD and the near anchorage damper is studied for higher modes of vibration. A comparison is also performed between passive dampers with constant damping properties and adaptive/semi-active dampers that can change in stiffness or viscous damping. The analysis is performed using a direct time incrementation. A harmonic unit load is applied with a linear increase in frequency from 0.5 Hz to 5.0 Hz during a total time of 2 h in the simulation, to approximate the steady-state response.

For the TMD, three different models are analysed; a passive damper tuned to first mode of vibration, an adaptive damper that can be retuned in increments corresponding to the first four modes and an adaptive/semi-active damper that can change frequency continuously. For all TMD-models, the viscous damping c_d = 127 Ns/m is used, corresponding to the optimal damping for the first mode. For the near anchorage damper, a passive viscous damper tuned to the first mode is compared with a damper that can change in increments of the first four modes of vibration. For all the adaptive/semi-active models, the real-time dominant frequency is evaluated every 5 s, based on the previous 5 s of response.

The results from the simulations are presented in Figure 9 and Figure 10. For the first mode, the passive and the incrementally adaptive dampers yield the same results. As presented in Figure 7, the TMD is about 3 times more efficient than the near anchorage damper. Even greater vibration mitigation is obtained with the continuously variable TMD. The reason is likely that a continuous update of the tuning frequency allows mitigating the two adjacent modes produced by the TMD. As a result, the largest magnitude is obtained closer to the fundamental frequency of the undamped cable.

For the higher modes, the passive TMD experience a significant loss of performance, due to detuning. The incrementally tuned TMD shows more pronounced double peaks for higher modes. This is due to the use of constant viscous damping, corresponding to a lower damping ratio for higher frequencies. A significant improvement is found using the continuously adaptive TMD.

The passive viscous near anchorage damper does not suffer from the same detuning as the TMD. The reason is that it mainly operates on increased cable damping rather than changing the dynamic modes of vibration. The difference between the passive and adaptive viscous damper is also less than the corresponding difference for the TMD. The reason is that the optimal viscous damping is inversely proportional to the mode number, Figure 5, where as the stiffness of the TMD depends on the square of the tuning frequency, Eq. (3).

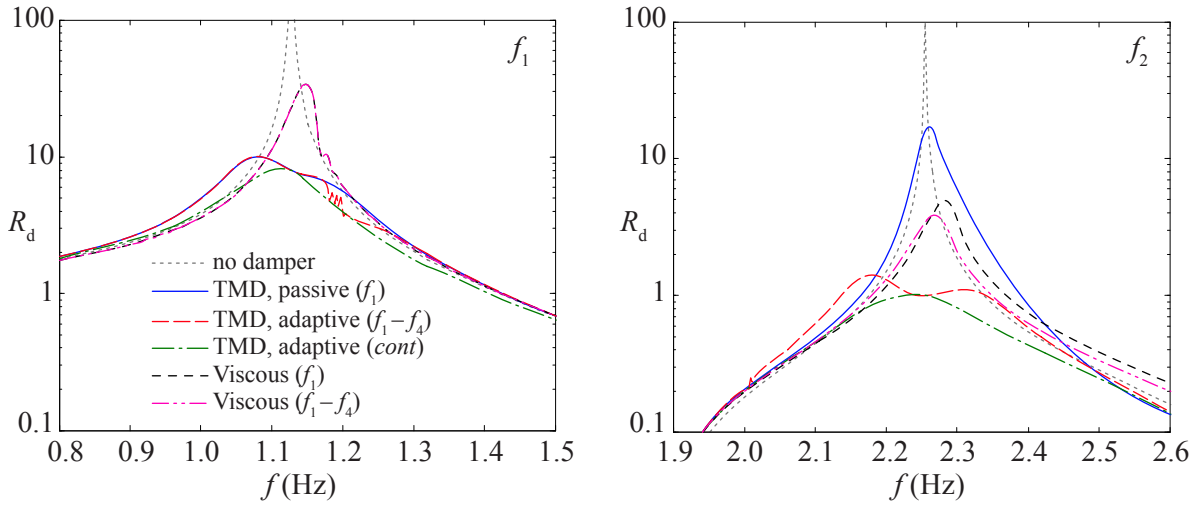

Figure 9: Steady-state response of the cable due to different damping systems, f_1 and f_2.

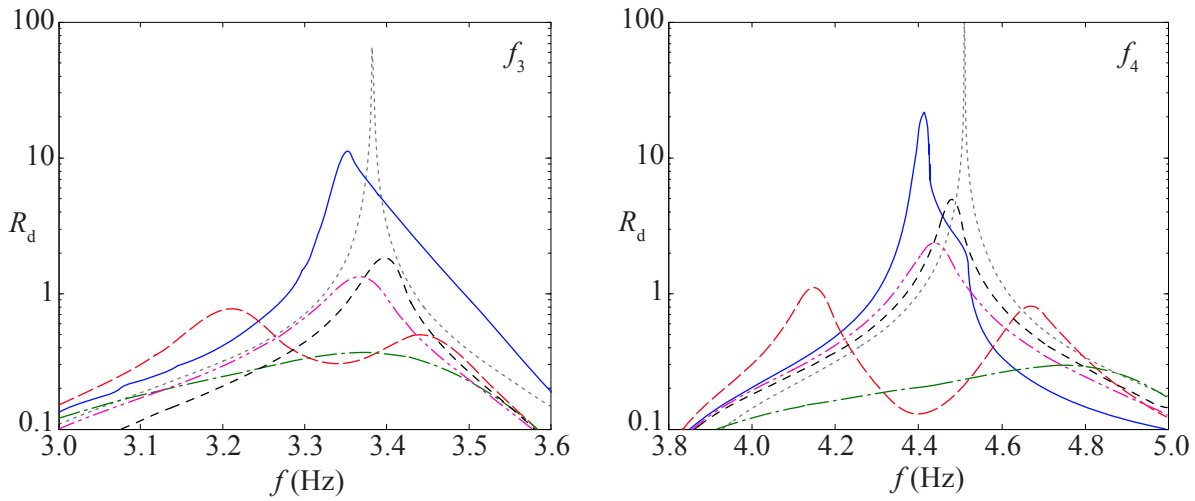

Figure 10: Steady-state response of the cable due to different damping systems, f_3 and f_4.

The peak response from Figure 9 and Figure 10 are summarised in Table 1. The dynamic amplification for all modes are related to the same static displacement. Since the static mode of displacement differs from the higher modes of vibrations, $R_d<1$ is sometimes obtained. The results aim at comparing the relative difference between different damping systems rather than estimating a realistic absolute value of the displacement magnitude.

Table 1: Peak steady-state dynamic amplification factor, based on vertical displacement at x_c/L = 0.4, comparison of different external damping systems.

	$R_{d,f1}$	$R_{d,f2}$	$R_{d,f3}$	$R_{d,f4}$
TMD, passive (f_1)	10.08	17.18	11.39	21.69
TMD, adaptive ($f_1 - f_4$)	10.08	1.41	0.78	1.17
TMD, adaptive (*cont.*)	8.24	1.04	0.37	0.29
Viscous (f_1)	33.93	5.05	1.83	5.09
Viscous ($f_1 - f_4$)	33.93	3.91	1.34	2.37

7. Conclusion

From the results presented in this paper, the following conclusions are made.

- Due to very low inherent damping of stay cables, very high dynamic response at resonance is obtained.
- The near anchorage viscous damper has a rather limited performance, depending on the relatively short distance between the anchorage point and the connection of the damper. This decreases the performance for longer cables.
- The adaptive viscous damper shows moderate improvement for higher modes compared to the corresponding passive damper.
- A TMD can result in significant vibration mitigation, even for a moderate damper mass.
- For the TMD, an optimal damping value exists, that increases with increased damper mass.
- The passive TMD is sensitive to detuning, resulting in a poor performance for higher modes.
- An adaptive/semi-active TMD can increase the vibration mitigation significantly for higher modes. The best performance was obtained by a continuously variable stiffness TMD.

The results presented in this paper contains several simplifications, the following should be addressed in further research.

- The influence of the cable flexural stiffness and cable sag may change the mode of vibration and the natural frequencies. The response may also be amplitude dependent.
- Further parametric studies to find optimal TMD tuning parameters for higher modes of vibration and optimal position along the cable.
- In practice, adaptive/semi-active damping devices often have a more complicated physical behaviour than a linear change in viscous damping or stiffness. The application of magneto-rheological dampers for near anchorage dampers have been studied by [8], similar procedures may be applicable for a adaptive/semi-active TMD.
- The use of coupled or uncoupled multi-passive dampers may serve as an alternative to the adaptive TMD.

Acknowledgements
The work presented in this paper was performed within the Long Life Bridges project, a Marie Curie Industry-Academia Partnerships and Pathways project, funded by the European Commission 7th Framework Programme (IAPP-GA-2011-286276).

References

[1] Gimsing, J.N., Georgakis, C.T., 2012. Cable Supported Bridges, Concept and Design. *3rd Ed., John Wiley & Sons*.

[2] SOLVIA, 2008. SOLVIA-PRE for Stress Analysis, User Manual. *Report SE 03-1, SOLVIA Finite Element Systems Version 03*.

[3] Tabatabai, H., Mehrabi, A.B., 2010. Evaluation of various damping treatments for stay cables. *IMAC XVIII, 7-10 Feb 2010, San Antonio, U.S.*

[4] Caetano, E., 2007. Cable Vibrations in Cable-Stayed Bridges. *International Association for Bridge and Structural Engineering*.

[5] Clough RW, Penzien J. Dynamics of Structures. *Computers & Structures, Inc, 3rd edition; 2003.*

[6] Wu, W.J., Cai, C.S., 2006. Cable Vibration Reduction with a Hung-on TMD System, Part II: Parametric Study. *Journal of Vibration and Control, 12(8): 881-899*.

[7] Pacheco, B.M., Fujino, Y., Sulekh, A., 1993. Estimation Curve for Modal Damping in Stay Cables with Viscous Damper. *Journal of Structural Engineering, 119(6): 1961-1979*.

[8] Johnson, E.A., Baker, G.A., Spencer, B.F., Fujino, Y., 2007. Semiactive Damping of Stay Cables. *ASCE Journal of Engineering Mechanics 133:1(1)*.